TECHNICAL REPORT

DESIGN AND DEVELOPMENT OF SMALL AND LARGE FORM FACTOR ON BODY ANTENNAS FOR SUB-6 GHZ 5G APPLICATIONS

Azremi Abdullah Al-Hadi Wee Fwen Hoon Saidatul Norlyana Azemi Surentiran Padmanathan Che Muhammad Nor Che Isa Soh Ping Jack



©Universiti Malaysia Perlis, 2025

All rights reserved. No part of this book may be reproduced or transmitted in any forms by any means, electronic, mechanical, or otherwise, whether now or hereafter devised, including photocopying, recording, or by any information storage and retrieval system without express written prior permission from the publishers.

e-ISBN 978-629-7715-xx-x

Published by:

Penerbit UniMAP Universiti Malaysia Perlis No. 11 & 13, Jalan Tiga Pusat Perniagaan Pengkalan Jaya 01000 Kangar, Perlis, MALAYSIA

Website: http://penerbit.unimap.edu.my E-mail: penerbitan@unimap.edu.my

TABLE OF CONTENTS

LIST OF TABLES LIST OF FIGURES ACKNOWLEGDEMENT PREFACE 1. INTRODUCTION 2. DUAL BAND CIRCULAR PATCH FLEXIBLE WEARABLE ANTENNA DESIGN FOR SUB-6 GHZ 5G APPLICATIONS 2.1 Circular Patch Wearable Antenna Design and Specification 2.2 Results and Discussion 2.2.1 Reflection Coefficient 2.2.2 Radiation Pattern 2.2.3 Surface Current Distribution 2.2.4 Gain and Efficiency 2.2.5 On-Body Performance Analysis 2.2.6 Bending Performance Analysis 3. FABRICATION OF A WEARABLE ANTENNA WITH DEFECTED GROUND STRUCTURE ON A FLEXIBLE TPU-POLYESTER SUBSTRATE 3.1 DGS Wearable Antenna Design 3.2 DGS Wearable Antenna Performance Analysis 4. ON-BODY PERFORMANCE ANALYSIS OF WEARABLE ANTIPODAL VIVALDI ANTENNA FOR 5G APPLICATIONS 5. ON-BODY ANALYSIS OF BENDING AND HUMAN BODY EFFECTS OF COMPACT FULL FLEXIBLE ANTIPODAL VIVALDI ANTENNA FOR 5G SUB-6 GHZ WEARABLE APPLICATIONS 5.1 Antenna Bending and On-body Analysis 6. ANTIPODAL VIVALDI ANTENNA WITH ANALYSIS NEAR HUMAN BODY AND UNDER BENDING CONDITIONS 7. CIRCULAR PATCH ANTENNA WITH ANALIS NEAR HUMAN	
ACKNOWLEGDEMENT PREFACE 1. INTRODUCTION 2. DUAL BAND CIRCULAR PATCH FLEXIBLE WEARABLE ANTENNA DESIGN FOR SUB-6 GHZ 5G APPLICATIONS 2.1 Circular Patch Wearable Antenna Design and Specification 2.2 Results and Discussion 2.2.1 Reflection Coefficient 2.2.2 Radiation Pattern 2.2.3 Surface Current Distribution 2.2.4 Gain and Efficiency 2.2.5 On-Body Performance Analysis 2.2.6 Bending Performance Analysis 3. FABRICATION OF A WEARABLE ANTENNA WITH DEFECTED GROUND STRUCTURE ON A FLEXIBLE TPU-POLYESTER SUBSTRATE 3.1 DGS Wearable Antenna Design 3.2 DGS Wearable Antenna Fabrication 3.3 DGS Wearable Antenna Performance Analysis 4. ON-BODY PERFORMANCE ANALYSIS OF WEARABLE ANTIPODAL VIVALDI ANTENNA FOR 5G APPLICATIONS 5. ON-BODY ANALYSIS OF BENDING AND HUMAN BODY EFFECTS OF COMPACT FULL FLEXIBLE ANTIPODAL VIVALDI ANTENNA FOR 3.5 GHZ IN 5G SUB-6 GHZ WEARABLE APPLICATIONS 5.1 Antenna Bending and On-body Analysis 6. ANTIPODAL VIVALDI ANTENNA WITH ANALYSIS NEAR HUMAN BODY AND UNDER BENDING CONDITIONS	V
PREFACE 1. INTRODUCTION 2. DUAL BAND CIRCULAR PATCH FLEXIBLE WEARABLE ANTENNA DESIGN FOR SUB-6 GHZ 5G APPLICATIONS 2.1 Circular Patch Wearable Antenna Design and Specification 2.2 Results and Discussion 2.2.1 Reflection Coefficient 2.2.2 Radiation Pattern 2.2.3 Surface Current Distribution 2.2.4 Gain and Efficiency 2.2.5 On-Body Performance Analysis 2.2.6 Bending Performance Analysis 3. FABRICATION OF A WEARABLE ANTENNA WITH DEFECTED GROUND STRUCTURE ON A FLEXIBLE TPU-POLYESTER SUBSTRATE 3.1 DGS Wearable Antenna Design 3.2 DGS Wearable Antenna Fabrication 3.3 DGS Wearable Antenna Performance Analysis 4. ON-BODY PERFORMANCE ANALYSIS OF WEARABLE ANTIPODAL VIVALDI ANTENNA FOR 5G APPLICATIONS 5. ON-BODY ANALYSIS OF BENDING AND HUMAN BODY EFFECTS OF COMPACT FULL FLEXIBLE ANTIPODAL VIVALDI ANTENNA FOR 3.5 GHZ IN 5G SUB-6 GHZ WEARABLE APPLICATIONS 5.1 Antenna Bending and On-body Analysis 6. ANTIPODAL VIVALDI ANTENNA WITH ANALYSIS NEAR HUMAN BODY AND UNDER BENDING CONDITIONS	vi
 INTRODUCTION DUAL BAND CIRCULAR PATCH FLEXIBLE WEARABLE ANTENNA DESIGN FOR SUB-6 GHZ 5G APPLICATIONS Circular Patch Wearable Antenna Design and Specification Results and Discussion Reflection Coefficient Reflection Coefficient Reflection Coefficient Surface Current Distribution Automated Galaxian and Efficiency Gain and Efficiency Gain and Formance Analysis FABRICATION OF A WEARABLE ANTENNA WITH DEFECTED GROUND STRUCTURE ON A FLEXIBLE TPU-POLYESTER SUBSTRATE JOGS Wearable Antenna Design DGS Wearable Antenna Fabrication JOGS Wearable Antenna Performance Analysis ON-BODY PERFORMANCE ANALYSIS OF WEARABLE ANTIPODAL VIVALDI ANTENNA FOR 5G APPLICATIONS ON-BODY ANALYSIS OF BENDING AND HUMAN BODY EFFECTS OF COMPACT FULL FLEXIBLE ANTIPODAL VIVALDI ANTENNA FOR 3.5 GHZ IN 5G SUB-6 GHZ WEARABLE APPLICATIONS Antenna Bending and On-body Analysis ANTIPODAL VIVALDI ANTENNA WITH ANALYSIS NEAR HUMAN BODY AND UNDER BENDING CONDITIONS 	X
 DUAL BAND CIRCULAR PATCH FLEXIBLE WEARABLE ANTENNA DESIGN FOR SUB-6 GHZ 5G APPLICATIONS Circular Patch Wearable Antenna Design and Specification Reflection Coefficient Reflection Coefficient Coefficient Coefficient Reflection Coefficient Coefficient Reflection Coefficient Resident Coefficient Reflection Coefficient Resident Coefficient <	xi
ANTENNA DESIGN FOR SUB-6 GHZ 5G APPLICATIONS 2.1 Circular Patch Wearable Antenna Design and Specification 2.2 Results and Discussion 2.2.1 Reflection Coefficient 2.2.2 Radiation Pattern 2.2.3 Surface Current Distribution 2.2.4 Gain and Efficiency 2.2.5 On-Body Performance Analysis 2.2.6 Bending Performance Analysis 3. FABRICATION OF A WEARABLE ANTENNA WITH DEFECTED GROUND STRUCTURE ON A FLEXIBLE TPU-POLYESTER SUBSTRATE 3.1 DGS Wearable Antenna Design 3.2 DGS Wearable Antenna Performance Analysis 4. ON-BODY PERFORMANCE ANALYSIS OF WEARABLE ANTIPODAL VIVALDI ANTENNA FOR 5G APPLICATIONS 5. ON-BODY ANALYSIS OF BENDING AND HUMAN BODY EFFECTS OF COMPACT FULL FLEXIBLE ANTIPODAL VIVALDI ANTENNA FOR 3.5 GHZ IN 5G SUB-6 GHZ WEARABLE APPLICATIONS 5.1 Antenna Bending and On-body Analysis 6. ANTIPODAL VIVALDI ANTENNA WITH ANALYSIS NEAR HUMAN BODY AND UNDER BENDING CONDITIONS	1
2.2 Results and Discussion 2.2.1 Reflection Coefficient 2.2.2 Radiation Pattern 2.2.3 Surface Current Distribution 2.2.4 Gain and Efficiency 2.2.5 On-Body Performance Analysis 2.2.6 Bending Performance Analysis 3. FABRICATION OF A WEARABLE ANTENNA WITH DEFECTED GROUND STRUCTURE ON A FLEXIBLE TPU-POLYESTER SUBSTRATE 3.1 DGS Wearable Antenna Design 3.2 DGS Wearable Antenna Fabrication 3.3 DGS Wearable Antenna Performance Analysis 4. ON-BODY PERFORMANCE ANALYSIS OF WEARABLE ANTIPODAL VIVALDI ANTENNA FOR 5G APPLICATIONS 5. ON-BODY ANALYSIS OF BENDING AND HUMAN BODY EFFECTS OF COMPACT FULL FLEXIBLE ANTIPODAL VIVALDI ANTENNA FOR 3.5 GHZ IN 5G SUB-6 GHZ WEARABLE APPLICATIONS 5.1 Antenna Bending and On-body Analysis 6. ANTIPODAL VIVALDI ANTENNA WITH ANALYSIS NEAR HUMAN BODY AND UNDER BENDING CONDITIONS	2
2.2.1 Reflection Coefficient 2.2.2 Radiation Pattern 2.2.3 Surface Current Distribution 2.2.4 Gain and Efficiency 2.2.5 On-Body Performance Analysis 2.2.6 Bending Performance Analysis 3. FABRICATION OF A WEARABLE ANTENNA WITH DEFECTED GROUND STRUCTURE ON A FLEXIBLE TPU-POLYESTER SUBSTRATE 3.1 DGS Wearable Antenna Design 3.2 DGS Wearable Antenna Fabrication 3.3 DGS Wearable Antenna Performance Analysis 4. ON-BODY PERFORMANCE ANALYSIS OF WEARABLE ANTIPODAL VIVALDI ANTENNA FOR 5G APPLICATIONS 5. ON-BODY ANALYSIS OF BENDING AND HUMAN BODY EFFECTS OF COMPACT FULL FLEXIBLE ANTIPODAL VIVALDI ANTENNA FOR 3.5 GHZ IN 5G SUB-6 GHZ WEARABLE APPLICATIONS 5.1 Antenna Bending and On-body Analysis 6. ANTIPODAL VIVALDI ANTENNA WITH ANALYSIS NEAR HUMAN BODY AND UNDER BENDING CONDITIONS	3
2.2.2 Radiation Pattern 2.2.3 Surface Current Distribution 2.2.4 Gain and Efficiency 2.2.5 On-Body Performance Analysis 2.2.6 Bending Performance Analysis 3. FABRICATION OF A WEARABLE ANTENNA WITH DEFECTED GROUND STRUCTURE ON A FLEXIBLE TPU-POLYESTER SUBSTRATE 3.1 DGS Wearable Antenna Design 3.2 DGS Wearable Antenna Fabrication 3.3 DGS Wearable Antenna Performance Analysis 4. ON-BODY PERFORMANCE ANALYSIS OF WEARABLE ANTIPODAL VIVALDI ANTENNA FOR 5G APPLICATIONS 5. ON-BODY ANALYSIS OF BENDING AND HUMAN BODY EFFECTS OF COMPACT FULL FLEXIBLE ANTIPODAL VIVALDI ANTENNA FOR 3.5 GHZ IN 5G SUB-6 GHZ WEARABLE APPLICATIONS 5.1 Antenna Bending and On-body Analysis 6. ANTIPODAL VIVALDI ANTENNA WITH ANALYSIS NEAR HUMAN BODY AND UNDER BENDING CONDITIONS	4 4
2.2.3 Surface Current Distribution 2.2.4 Gain and Efficiency 2.2.5 On-Body Performance Analysis 2.2.6 Bending Performance Analysis 3. FABRICATION OF A WEARABLE ANTENNA WITH DEFECTED GROUND STRUCTURE ON A FLEXIBLE TPU-POLYESTER SUBSTRATE 3.1 DGS Wearable Antenna Design 3.2 DGS Wearable Antenna Fabrication 3.3 DGS Wearable Antenna Performance Analysis 4. ON-BODY PERFORMANCE ANALYSIS OF WEARABLE ANTIPODAL VIVALDI ANTENNA FOR 5G APPLICATIONS 5. ON-BODY ANALYSIS OF BENDING AND HUMAN BODY EFFECTS OF COMPACT FULL FLEXIBLE ANTIPODAL VIVALDI ANTENNA FOR 3.5 GHZ IN 5G SUB-6 GHZ WEARABLE APPLICATIONS 5.1 Antenna Bending and On-body Analysis 6. ANTIPODAL VIVALDI ANTENNA WITH ANALYSIS NEAR HUMAN BODY AND UNDER BENDING CONDITIONS	5
2.2.5 On-Body Performance Analysis 2.2.6 Bending Performance Analysis 3. FABRICATION OF A WEARABLE ANTENNA WITH DEFECTED GROUND STRUCTURE ON A FLEXIBLE TPU-POLYESTER SUBSTRATE 3.1 DGS Wearable Antenna Design 3.2 DGS Wearable Antenna Fabrication 3.3 DGS Wearable Antenna Performance Analysis 4. ON-BODY PERFORMANCE ANALYSIS OF WEARABLE ANTIPODAL VIVALDI ANTENNA FOR 5G APPLICATIONS 5. ON-BODY ANALYSIS OF BENDING AND HUMAN BODY EFFECTS OF COMPACT FULL FLEXIBLE ANTIPODAL VIVALDI ANTENNA FOR 3.5 GHZ IN 5G SUB-6 GHZ WEARABLE APPLICATIONS 5.1 Antenna Bending and On-body Analysis 6. ANTIPODAL VIVALDI ANTENNA WITH ANALYSIS NEAR HUMAN BODY AND UNDER BENDING CONDITIONS	6
 2.2.6 Bending Performance Analysis 3. FABRICATION OF A WEARABLE ANTENNA WITH DEFECTED GROUND STRUCTURE ON A FLEXIBLE TPU-POLYESTER SUBSTRATE 3.1 DGS Wearable Antenna Design 3.2 DGS Wearable Antenna Fabrication 3.3 DGS Wearable Antenna Performance Analysis 4. ON-BODY PERFORMANCE ANALYSIS OF WEARABLE ANTIPODAL VIVALDI ANTENNA FOR 5G APPLICATIONS 5. ON-BODY ANALYSIS OF BENDING AND HUMAN BODY EFFECTS OF COMPACT FULL FLEXIBLE ANTIPODAL VIVALDI ANTENNA FOR 3.5 GHZ IN 5G SUB-6 GHZ WEARABLE APPLICATIONS 5.1 Antenna Bending and On-body Analysis 6. ANTIPODAL VIVALDI ANTENNA WITH ANALYSIS NEAR HUMAN BODY AND UNDER BENDING CONDITIONS 	6
 FABRICATION OF A WEARABLE ANTENNA WITH DEFECTED GROUND STRUCTURE ON A FLEXIBLE TPU-POLYESTER SUBSTRATE 3.1 DGS Wearable Antenna Design 3.2 DGS Wearable Antenna Fabrication 3.3 DGS Wearable Antenna Performance Analysis ON-BODY PERFORMANCE ANALYSIS OF WEARABLE ANTIPODAL VIVALDI ANTENNA FOR 5G APPLICATIONS ON-BODY ANALYSIS OF BENDING AND HUMAN BODY EFFECTS OF COMPACT FULL FLEXIBLE ANTIPODAL VIVALDI ANTENNA FOR 3.5 GHZ IN 5G SUB-6 GHZ WEARABLE APPLICATIONS	7
GROUND STRUCTURE ON A FLEXIBLE TPU-POLYESTER SUBSTRATE 3.1 DGS Wearable Antenna Design 3.2 DGS Wearable Antenna Fabrication 3.3 DGS Wearable Antenna Performance Analysis 4. ON-BODY PERFORMANCE ANALYSIS OF WEARABLE ANTIPODAL VIVALDI ANTENNA FOR 5G APPLICATIONS 5. ON-BODY ANALYSIS OF BENDING AND HUMAN BODY EFFECTS OF COMPACT FULL FLEXIBLE ANTIPODAL VIVALDI ANTENNA FOR 3.5 GHZ IN 5G SUB-6 GHZ WEARABLE APPLICATIONS 5.1 Antenna Bending and On-body Analysis 6. ANTIPODAL VIVALDI ANTENNA WITH ANALYSIS NEAR HUMAN BODY AND UNDER BENDING CONDITIONS	9
 3.1 DGS Wearable Antenna Design 3.2 DGS Wearable Antenna Fabrication 3.3 DGS Wearable Antenna Performance Analysis 4. ON-BODY PERFORMANCE ANALYSIS OF WEARABLE ANTIPODAL VIVALDI ANTENNA FOR 5G APPLICATIONS 5. ON-BODY ANALYSIS OF BENDING AND HUMAN BODY EFFECTS OF COMPACT FULL FLEXIBLE ANTIPODAL VIVALDI ANTENNA FOR 3.5 GHZ IN 5G SUB-6 GHZ WEARABLE APPLICATIONS 5.1 Antenna Bending and On-body Analysis 6. ANTIPODAL VIVALDI ANTENNA WITH ANALYSIS NEAR HUMAN BODY AND UNDER BENDING CONDITIONS 	12
 3.2 DGS Wearable Antenna Fabrication 3.3 DGS Wearable Antenna Performance Analysis 4. ON-BODY PERFORMANCE ANALYSIS OF WEARABLE ANTIPODAL VIVALDI ANTENNA FOR 5G APPLICATIONS 5. ON-BODY ANALYSIS OF BENDING AND HUMAN BODY EFFECTS OF COMPACT FULL FLEXIBLE ANTIPODAL VIVALDI ANTENNA FOR 3.5 GHZ IN 5G SUB-6 GHZ WEARABLE APPLICATIONS 5.1 Antenna Bending and On-body Analysis 6. ANTIPODAL VIVALDI ANTENNA WITH ANALYSIS NEAR HUMAN BODY AND UNDER BENDING CONDITIONS 	12
 4. ON-BODY PERFORMANCE ANALYSIS OF WEARABLE ANTIPODAL VIVALDI ANTENNA FOR 5G APPLICATIONS 5. ON-BODY ANALYSIS OF BENDING AND HUMAN BODY EFFECTS OF COMPACT FULL FLEXIBLE ANTIPODAL VIVALDI ANTENNA FOR 3.5 GHZ IN 5G SUB-6 GHZ WEARABLE APPLICATIONS 5.1 Antenna Bending and On-body Analysis 6. ANTIPODAL VIVALDI ANTENNA WITH ANALYSIS NEAR HUMAN BODY AND UNDER BENDING CONDITIONS 	14
ANTIPODAL VIVALDI ANTENNA FOR 5G APPLICATIONS 5. ON-BODY ANALYSIS OF BENDING AND HUMAN BODY EFFECTS OF COMPACT FULL FLEXIBLE ANTIPODAL VIVALDI ANTENNA FOR 3.5 GHZ IN 5G SUB-6 GHZ WEARABLE APPLICATIONS 5.1 Antenna Bending and On-body Analysis 6. ANTIPODAL VIVALDI ANTENNA WITH ANALYSIS NEAR HUMAN BODY AND UNDER BENDING CONDITIONS	16
EFFECTS OF COMPACT FULL FLEXIBLE ANTIPODAL VIVALDI ANTENNA FOR 3.5 GHZ IN 5G SUB-6 GHZ WEARABLE APPLICATIONS 5.1 Antenna Bending and On-body Analysis 6. ANTIPODAL VIVALDI ANTENNA WITH ANALYSIS NEAR HUMAN BODY AND UNDER BENDING CONDITIONS	20
6. ANTIPODAL VIVALDI ANTENNA WITH ANALYSIS NEAR HUMAN BODY AND UNDER BENDING CONDITIONS	24
HUMAN BODY AND UNDER BENDING CONDITIONS	24
7. CIRCULAR PATCH ANTENNA WITH ANALIS NEAR HUMAN	28
BODY AND UNDER BENDING CONDITIONS	43
8. ANALYSIS OF BENDING AND HUMAN BODY EFFECTS OF COMPACT FULL FLEXIBLE ANTIPODAL VIVALDI ANTENNA FOR 3.5 GHZ IN 5G SUB-6 GHZ WEARABLE APPLICATIONS	57 57
8.1 Antenna Performance Analysis, Results, and Discussion	
 9. COMPACT FULL FLEXIBLE VIVALDI ANTENNA FOR 3.5 GHZ WEARABLE APPLICATIONS 9.1 Antenna Performance Analysis, Results, and Discussion 	60 60

10. CONCLUSION	63
11. REFERENCES	64
12. APPENDIX	67

LIST OF TABLES

Table 2.1	The Dimension Details of the Circular Patch Wearable Antenna	3
Table 2.2	The Comparison Results with Previous Studies	11
Table 3.1	DGS Wearable Antenna Design Specifications	13
Table 3.2	DGS Wearable Antenna Screen Printing Parameter	15
Table 3.3	Performance Comparison of the Proposed Antenna, DGS Wearable Antenna	17
Table 4.1	SAR Performance of Wearable Antipodal Vivaldi Antenna	23
Table 6.1	Dimensions of the Antipodal Vivaldi Antenna	29
Table 6.2	SAR for Single Port Antipodal Antenna	34
Table 6.3	SAR Values for Two-Port Antipodal Vivaldi Antenna	42
Table 7.1	Dimensions of the Single Circular Patch Antenna	43
Table 7.2	SAR Values for Circular Patch Single Port Antenna	48

LIST OF FIGURES

Figure 2.1	Configuration of the designed Circular Patch Wearable antenna (a) Top view (b) Rear view			
Figure 2.2	Configuration of the fabricated antenna (a) Front view (b) Rear view (c) Measurement setup			
Figure 2.3	Simulated and measured reflection coefficient			
Figure 2.4	Simulated radiation pattern at 3.63 (a) H-Plane (b) E-Plane and at 4.95 (c) H-plane (d) E-Plane	6		
Figure 2.5	Current distribution of the antenna at (a) 3.63 and (b) 4.95 Hz	6		
Figure 2.6	Gain and efficiency vs frequency	7		
Figure 2.7	Antenna near human body model (on chest)	7		
Figure 2.8	Antenna near human body model (on back)	8		
Figure 2.9	Reflection coefficient performances with different distances placing on the (a) Chest and (b) Back of the human model	8		
Figure 2.10	Antenna bending with radius of (a) 50 mm (b) 40 mm (c) 30 mm	9		
Figure 2.11	Antenna performances under bending conditions (a) Reflection coefficient (b) Efficiency (c) Gain	10		
Figure 3.1	DGS wearable antenna dimensions without DGS (a) Front view (b) Back view (c) Cross section			
Figure 3.2	Antenna dimensions with DGS (a) Front view (b) Back view	14		
Figure 3.3	Layer stack-up of the screen-printed antenna on TPU a) TPU Substrate b) Conductive Ground Layer screen printing c) Flip the substrate and screen print the Conductive Patch Layer d) Dielectric Patch Layer Screen Printing	15		
Figure 3.4	Screen printing process	16		
Figure 3.5	Fabricated antennas (a) Without DGS (b) with DGS	16		
Figure 3.6	Comparison of S ₁₁ of the antenna with and without DGS	16		
Figure 3.7	3D antenna radiation pattern for single element patch antenna (a) Without DGS (b) With DGS	17		
Figure 3.8	DGS Antenna measurement setup	18		
Figure 3.9	1			
Figure 4.1				
Figure 4.2	Reflection coefficient simulation vs measurement	21		
Figure 4.3	Simulated efficiency vs gain	21		
Figure 4.4	Antenna placement near human model in CST (a) On the back of the model (b) On the chest of the model			
Figure 4.5	Simulated S ₁₁ near human body model on (a) Back (b) Chest with different distances	22		

Figure 5.1	Flexible antipodal Vivaldi Antenna (a) Front (b) Back side of fabricated antenna and the (c) Measurement set up			
Figure 5.2	Different bending angles of proposed antenna (a) 120° (b) 60° (c) 20° in vertical direction (d) 120° (e) 60° (f) 20° in horizontal direction			
Figure 5.3	Simulated reflection coefficient with its effect in different bending angles in Horizontal (H) and Vertical (V) directions			
Figure 5.4	Placement of antenna with different body parts (a) Chest (b) Back and (c) Arm (d) Gap between arm and antenna, x=0, indicates the antenna is very close to the arm			
Figure 6.1	Geometry of antipodal Vivaldi antenna (a) Front (b) Back (c) Side view	29		
Figure 6.2	Simulated S-parameter result of modified and conventional antipodal	29		
Figure 6.3	Simulated and measured reflection coefficient	30		
Figure 6.4	(a) Simulated efficiency and realized gain (b) Simulated vs measured efficiency and gain	30		
Figure 6.5				
Figure 6.6	Antenna measurement arrangement at bending radius (a) 30 mm (b) 50 mm and (c) 100 mm			
Figure 6.7	(a) Simulated reflection coefficient with different bending conditions vs reflection coefficient in flat condition (b) Simulated vs measured reflection coefficient in bending conditions	33		
Figure 6.8	Antenna simulated near human body model in computation software	33		
Figure 6.9	Simulated reflection coefficient for on-body condition	34		
Figure 6.10	Two-port antenna structures (a) Front (b) Rear view	35		
Figure 6.11	Two port simulated S-parameters (feeding in same vs opposite direction)	35		
Figure 6.12	Two-port simulated and measured S-parameters	36		
Figure 6.13	(a) Simulated two-port antipodal antenna efficiency and gain; simulated vs measure efficiency vs gain (b) Port 1 (c) Port 2			
Figure 6.14	Antenna in different bending situation with different radius of cylinder (a) 250 mm (b) 160 mm (c) 100 mm			
Figure 6.15	Antipodal Vivaldi dual port antenna measurement arrangement at bending radius (a) 50 mm (b) 100 mm			
Figure 6.16				
Figure 6.17	Simulated antenna near human body model in computation software	40		

Figure 6.18	(a) Simulated S-parameters for on-body vs free space (b) 4 Simulated vs measured s parameters			
Figure 7.1	(a) Simulated S-parameters for on-body vs free space (b) Simulated vs measured s parameters	43		
Figure 7.2	Simulated and measured reflection coefficient performance of circular patch antenna	44		
Figure 7.3	(a) Simulated efficiency and gain (b) Simulated vs measurement efficiency and gain			
Figure 7.4	Simulated bending setup for single port circular patch antenna	45		
Figure 7.5	Circular patch single port antenna measurement arrangement at bending radius (a) 30 mm (b) 50 mm (c) 100 mm	46		
Figure 7.6	(a) Simulated reflection coefficient with different bending conditions vs reflection coefficient in flat condition (b) simulated vs measured reflection coefficient in bending conditions	47		
Figure 7.7	Simulated antenna near human body model in computation software	47		
Figure 7.8	Simulated S-parameters for on-body condition	48		
Figure 7.9	Antenna designing steps from (a) Single antenna to (b) Two port two element/ radiator antenna to (c) Shared radiator two port antenna and afterward (d) Inserting slot in the radiator	49		
Figure 7.10	Simulated and fabricated finalized two-port circular patch antenna (a) Front view (b) Rear view			
Figure 7.11	Simulated antenna performance S ₁₁ , single antenna vs shared two-port antenna			
Figure 7.12	(a) S_{11} and S_{22} in two-port (before and after adding slot) (b) S_{21} and S_{12} in two-port antenna (before and after adding slot)			
Figure 7.13	S_{12}			
Figure 7.14	Simulated and measured S-parameters in two-port circular patch, S_{11} and S_{22}			
Figure 7.15	(a) Simulated efficiency and gain; simulated vs measured efficiency and gain (b) Port 1 (c) Port 2	52		
Figure 7.16	7.16 Antenna in different bending position with different cylinder radius for bending (a) 150 mm; (b) 100 mm (c) 50 mm			
Figure 7.17	Circular patch single port antenna measurement arrangement at bending radius (a) 50 mm (b) 100 mm	54		
Figure 7.18	(a) Simulated reflection coefficient with different bending conditions vs reflection coefficient in flat condition (b) Simulated vs measured reflection coefficient in bending conditions; simulated vs measured (c) Efficiency (d) Gain			
Figure 7.19	On-body analysis simulation set-up	56		
Figure 7.20	(a) Simulated on-body vs free space s-parameters (b) Simulated vs measured s parameters	56		

Figure 8.1	Flexible antipodal Vivaldi antenna (a) Front (b) Back side of fabricated antenna (c) Measurement set up	58	
Figure 8.2	Different bending angles of proposed antenna (a) 120° (b) 60° (c) 20° in vertical direction and (d) 120° (e) 60° (f) 20° in horizontal direction		
Figure 8.3	Simulated reflection coefficient with its effect in different bending angles in Horizontal (H) and Vertical (V) directions	58	
Figure 8.4	Placement of antenna with different body parts (a) Chest (b) Back and (c) Arm (d) Gap between arm and antenna, x=0, indicates the antenna is very close to the arm	59	
Figure 8.5	Simulated reflection coefficient on different places of body along with in free space	59	
Figure 9.1	(a) Geometry of Vivaldi antenna with all parameters, fabricated antenna (b) Front view (c) Rear view (d) Measurement setup	60	
Figure 9.2	(a) Simulated and measured reflection coefficient, simulated(b) Surface current density (c) Gain and efficiency (d) XZ-plane(c) XY-plane radiation pattern	62	

ACKNOWLEDGEMENT

The authors would like to acknowledge the support from University-Private Matching Fund (UniPRIMA) under grants number of 9001-0064/9002-00125 and 9001-00645/9002-00126 from Universiti Malaysia Perlis and Jabil Circuits Sdn.Bhd. We thank everyone who helped us, directly or indirectly, in completing our project. We are grateful to all those we had the pleasure of working with. Special thanks to our group members for their cooperation and teamwork from start to finish. Each person played an important role in making this project a success.

PREFACE

The continuous evolution of wireless technology has profoundly influenced the development of wearable devices, transforming how we interact with technology and monitor health in our daily lives. Among these advancements, Wireless Body Area Networks (WBANs) represent a significant leap forward, enabling seamless communication and data collection via wearable sensors and antennas. These technologies have the potential to revolutionize healthcare, sports, and communication by providing real-time monitoring and feedback while reducing the dependence on traditional medical infrastructure.

This report delves into the design and optimization of wearable antennas tailored for WBANs, focusing specifically on integrating 5G capabilities to enhance system performance. Through the collaborative efforts of researchers and industry professionals, this report examines innovative approaches to overcoming the challenges associated with wearable antenna design, including their proximity to the human body and mechanical deformations caused by movement. The findings and methodologies presented herein are intended to guide future research and contribute to the advancement of wearable technology, particularly in areas requiring high-performance wireless communication.

1. INTRODUCTION

Wearable technology has emerged as a cornerstone of modern innovation, merging electronic systems with clothing and accessories to provide continuous connectivity and functionality. Central to this revolution are Wireless Body Area Networks (WBANs), which employ wearable antennas to facilitate wireless communication between devices and sensors positioned on the human body. These networks are crucial for applications ranging from patient monitoring in healthcare to performance tracking in sports and fitness. By enabling real-time data collection and analysis, WBANs empower users and professionals to make informed decisions, enhancing outcomes in critical scenarios.

Despite their immense potential, wearable antennas face unique challenges due to their close proximity to the human body, which can degrade performance by detuning the antenna and reducing radiation efficiency. Furthermore, antennas must be lightweight, compact, and conformal to ensure user comfort while maintaining robust wireless communication. Recent advancements in materials, design, and fabrication techniques have begun addressing these issues, particularly in integrating 5G capabilities, which promise higher data rates, improved reliability, and enhanced capacity.

This report aims to explore the development of a novel stretchable 5G antenna array optimized for WBANs. It discusses the methodology for designing and fabricating these antennas, evaluates their performance under various conditions, and investigates their integration into wearable applications such as smart clothing. Additionally, the report examines the implications of multipath fading, Specific Absorption Rate (SAR) considerations, and the role of multiple-input multiple-output (MIMO) systems in overcoming communication challenges. By presenting comprehensive findings, this report seeks to contribute to the advancement of wearable technology and its integration with 5G networks for diverse applications.

2. DUAL BAND CIRCULAR PATCH FLEXIBLE WEARABLE ANTENNA DESIGN FOR SUB-6 GHZ 5G APPLICATIONS

Wearable computing devices which are integrated in wireless body area networks (WBAN) have seen enormous developments in recent years, specifically in the sports and medical fields. Wearable computing devices can be used in hospitals to monitor patients' health on a regular basis, allowing health professionals to make critical decisions in life-threatening situations [1]. Moreover, athletes can use this device to track and receive real-time feedback during their training, which eventually helps them to improve their own performances, besides being coached by trainers [2]. Wearable antenna plays a significant role in wearable computing devices to efficiently transmit and receive wireless signals [3]. Realizing this, tremendous research efforts have been channelled toward designing efficient wearable antennas to enhance the performance of wearable computing devices.

Wearable antennas can be classified into two categories: rigid antennas, which exhibit more stability in radiation pattern performance and flexible antennas, which offer advantages such as lightweight and convenient attachment, both are important for human comfort [4]. The fabric textile materials with low dielectric constant (ε_r) are the most commonly used substrates for flexible antenna designs due to their capability in achieving wideband and good radiation pattern characteristics. Besides this, other commonly used substrate materials for flexible antenna designs are wool felt [5]-[6], felt [7]-[8], and felt textile [9]. These materials, however, are thicker than fabric textiles, which increases manufacturing costs and reduces the comfort of the wearer. Therefore, flexible wearable antenna designs preferably embrace fabric textile materials as substrate due to their thinness and low dielectric constant value ($\varepsilon_r < 2$), in addition to their advantages and being comfortable to wear [10].

Polyester fabric is an excellent choice for flexible wearable antenna design since it is thin and has a lower dielectric value. The dielectric characteristics property of polyester fabric makes it preferable as it has improved dielectric characteristics in comparison with other available textile materials including linen, cotton, and silk [11]. Besides that, lower values of dielectric constants are preferred to achieve higher bandwidth since bandwidth is inversely proportional to permittivity or dielectric constant [12]. Nevertheless, attaching multiple layers of polyester fabrics makes the substrate thicker [11], and thus complicates the fabrication process [11]-[13].

The Third Generation Partnership Project (3GPP) recently has released various Fifth Generation New Radio (5G-NR) frequency bands in sub- 6 GHz region that can be utilized for 5G applications. Among these bands, 3.5 GHz becomes one of most important one as it is being widely utilized in 5G for various applications such as medical, sports, education etc. [14]. Furthermore, 3.5 GHz band has received the most attention in the World Radio Communication Conference (WRC) due to its widespread use in most of the countries across the world when compared to other 5G-NR sub – 6 GHz bands [15]. Considering all these requirements, a simple dual ring circular patch antenna placed on a single-layer polyester substrate is proposed in this paper.

The research work presented in this report advances the flexible wearable antenna design by utilizing thin substrate material with low dielectric value that potentially provides desired resonant band and good radiation pattern. In addition, besides being comfortable to wear, the thin and soft fabric material also reduces manufacturing costs.

2.1 Circular Patch Wearable Antenna Design and Specification

Figure 2.1 shows the modelled dual-ring circular patch antenna design. Dual ring structure creates inductive capacitive coupling in the radiator, which increases bandwidth coverage [16].

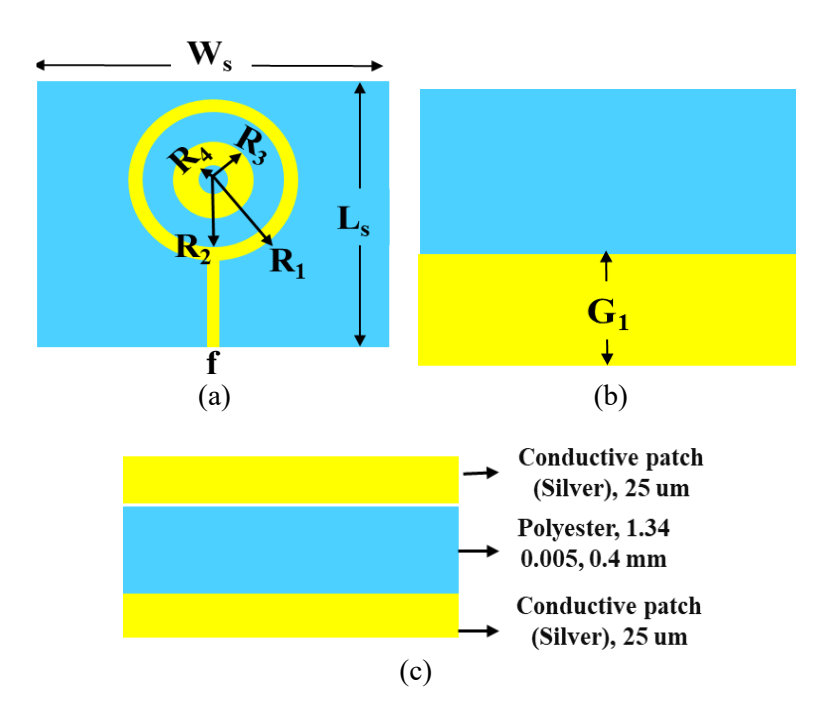


Figure 2.1. Configuration of the designed Circular Patch Wearable antenna (a) Top view (b) Rear view.

Table 2.1 The Dimension Details of the Circular Patch Wearable Antenna

Parameter	Description	Dimension (mm)
Ws	Width of Substrate	55
Ls	Length of Substrate	46
R1	Outer Radius of Circular Patch 17	
R2	Inner Radius of Circular Patch 15	
R3	Outer Radius of Inner Circle 5.5	
R4	Inner Radius of Inner Circle 2	
f	Width of Feedline 1.3	
G1	Ground Height 31	
	1	

This antenna was modelled and simulated in CST Microwave Studio software. Two circular ring patches (inner and outer) with a thickness of 3.5 and 2 mm respectively, are designed on top of a polyester fabric substrate (55 mm x 46 mm x 0.4 mm) as shown in Figure 2.1(a). The polyester substrate is with a relative dielectric constant (ϵ_r) of 1.40 and loss tangent ($\tan \delta$) of 0.005. Furthermore, a 50 Ω microstrip feedline is attached to the outer circular ring patch to feed RF power. A partial ground plane with the size of 55 mm x 31 mm is introduced on the bottom of the substrate to obtain wider bandwidth. The dimensions were initially chosen according to [16] and later optimized through iteration in CST Microwave Studio software. The dimensions of the proposed antenna are summarized in Table 2.1.

2.2 Results and Discussion

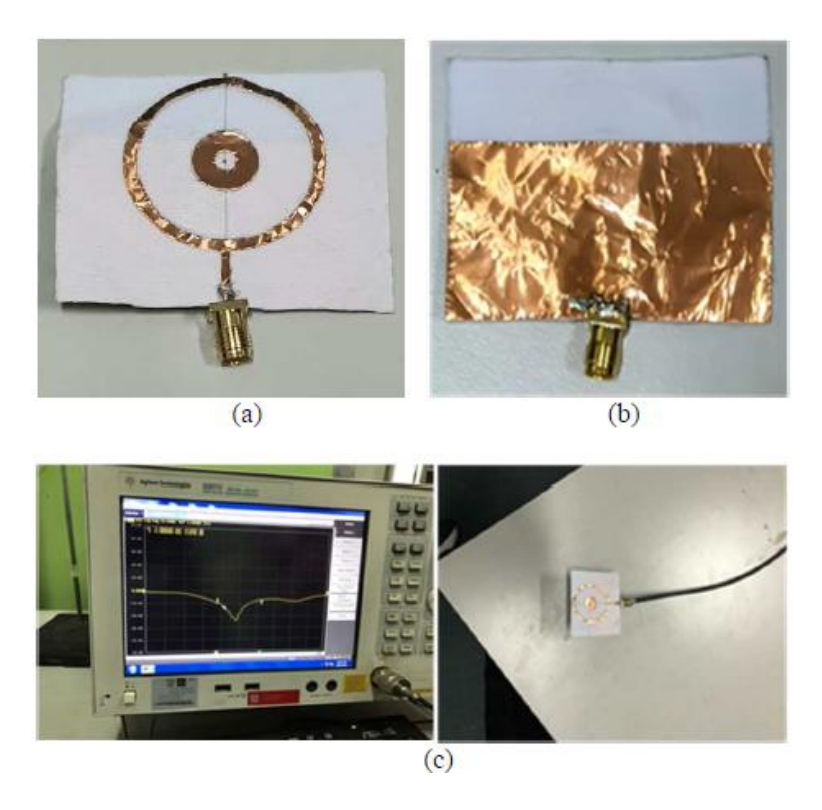


Figure 2.2. Configuration of the fabricated antenna (a) Front view (b) Rear view (c) Measurement setup.

The front and rear view of the fabricated prototype of the proposed antenna are shown in Figure 2.2 (a) and (b), respectively. The fabrication was performed in the laboratory. The patch and ground plane of the antenna were fabricated using copper tape with the thickness of 0.05 mm. A 50 Ω SMA connector is attached to the microstrip feedline using lead solder. Figure 2.2 (c) on the other hand, shows the setup during the s-parameter measurement using vector network analyser (VNA; model: E5071C) in the laboratory. The simulated and measured results (reflection coefficient) will be discussed in the following subsections.

2.2.1 Reflection Coefficient

Figure 2.3 presents the simulated and measured reflection coefficient results of dual ring circular patch antenna. From the figure, it can be observed that the measured result is comparable to the simulation. In the simulation, the dual ring circular patch antenna successfully achieved resonances at 3.63 and 4.95 GHz with at least S11 < -10 dB. This translates to dual -10 dB bandwidths of 300 MHz (from 3.50 to 3.80 GHz) and 160 MHz (from 4.86 to 5.02 GHz), covering sub-6 GHz 5G-NR bands such as n48, n77, n78, and n79. In measurement on the other hand, antenna resonates from 3.50 GHz to 4.16 GHz which implies the antenna covered the same sub-6 GHz 5G-NR bands as the simulation result except n79 due to fabrication tolerance.

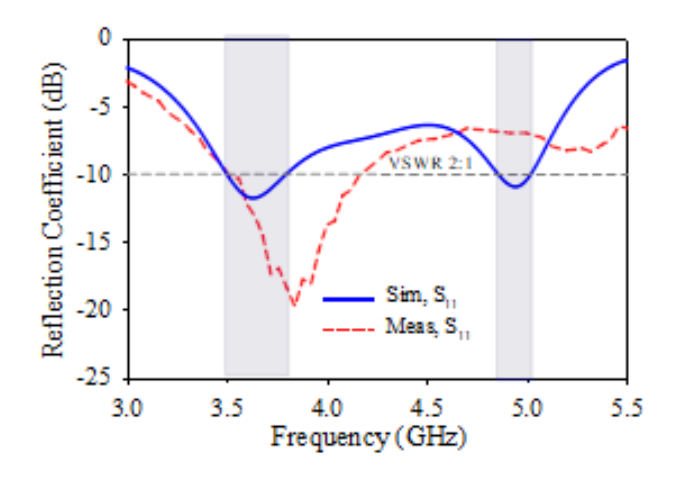
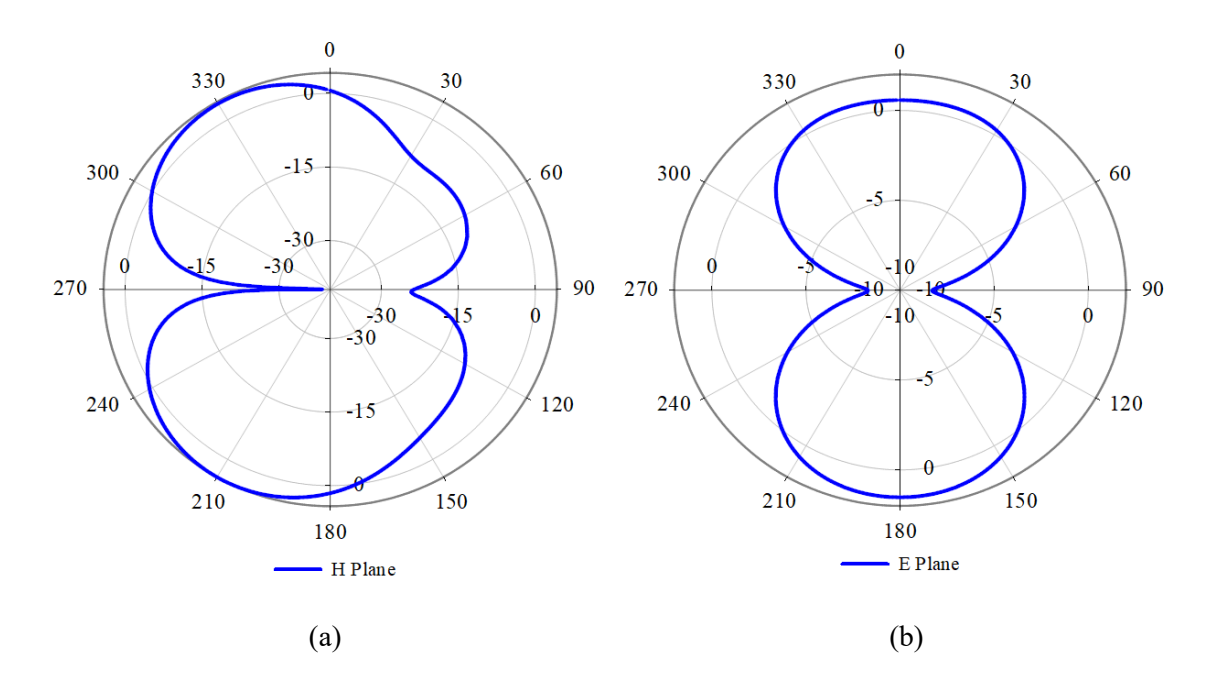


Figure 2.3. Simulated and measured reflection coefficient.

2.2.2 Radiation Pattern

The proposed antenna's simulated radiation patterns observed at 3.63 GHz are illustrated in Figure 2.4 (a) and (b), respectively in E-plane and H-plane and at 4.95 GHz in Figure 2.2.4(c) and (d), respectively in E-plane and H-plane. It can be noticed that the proposed antenna has a dipole-shaped radiation pattern at resonant frequency due to the dual circular ring patch design with a partial ground plane.



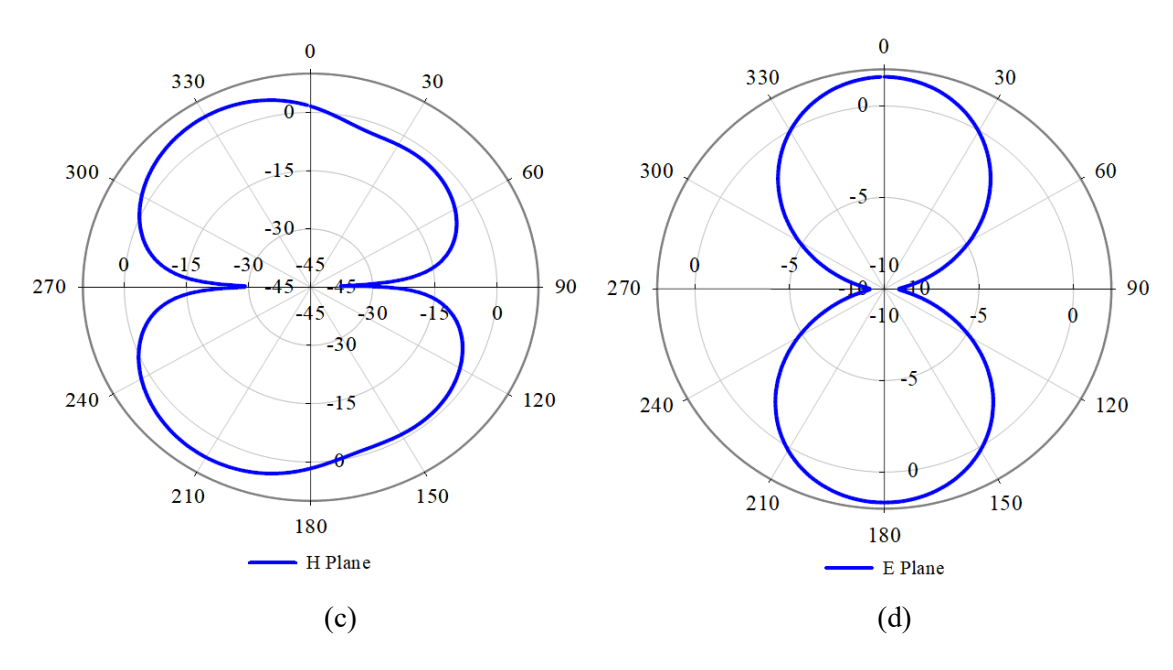


Figure 2.4. Simulated radiation pattern at 3.63 (a) H-Plane (b) E-Plane and at 4.95 (c) H-plane (d) E-Plane.

2.2.3 Surface Current Distribution

The current distribution of the antenna illustrated in Figure 2.5 (a) and (b) indicates the efficiency of the patch in radiating the RF current. Moreover, it can be noticed that along with the radiating patch, the current distribution on inner circle patch indicates its significant role in achieving dual resonances.

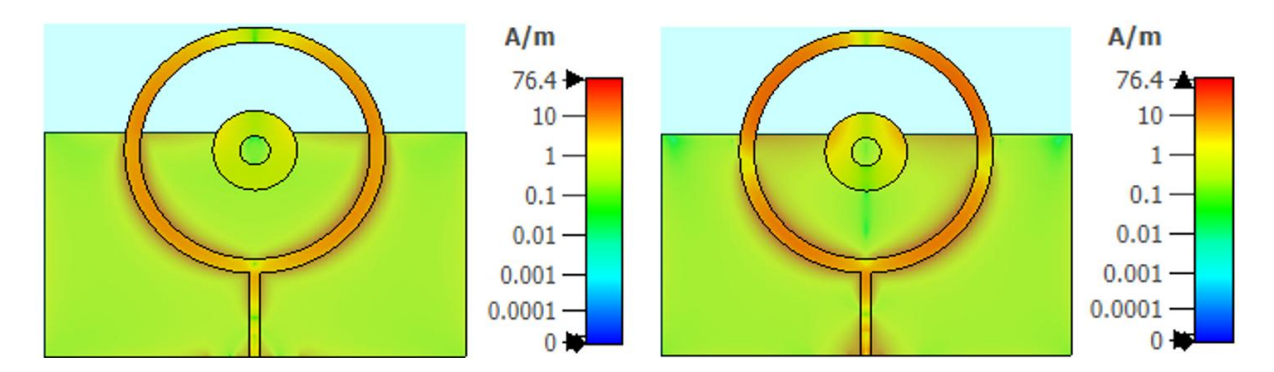


Figure 2.5. Current distribution of the antenna at (a) 3.63 and (b) Hz.

2.2.4 Gain and Efficiency

The simulated realized gain and simulated total efficiency of the proposed antenna are illustrated in Figure 2.6 The proposed antenna achieved a realized gain of 4.2 and 5.78 dBi at 3.63 and 4.95 GHz respectively, with a total efficiency of 90.5% and 82.3%.

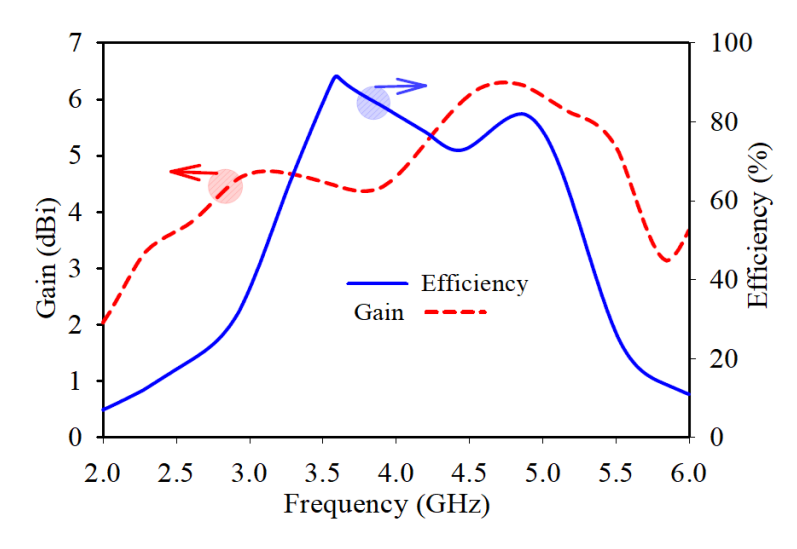


Figure 2.6. Gain and efficiency vs frequency.

2.2.5 On-Body Performance Analysis

A realistic homogeneous human body model from CST Microwave Studio was employed to assess the impact of the human body on antenna performance, as it closely replicates the characteristics of a real human body. The antenna was placed at two specific locations on the model, on the chest and back (illustrated in Figure 2.7 and Figure 2.8) to examine its resonance since high permittivity of the human body results in a shift in the antenna's resonance.

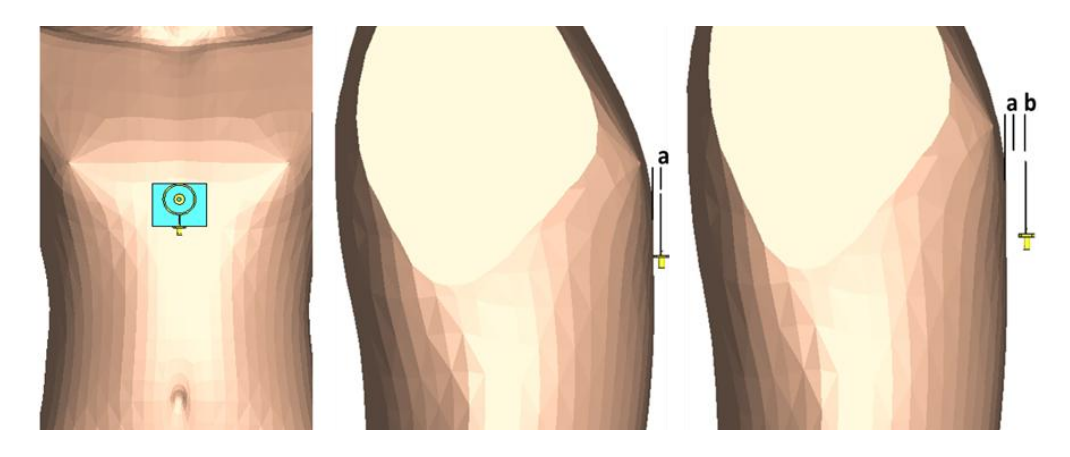


Figure 2.7. Antenna near human body model (on chest).

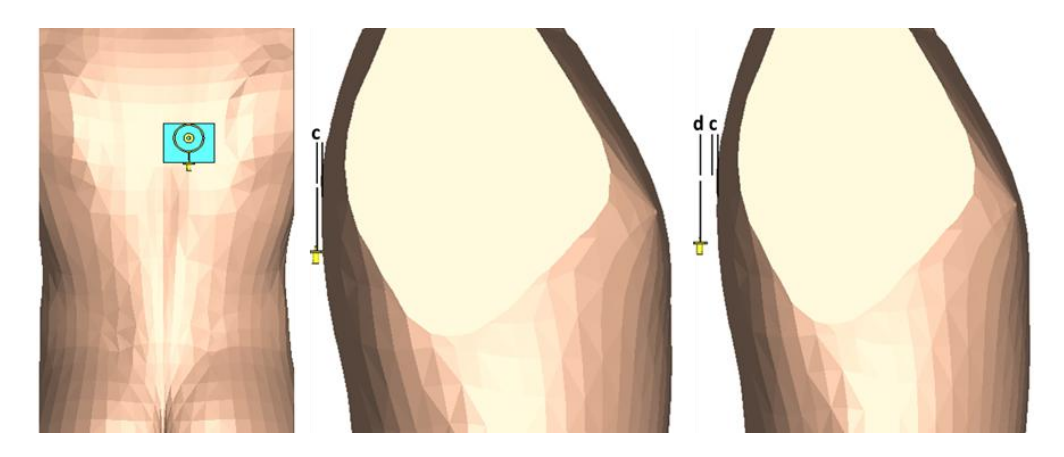


Figure 2.8. Antenna near human body model (on back).

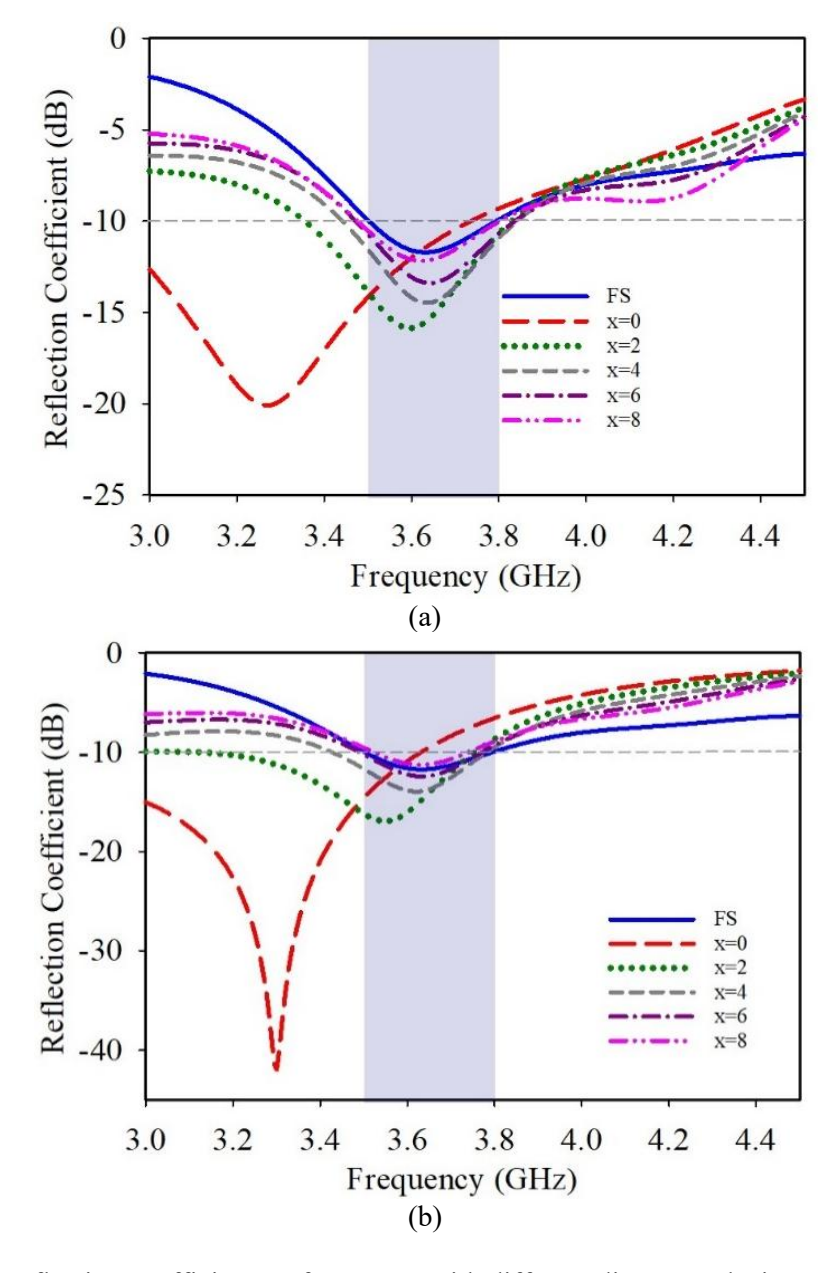


Figure 2.9. Reflection coefficient performances with different distances placing on the (a) Chest (b) Back of the human model.

When the antenna is placed on the chest, its performance closely aligns with free space antenna performances, apart from the initial position. The initial position, labelled as x=0, represents the closest proximity of 5.45 mm to the human body model. To ensure the antenna's proper functionality, a minimum distance of x=2, corresponding to 7.54 mm, must be maintained as the threshold distance. Similarly, when the antenna is placed on the back of the human model, its performance closely resembles that observed on the chest and in free space, apart from the initial position. The initial position, labeled as x=0, represents the closest proximity of 3.02 mm to the human body model. To maintain the antenna's functionality, a minimum distance of x=2, corresponding to 5.02 mm, must be observed as the threshold distance.

2.2.6 Bending Performance Analysis

For the bending simulation, a vacuum cylinder was employed as the supporting structure. Vacuum was chosen as the cylinder material to ensure that the cylinder itself does not influence the antenna's performance, allowing the analysis to focus solely on the effects of bending. The degree of antenna bending is determined by the radius of the cylinder: a larger radius corresponds to a less curved structure, while a smaller radius results in a more pronounced bending of the antenna. Figure 2.10 (a) illustrates the reflection coefficient of the antenna under various bending conditions. The analysis reveals a shift in the resonance frequency toward lower values, attributed to impedance changes induced by bending. Despite this frequency shift, the antenna demonstrates satisfactory resonance bandwidth across most bending scenarios. However, in cases of strong deformation, such as when the bending radius is reduced to R=30mm, resonance performance of the antenna degrades significantly. Based on these observations, the threshold bending radius for maintaining acceptable performance can be identified as R=40mm, below which the antenna's operational reliability is compromised. In addition to the reflection coefficient, other key performance parameters, such as antenna gain and efficiency, were thoroughly examined under various bending conditions. The results indicate that the antenna maintains a satisfactory efficiency, exceeding 60 percent, across the entire operational bandwidth for all bending scenarios. A noticeable shift in peak efficiency, consistent with the behaviour of S₁₁ under bending conditions, was observed, reflecting the impact of structural deformation on performance. Similarly, the antenna demonstrates robust gain performance, consistently achieving values above 4 dBi throughout the bandwidth, confirming its suitability for wearable applications even under deformation.

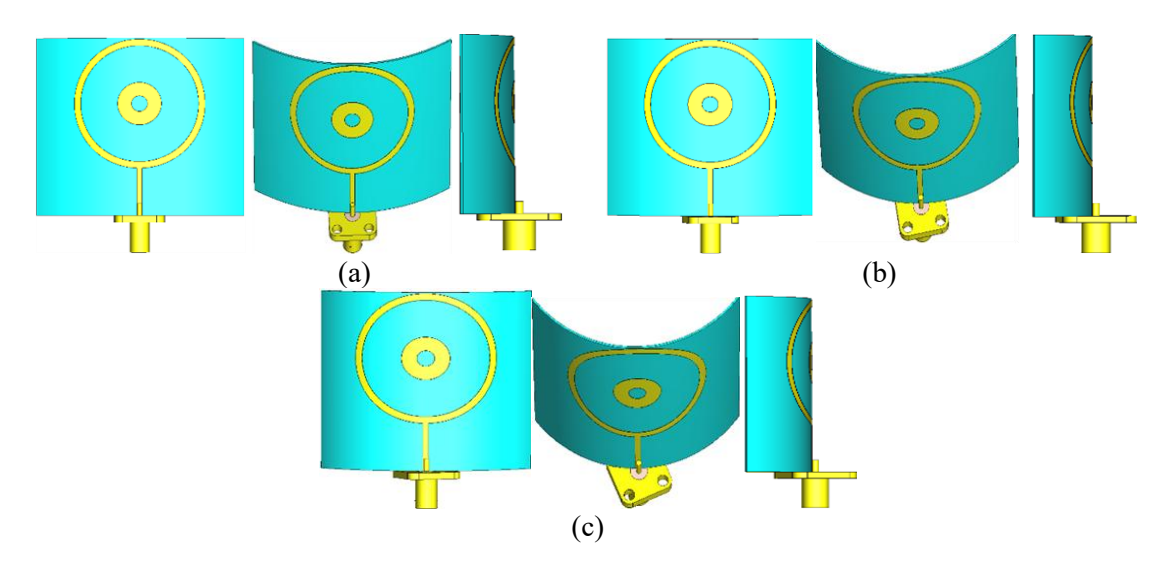


Figure 2.10. Antenna bending with radius of (a) 50 mm (b) 40 mm (c) 30 mm.

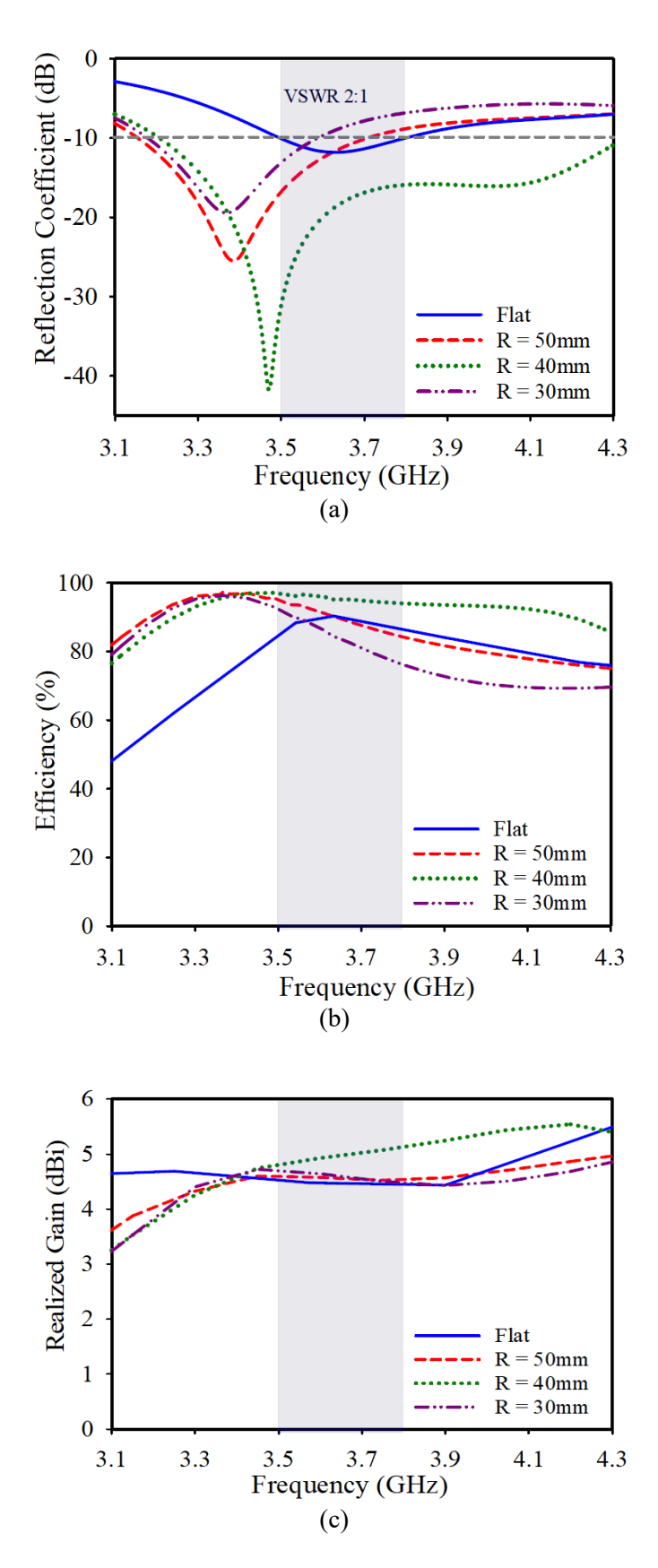


Figure 2.11. Antenna performances under bending conditions (a) Reflection coefficient (b) Efficiency (c) gain.

DESIGN AND DEVELOPMENT OF SMALL AND LARGE FORM FACTOR ON BODY ANTENNAS FOR SUB-6 GHZ ${\bf 5G}$ APPLICATIONS

Table 2.2 The Comparison Results with Previous Studies

Ref.	Frequency (GHz)	Size (mm3)	Material	Gain (dBi)	Efficiency (%)	Bandwidth (MHz)
[5]	5.0	42 x 28 x 4	Wool Felt; Nylon Conductive Textile	6.70 (maximum); 5.67 (average)	77 (average)	940
[6]	2.45	40 x 32 x 2	Wool Felt; Nylon Conductive Textile	7.3 (maximum)	More than 70	380
[8]	2.45 and 3.45	60 x 60 x 3	Felt, Taconic TLY-5; Shieldit TM	Free Space: 6.6-6.8 and 8.9-9.0 On Body: 4.9-5.1 and 8.5-8.6	91 and 94 respectively	120 and 230
[17]	2.4 and 5.8	15 x 40 x 0.8	FR4: Nylon Conductive Textile	1.1-1.5 and 3.8-4.2	65-76 and 88	100 and 150
Proposed	3.5 and 4.95	55 x 46 x 0.4	Polyester; Copper	4.2 and 5.78	90.5 and 82.3	300 and 160

In this research study, a dual circular ring patch antenna is designed on a flexible material for sub-6 GHz 5G applications. The proposed antenna is made using a thin polyester fabric substrate and copper tape. The simulation exhibited a dual band characteristic centred at 3.63 GHz (covering the sub-6 GHz 5G-NR bands n48, n77, n78) and 4.95 GHz (covering the sub-6 GHz 5G-NR band n79) with a dipole-like radiation pattern. Additionally, the antenna provided a comparable reflection coefficient performance in measurement covering the sub-6 GHz 5G-NR bands (n48, n77, n78). Nevertheless, the second band at 4.95 GHz (n79) couldn't be achieved due to the fabrication tolerance. It featured a satisfactory simulated realized gain of 4.2 and 5.78 dBi indicating suitability for 5G sub- 6 GHz wearable antenna applications. This antenna will be utilized for further analysis, which includes the study of on-body placement and SAR calculation. The comparison results with previous studies can be found in Table 2.2.

3. FABRICATION OF A WEARABLE ANTENNA WITH DEFECTED GROUND STRUCTURE ON A FLEXIBLE TPU-POLYESTER SUBSTRATE

During the past decade, wearable devices have been known to be useful in multiple applications, including medical military, and emergency rescue systems. Wearable electronics that could be flexed, reconfigured, and bent will extend the capabilities of conventional mobile devices [18]. In wearable devices, high-speed data communication is preferred, and their wireless modules are usually integrated with other devices, such as sensors, batteries, and antennas. Wearable antenna is an important component of wearable devices as they are critical in ensuring the overall efficiency of the devices [19].

While developing wearable antennas for use as part of the clothes, they should be unobtrusive, adaptable, and capable of working close to the human body with limited degradation [20-21]. Wearable antennas are often challenging to develop due to the influence of the users' body. The efficiency loss caused by structural deformation is another issue which needs to be addressed throughout the design process [22-23].

This research aims to design a wearable antenna with defected ground structure operating at a 2.45 GHz using a customized substrate combining two different dielectric materials, thermoplastic polyurethane (TPU) and polyester fabric. Simulations is performed using CST Microwave Studio software whereas fabrication is performed using the in-house screen-printing process developed by Jabil. Based on the results of the simulation process, the antenna with the defected ground structure shows better performance compared to the one without DGS.

3.1 DGS Wearable Antenna Design

The two designs fabricated in this work are as follows. The first is a rectangular patch antenna as shown in Figure 3.1, whereas the second is a rectangular patch antenna with DGS (Defected Ground Structure) as shown in Figure 3.2. Both antennas are fed by a $50-\Omega$ inset feed. The antenna consists of a substrate with a layer of TPU integrated on polyester fabric. The overall substrate is 0.3 mm in height, with a relative permittivity (ε_r) of 2.1 and a loss tangent ($tan\delta$) of 0.009. The conductive sections (patch and ground) are fabricated using silver ink with a height (h) of 0.1 mm. Table 3.1 summarizes the antenna design specifications.

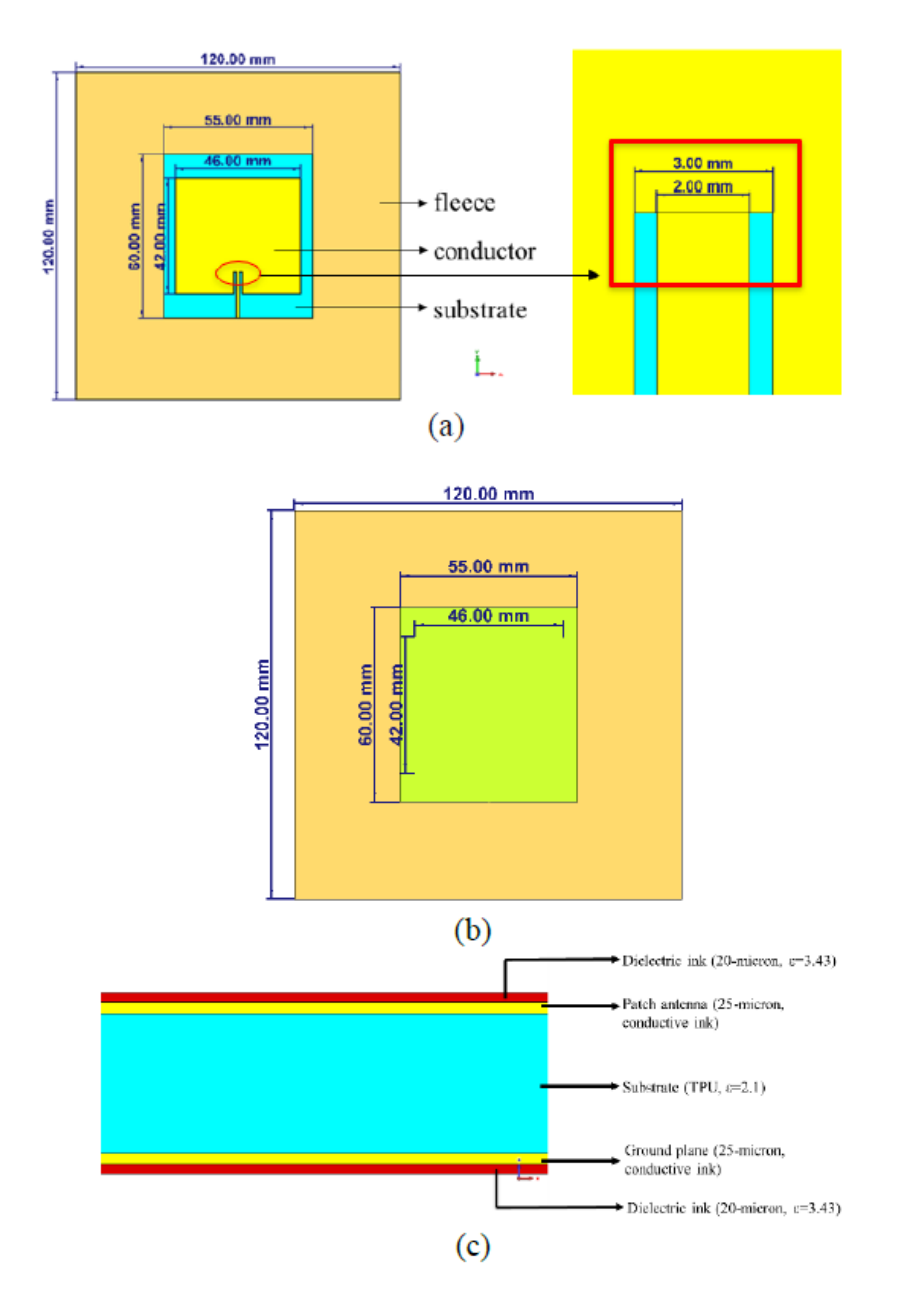


Figure 3.1. DGS wearable antenna dimensions without DGS (a) Front view (b) Back view (c) Cross section.

Table 3.1 DGS Wearable Antenna Design Specifications

Center Frequency	2.45 GHz
Substrate	Thermoplastic polyurethane (TPU) on polyester fabric
Height of substrate	0.3 mm
Dielectric Constant, εr	2.1
Loss Tangent	0.009
Conductive Material	Silver ink
Height of Conductor, h	0.020 mm

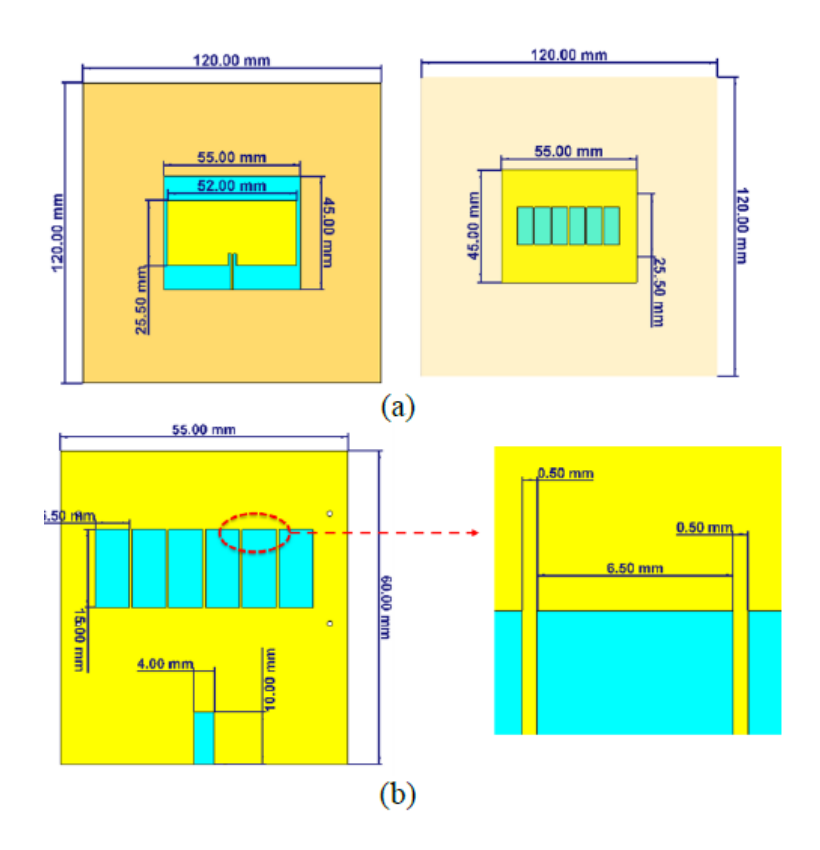


Figure 3.2. Antenna dimensions with DGS (a) Front view (b) Back view.

3.2 DGS Wearable Antenna Fabrication

The fabrication process of both antennas is performed using the screen-printing technique. The antenna is screen printed on the TPU substrate as shown in Figure 3.3 Silver ink is used as the conductive sections to form the patch and ground plane. Dielectric ink is used as an overcoat layer to prevent oxidation of the silver conductive patch antenna layer over time, which may reduce the antenna efficiency. For silver conductive ground layer and silver conductive patch antenna layer, the 25 μ m-thick silver ink was printed using a 230 thread/inch meshes with a 20 μ m emulsion thickness and 25N tension of polyester screen mesh. On the other hand, the 25 μ m emulsion thickness and 25N tension of polyester screen mesh. All the printing process was printed using an automatic Micro-tec (MTP-1000) printer machine and cured in a force convection oven (binder drying and heating chamber) at MTI Lab, Jabil Circuits, Penang. The screen-printing parameters are summarized in Table 3.2 The screen-printed antenna in Figure 3.4 was then laminated onto a 100% polyester textile using a heat press laminator machine (Hotronix). The 50 Ω PCB-mount SMA connector was attached to the antenna using screws, with its pin connected with the feedline. The fabricated prototypes are shown in Figure 3.5.

DESIGN AND DEVELOPMENT OF SMALL AND LARGE FORM FACTOR ON BODY ANTENNAS FOR SUB-6 GHZ $5\mathrm{G}$ APPLICATIONS

Table 3.2 DGS Wearable Antenna Screen Printing Parameter

Parameter	Value
Printing mode	Double-pass (flood and print)
Printing speed (mm/s)	100
Flooding speed (mm/s)	50
Squeegee pressure (Mpa)	0.250
Counter pressure (MPa)	0.130
Squeegee angle ()	70
Snap-off distance (mm)	5
Peel-off speed (mm/s)	10

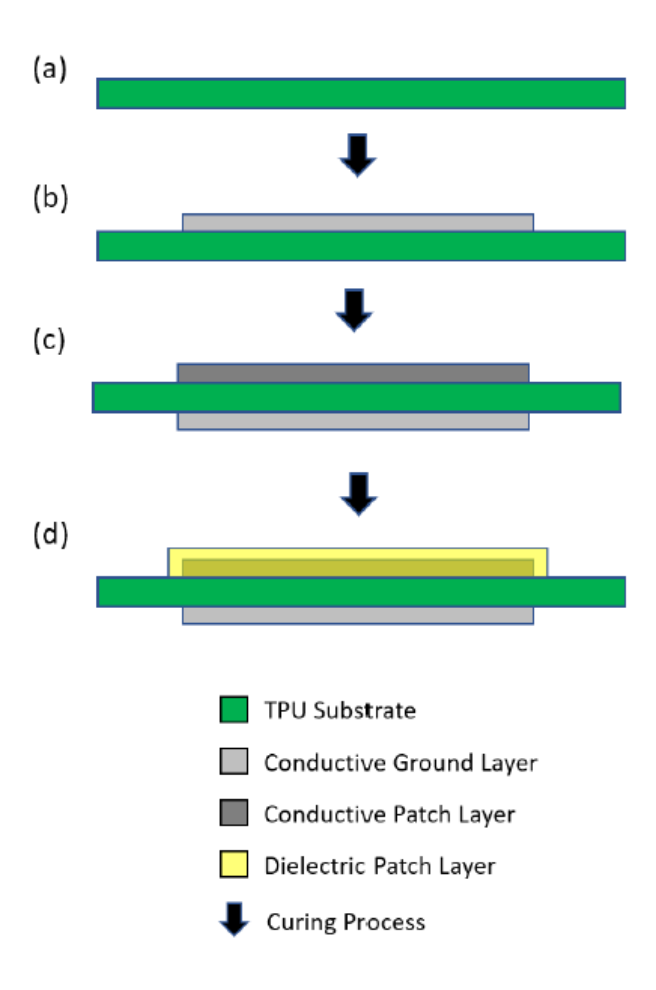


Figure 3.3. Layer stack-up of the screen-printed antenna on TPU a) TPU Substrate b) Conductive Ground Layer screen printing c) Flip the substrate and screen print the Conductive Patch Layer d) Dielectric Patch Layer Screen Printing.

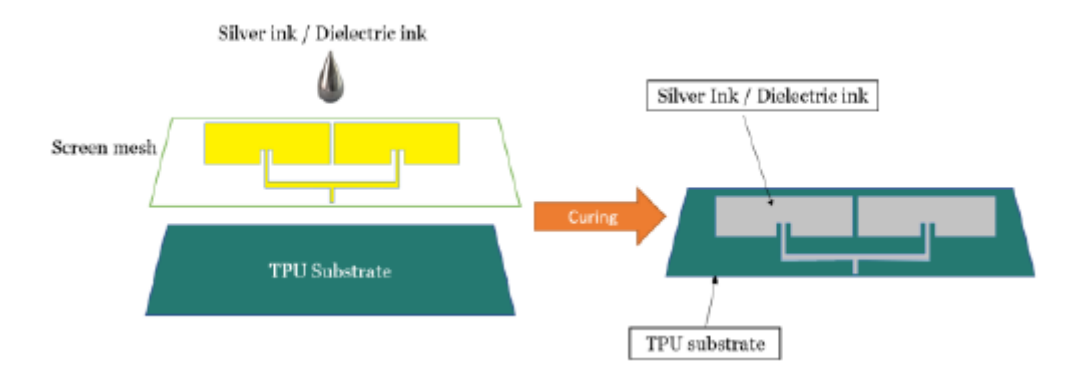


Figure 3.4. Screen printing process.

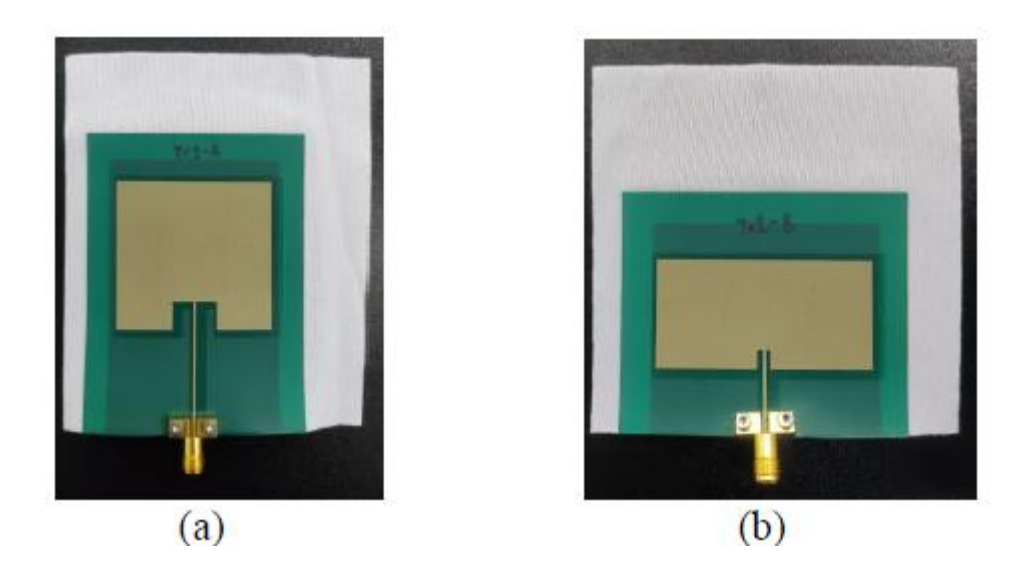


Figure 3.5. Fabricated antennas (a) Without DGS (b) With DGS.

3.3 DGS Wearable Antenna Performance Analysis

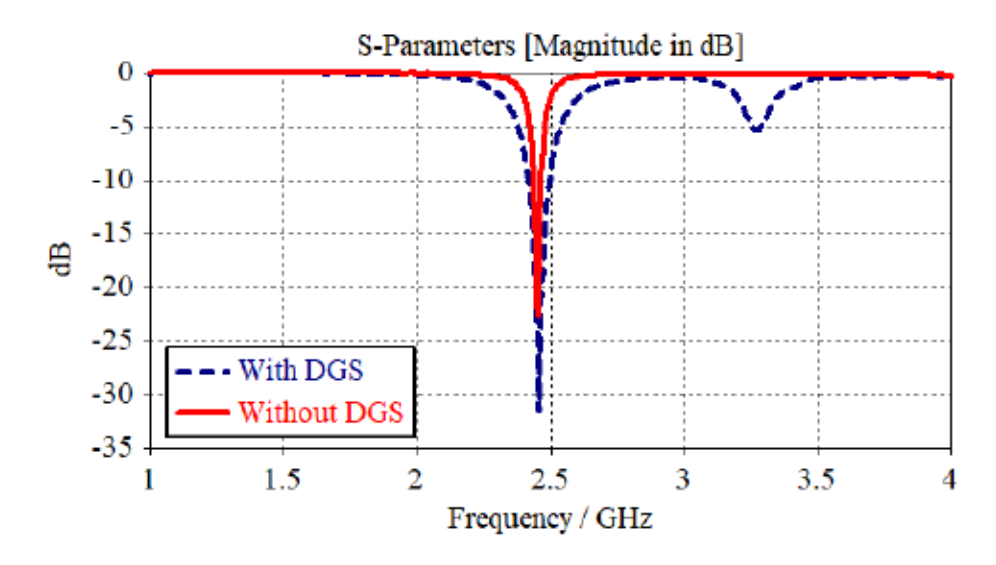


Figure 3.6. Comparison of S_{11} of the antenna with and without DGS.

DESIGN AND DEVELOPMENT OF SMALL AND LARGE FORM FACTOR ON BODY ANTENNAS FOR SUB-6 GHZ 5G APPLICATIONS

This section shows the simulation results of the two antennas. Simulation results indicated that both the antenna with and without DGS operated with at least -10 dB of reflection coefficient (S11), as illustrated in Figure 3.6 and summarized in Table 3.3. On the other hand, the 3D antenna radiation patterns for both designs are shown in Figure 3.7. Based on the comparison in Table 3.3, the patch antenna with DGS showed better performance.

	With DGS	Without DGS
Reflection Coefficient, S11 (dB)	-31.6	-22.2
Bandwidth MHz	79.3	28.4
Efficiency, %	30%	74 %
Gain (dBi)	2.01	3.62

Table 3.3 Performance Comparison of the Proposed Antenna, DGS Wearable Antenna

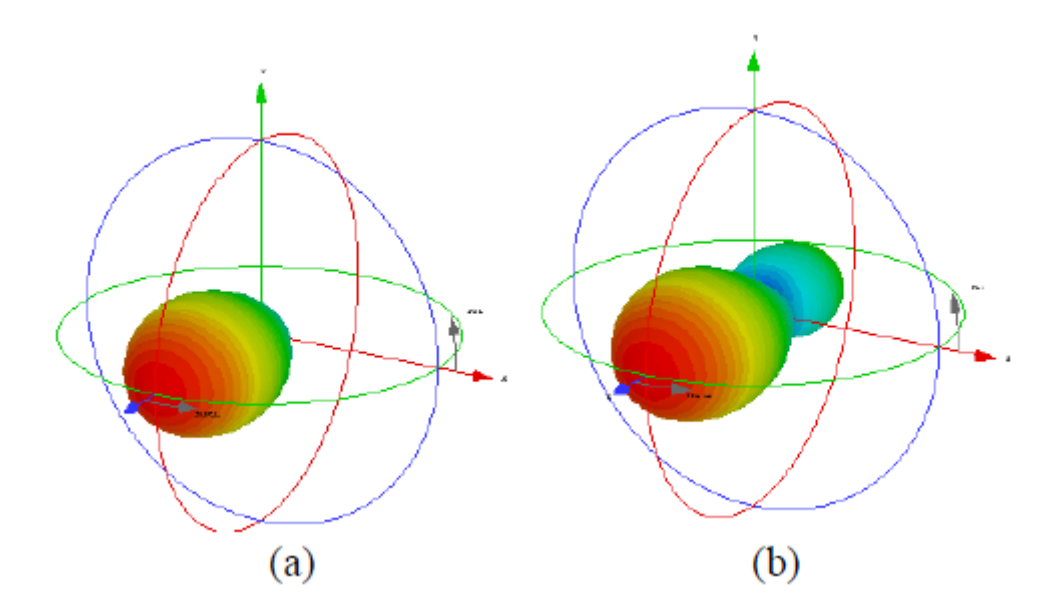


Figure 3.7. 3D antenna radiation pattern for single element patch antenna (a) Without DGS (b) With DGS

Efficiency and directivity results of both designs area also tabulated in Table 3.3. Based on the results, a single element patch antenna with DGS shows a better efficiency and performance compared to the one without DGS.

The fabricated antenna prototypes are then experimentally evaluated, as shown in Figure 3.8. Measurements were performed in ACE CoE lab, Universiti Malaysia Perlis. Based on the results shows in Figure 3.9, the measurement result for the antenna without DGS is shifted to higher frequencies. This is potentially due to fabrication. Since the feedline is too narrow, the alignment of the feedline with the port is shifted and missed the feedline. This can be seen in Figure 3.9 (a) where the frequency is way shifted from the simulation. On the other hand, it is evident that the reflection coefficient for the antenna with DGS agreed with simulations, despite being broader in bandwidth. This is potentially caused by increment of the thickness and gap of the substrate during the fabrication.



Figure 3.8. DGS antenna measurement setup.

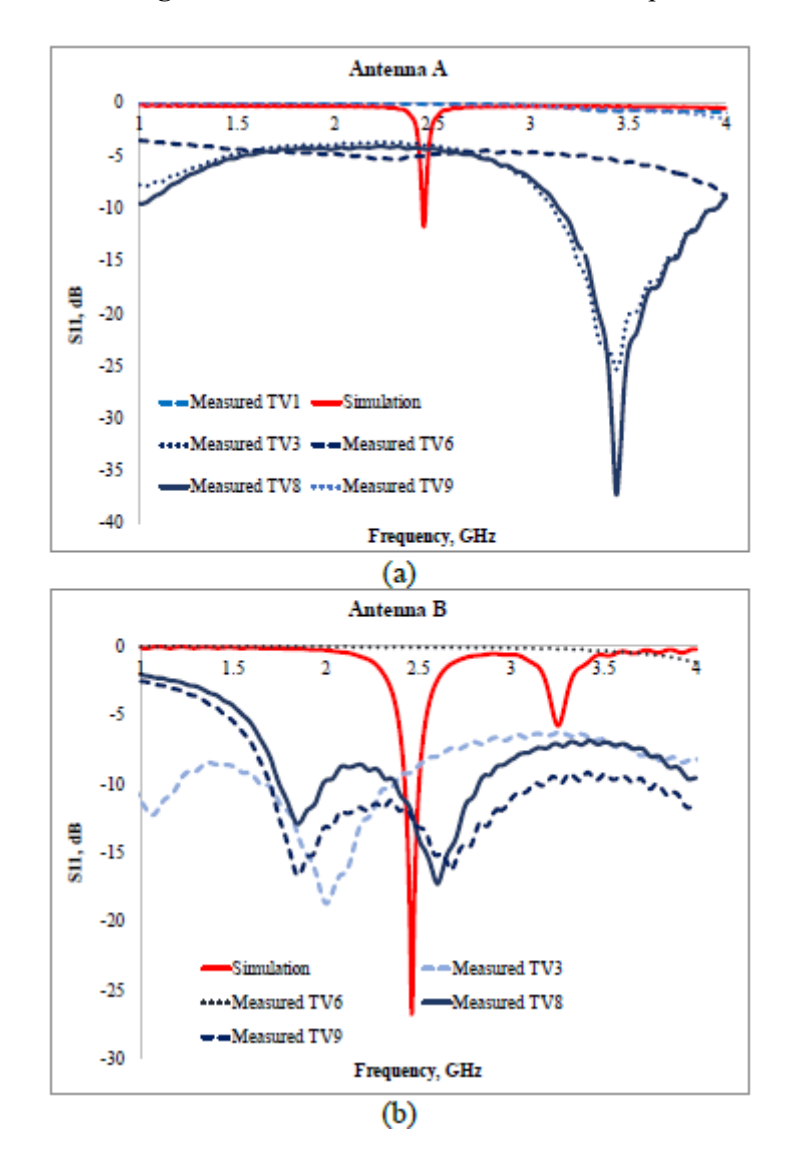


Figure 3.9. Comparison of the simulated and measured S₁₁ (a) Without DGS (b) With DGS.

DESIGN AND DEVELOPMENT OF SMALL AND LARGE FORM FACTOR ON BODY ANTENNAS FOR SUB-6 GHZ ${\bf 5G}$ APPLICATIONS

This research presented the design and fabrication process of two wearable antennas on a customized flexible TPU polyester substrate, with and without DGS. Both antennas operate at 2.45 GHz and are operating with at least -10 dB of reflection coefficients. However, performance of the antennas compared in terms of bandwidth, radiation patterns, and gain indicated that the antenna with DGS showed better performance. Bandwidth for the antenna with DGS is improved from 28.4 MHz (without DGS) to 79.3 MHz. Besides that, its gain is also improved from 2.01 dBi (without DGS) to 3.62 dBi and efficiency from 30% (without DGS) to 74%.

4. ON-BODY PERFORMANCE ANALYSIS OF WEARABLE ANTIPODAL VIVALDI ANTENNA FOR 5G APPLICATIONS

Body Area Networks (BANs) are extensively employed in diverse fields such as health and sports monitoring, emergency response, and navigation [24]. In BAN communication systems wearable devices depend significantly on wearable antennas for effective wireless signal transmission and reception [25]. Besides, The latest cellular technology, 5G, brings improvements such as higher data rates, increased user capacity, larger bandwidth, enhanced security, better resolution, and energy efficiency [26]. To accommodate multiple 5G applications, a wideband antenna capable of resonance bandwidth covering the sub-6 GHz 5G frequencies is necessary; the Vivaldi structure is selected due to its high bandwidth, low cost, lightweight, and ease of feeding. For wearable applications, a combination of polyimide and polyester substrates is proposed to provide a stable, durable, and flexible antenna design.

A bandwidth from 3.4 GHz to 4.2 GHz is covered by the antenna in both simulation and measurement (showed in Figure 4.2). So, the measured reflection coefficient performance is compatible with the simulation performance. Although in the measurement the resonating frequency got slightly shifted due to the screen-printing technique fabrication procedure. In the screen-printing procedure, the layers got diffused with one another which led to this shifting. The simulated realized gain and simulated total efficiency of the proposed antenna are illustrated in Figure 4.3 and both gain and efficiency were satisfactory throughout the entire bandwidth.

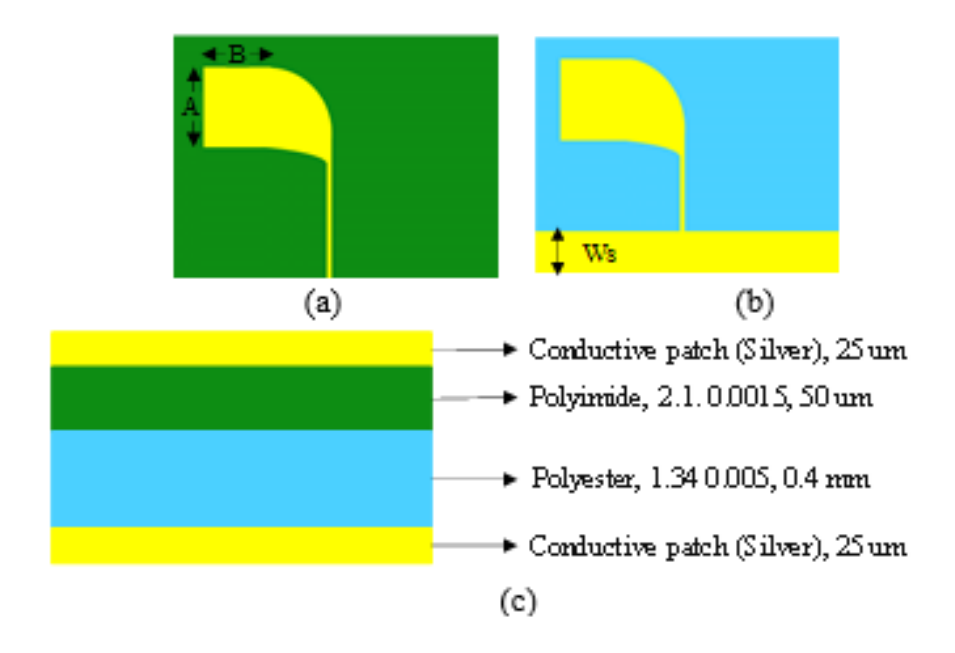


Figure 4.1. Geometry of antipodal Vivaldi antenna (a) Front (b) Back (c) Side view.

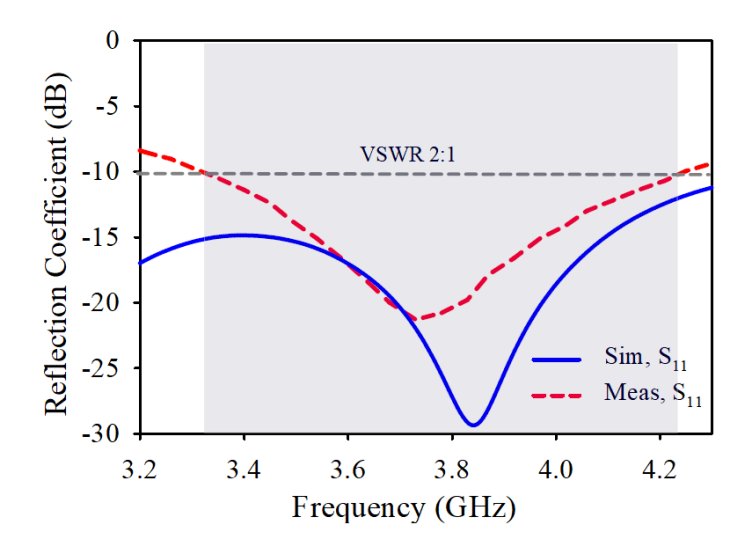


Figure 4.2. Reflection coefficient simulation vs measurement.

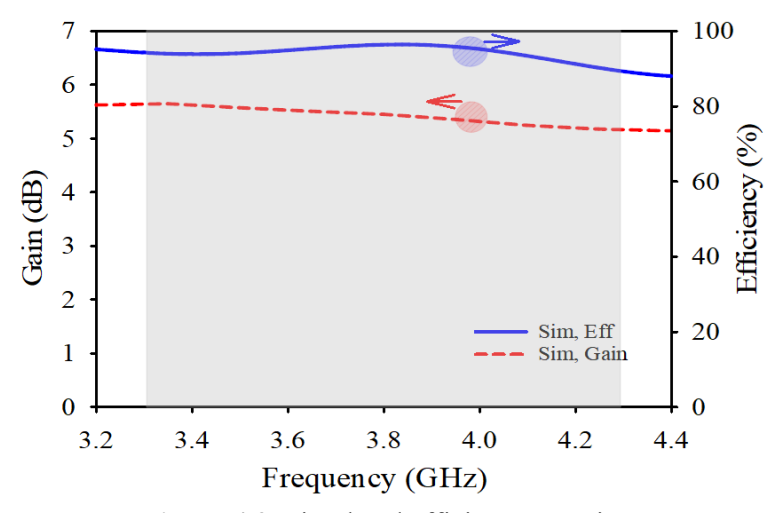


Figure 4.3. Simulated efficiency vs gain.

Since the antenna is wearable, antenna performance near human body must be investigated. The presence of the human body significantly influences antenna performance, which often leads to performance degradation due to its characteristics as a lossy medium [28]. Along with that, since electromagnetic radiation can be harmful to the human body the SAR (Specific absorption rate) is required to adhere to restrictions settled by the American and EU standards i.e. lower than 1.6 W/kg and 2 W/kg, respectively. [29].

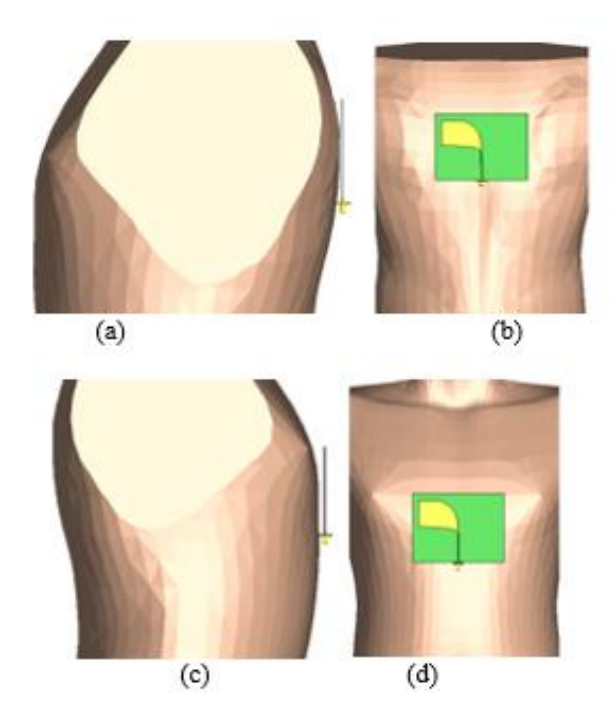


Figure 4.4. Antenna placement near human model in CST (a) On the back of the model (b) On the chest of the model.

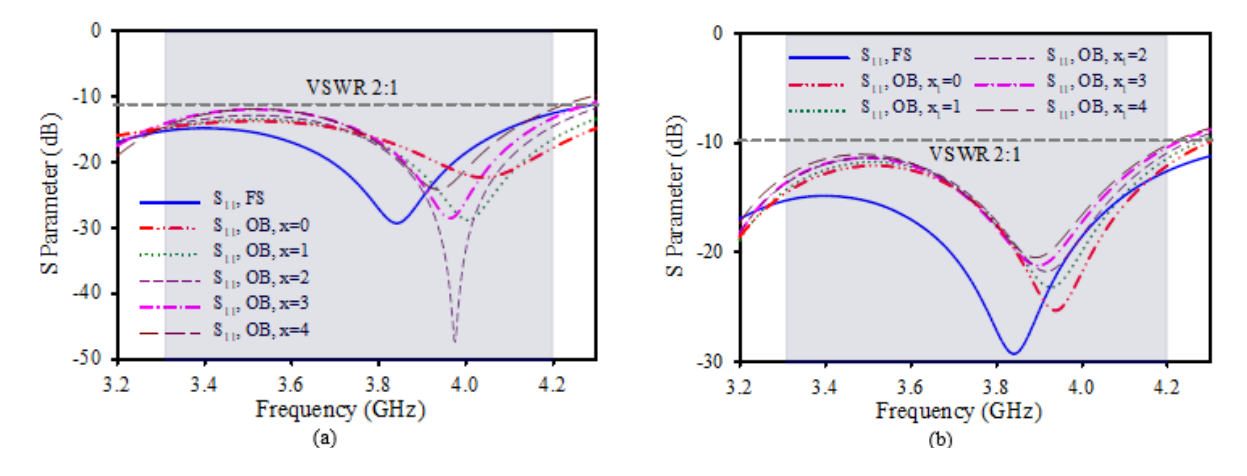


Figure 4.5. Simulated S₁₁ near human body model on (a) Back (b) Chest with different distances.

A realistic homogeneous human body model from CST Microwave Studio has been utilized to analyze the impact of the human body on antenna performance since the model contains characteristics similar to the real human body. The antenna is placed at two distinct locations on the human model, specifically on the chest and back (as shown in Figure 4.4), to study its resonance. The antenna is positioned at the nearest possible distance, considering the constraints of the SMA and antenna structure. Additionally, antenna performance at farther distances from body model has been studied. The high permittivity of the human body causes a shift in the antenna's resonance.

Figure 4.5 presents the simulated S₁₁ values comparing free space (FS) with on-body (OB) conditions. The antenna is positioned on both the chest and back because its size is too large for placement on areas like the shoulder or leg. Additionally, the human body's shape is curved and varies at different positions. Consequently, considering the contours of the chest and back,

DESIGN AND DEVELOPMENT OF SMALL AND LARGE FORM FACTOR ON BODY ANTENNAS FOR SUB-6 GHZ ${\bf 5G}$ APPLICATIONS

the antenna is placed as close as possible to the body (1.6 mm and 5.8 mm for the back and chest, respectively), with the nearest distance being defined as position 0. The distance between the antenna and the human model is then incrementally increased by 1 mm. The antenna positions are designated as x (back) and x1 (front), and this distance is increased up to 4. Figure 4.1.1 shows that when the antenna is placed on the body, its resonance shifts towards a higher frequency. Despite this shift, the antenna maintains a similar resonance bandwidth (from 3.3 GHz to 4.2 GHz) across both placement locations and all measured distances. Another critical parameter to consider is the Specific Absorption Rate (SAR), which is essential for ensuring the safety of the wearer. SAR values have been determined across the entire bandwidth for both positions (chest and back, nearest to the body), and the results are presented in Table 4.1.

Table 4.1 SAR Performance of Wearable Antipodal Vivaldi

Frequency (GHz)	SAR(W/Kg) (Back)	Frequency (GHz)	SAR(W/Kg) (Chest)
3.3	1.68	3.3	0.98
3.5	1.79	3.5	0.84
3.7	1.89	3.7	0.92
3.9	1.95	3.9	1.00
4.1	1.93	4.1	1.046

Additionally, for the SAR analysis, the input power was initially set to 100 mW, as suggested by the literature. However, for the back position, the SAR exceeded regulatory limits. Consequently, the threshold power for this position was determined to be 85 mW, at which all SAR values were found to be below 2 W/kg.

In this research, a brief on-body analysis was conducted on a wearable antipodal Vivaldi antenna proposed for 5G Sub-6 GHz applications. The antenna resonated efficiently near the human model in simulations at various distances and locations. Furthermore, the SAR values were managed within the safety regulation of 2 W/kg per 10 grams of tissue, as stipulated by ICNIRP.

5. ON-BODY ANALYSIS OF BENDING AND HUMAN BODY EFFECTS OF COMPACT FULL FLEXIBLE ANTIPODAL VIVALDI ANTENNA FOR 3.5 GHZ IN 5G SUB-6 GHZ WEARABLE APPLICATIONS

In the search for ubiquitous connectivity, the increasing demand for fifth-generation (5G) wireless technology has sparked innovation across various sectors, such as biomedical, healthcare, sports, military, smart display, radar, 5G communication, WBAN, WLAN, IoT, Satellite, UHF RFID, tracking, navigation, remote computing, wearable applications, etc [31]. Among the numerous challenges in this domain, the design of compact, flexible antennas capable of operating effectively across the sub-6 GHz spectrum stands as a paramount concern. In this context, the antipodal Vivaldi antenna emerges as a promising contender, offering versatility, compactness, and broadband capabilities crucial for 5G-enabled wearable devices [32].

This research explained an in-depth analysis of the bending conditions and effect of the antenna when placed in close proximity to the human body, specifically for sub-6 GHz 5G wearable applications. Bending and crumpling introduce mechanical stress, potentially altering the antenna's electrical properties, gain, efficiency and radiation pattern, which leads to impedance mismatch and signal loss [33]. This can cause changes in the electromagnetic fields around the antenna, resulting in changes to its radiated power and directionality. Moreover, the human body, with its varying dielectric properties and proximity effects, can significantly influence antenna performance [34].

5.1 Antenna Bending and On-body Analysis

Figure 5.1 (a) and (b) show the front and rear side view of the fabricated antipodal Vivaldi antenna, designed using a 100 % polyester substrate with a dielectric constant of 1.34, a loss tangent of 0.005, and a thickness of 0.4 mm, whereas Figure 5.1.1 (c) shows the measurement setup using a vector network analyzer (VNA; model: E5071C) in the UNIMAP laboratory. All the design procedures, parameters and measurement results have been explained more detail in previous work [32]. The total antenna dimensions (i.e. substrate dimensions, $SL \times SW \times ST$) are $33 \times 33 \times 0.4 \text{ mm}^3$.

As this antenna is going to be used in wearable purpose, it is very important to observe antenna's performance under different bending conditions. The antenna is placed upon a cylinder and by varying the radius or angle of the cylinder with reference to the UV-plane, we can bend the antenna with different angles. Figure 5.2 shows the antenna structures with different bending angles from 20° to 120° in both horizontal (H) and vertical (V) directions, whereas Figure 5.3 represents the effect of bending of antipodal Vivaldi antenna on reflection coefficient with different angles in both directions. As the bending angle increases from 20° to 120° in horizontal and vertical directions, resonance shifts towards positive frequencies along with bit degradation in bandwidth. Although, minimal degradation in performance, still it is within required bands, which shows the antenna's function ability under bending conditions.

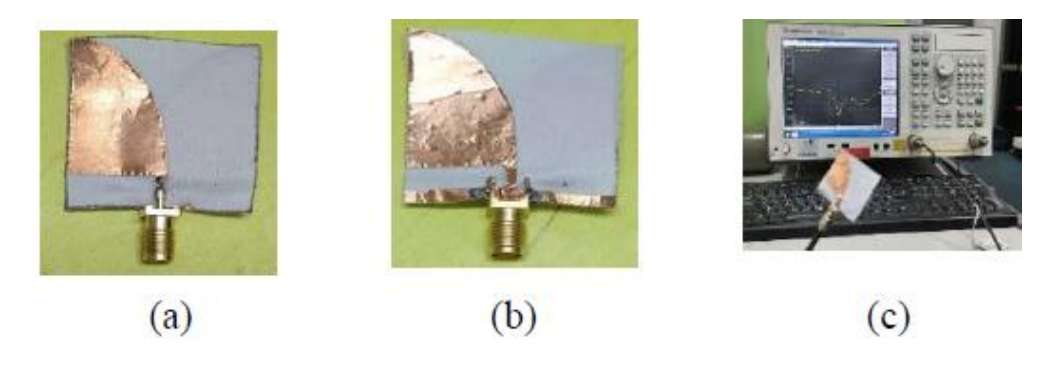


Figure 5.1. Flexible antipodal Vivaldi antenna (a) Front (b) Back side of fabricated antenna (c) Measurement set up.

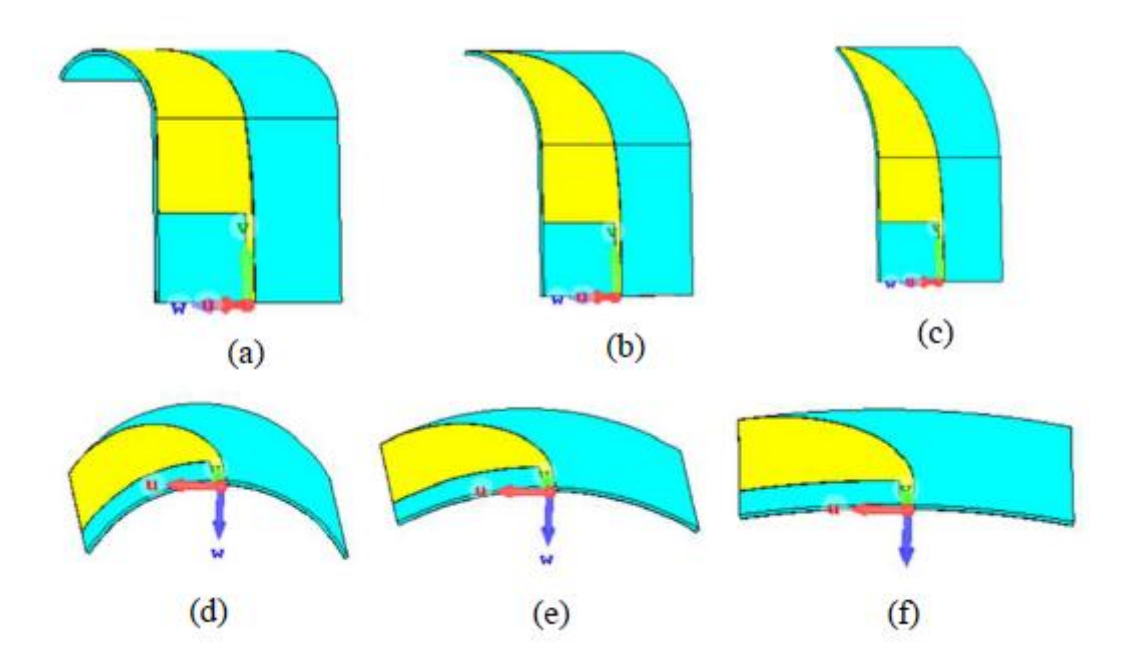


Figure 5.2. Different bending angles of proposed antenna (a) 120° (b) 60° (c) 20° in vertical direction (d) 120° (e) 60° (f) 20° in horizontal direction.

An on-body analysis of the antenna has been performed on different body parts using a homogeneous human model from CST studio, as shown in Figure 5.4. The wideband characteristics of the antenna is very important for less detuned effect on the antenna operational frequency in the presence of body.

At first the antenna was placed on chest and back and started varying the gap (x) between the body and the antenna. Even after placing at 10 mm distance, the antenna's performance did not match with the requirement, this is because of the large surface area as compared to smaller sized antenna. Then the antenna is placed upon arm and started varying the gap (x). Figure 5.4 shows the reflection coefficient plot of the antenna with different body parts, along with its effect when placed at specific distances from the arm, it depicts when the antenna is at least 2 mm far away from the arm, its performance maintained.

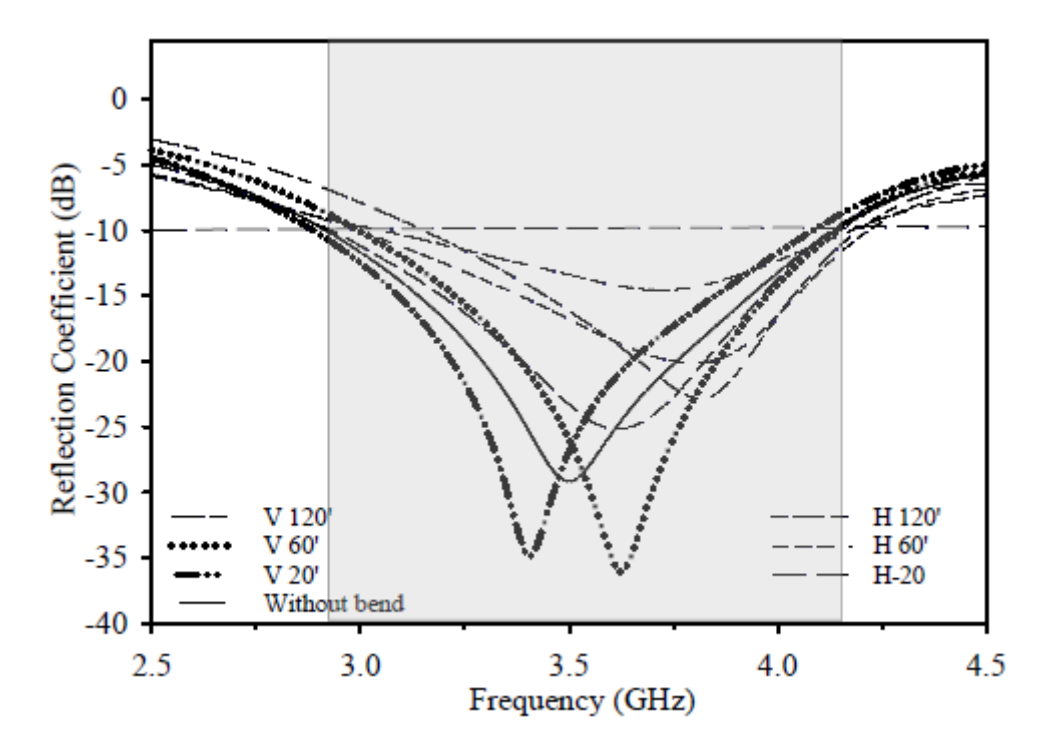


Figure 5.3. Simulated reflection coefficient with its effect in different bending angles in Horizontal (H) and Vertical (V) directions.

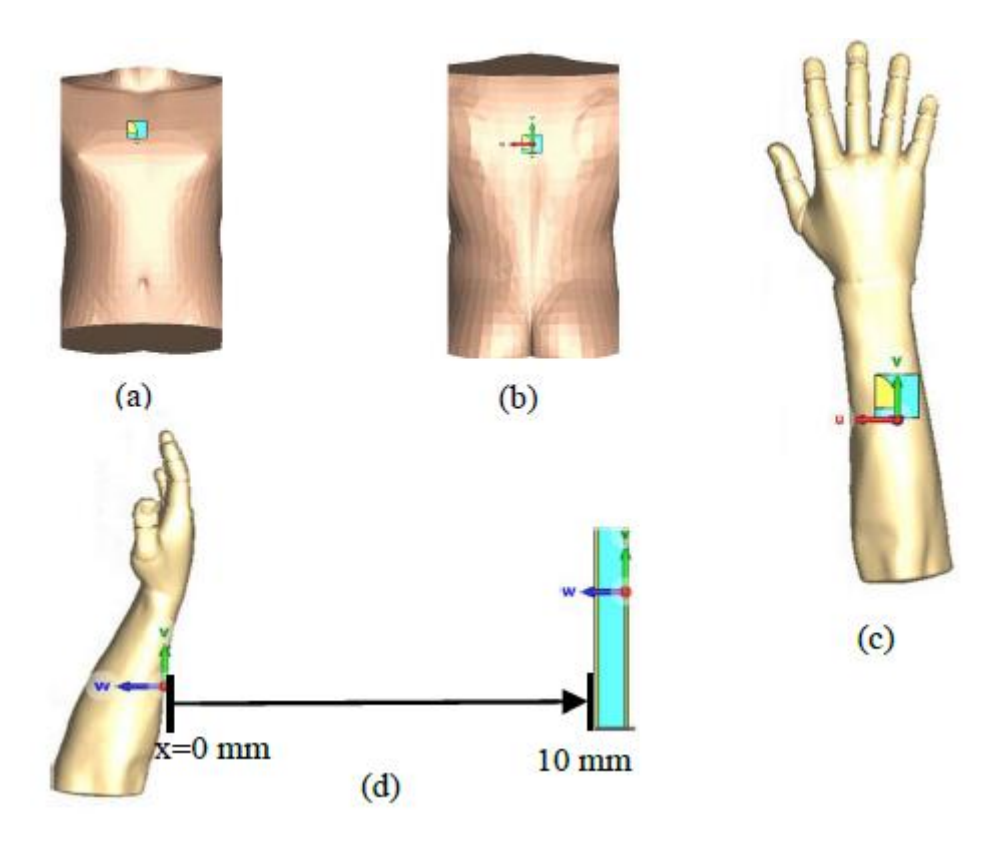


Figure 5.4. Placement of antenna with different body parts (a) Chest (b) Back (c) Arm (d) Gap between arm and antenna, x=0, indicates the antenna is very close to the arm.

DESIGN AND DEVELOPMENT OF SMALL AND LARGE FORM FACTOR ON BODY ANTENNAS FOR SUB-6 GHZ ${\bf 5G}$ APPLICATIONS

This paper proposes a flexible antipodal Vivaldi antenna for 5G wearable applications. It uses a polyester fabric substrate with a low dielectric value and operates at 3.5 GHz, with a bandwidth of 34.9% (1.224 GHz). Finally, bending, and on body analysis have been proposed. These indicates the antenna's suitability for wearable applications in the 5G n77 and n78 bands. Radiation pattern, gain, efficiency and on body measurements for this design will be investigated in the future.

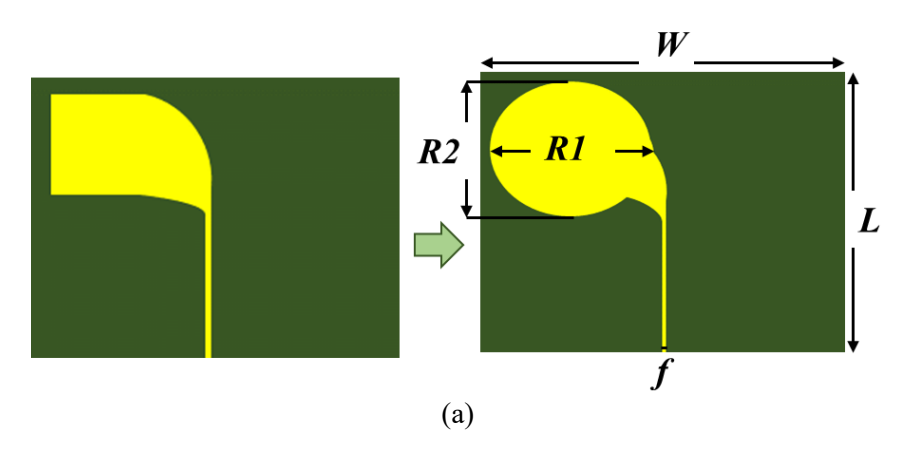
6. ANTIPODAL VIVALDI ANTENNA WITH ANALYSIS NEAR HUMAN BODY AND UNDER BENDING CONDITIONS

Since, the Vivaldi-type structure offers wideband performance due to its structural characteristics, the antipodal structure was chosen for antenna design structure showed in Figure 6.1 and the parameters are tabulated in Table 6.1.

The antenna's performance, including the reflection coefficient, efficiency, and gain, is depicted in Figures 6.2, 6.3, and 6.4, respectively. From Figure 6.2, it can be observed that the conventional antipodal Vivaldi antenna structure failed to achieve resonance at certain frequencies (1.95 to 2.27 GHz, 3.14 to 3.41 GHz, and 4.17 to 4.41 GHz) within the targeted bandwidth. To address this limitation, modifications were made to the antenna structure, resulting in a shift of the resonance bandwidth toward lower frequencies (from 1.47 GHz to 1.40 GHz). Additionally, shifts in resonance frequencies were observed in the lower bands (from 1.60 GHz to 1.54 GHz, 2.75 GHz to 2.56 GHz, and 3.79 GHz to 3.40 GHz), along with a more pronounced and deeper notch in the reflection coefficient graph due to the uniformity of the circle type structure in the flares of the Vivaldi antenna compared to the conventional Vivaldi design. As a result of these modifications, the antenna successfully achieved the entire bandwidth (<-10 dB), even including previously unattained frequency bands. The final design exhibited a bandwidth of 4264 MHz (1.412 to 5.676 GHz), encompassing all the required resonance frequencies.

The measurement results for the reflection coefficient align well with the simulated results, following a similar pattern in the graph while covering the desired frequency bands, as illustrated in Figure 4.4. A slight shift and reduced resonance depth were observed in the measured reflection coefficient, attributed to the screen-printing fabrication technique. During the fabrication process, the material layers merged or blended into one another a bit, whereas in simulation, the layers were ideally separated and stacked, resulting in the mild mismatch.

Additionally, the antenna demonstrated satisfactory simulated efficiency and gain performance across the entire bandwidth (portrayed in Figure 4.5 (a)), achieving a maximum efficiency of 96.90% and a maximum gain of 5.65 dBi. The gain closely followed an upward trend throughout the bandwidth, except at the higher frequency end. The observed reduction in gain at higher frequencies is due to the relationship between gain and efficiency. Gain is the product of efficiency and directivity, and at higher frequencies, the directivity decreases, leading to a gain lower than the efficiency. In the measurements, the observed efficiency and gain exhibit a similar trend to the simulation results, although the measured values are slightly lower. This discrepancy is attributed to fabrication-related factors, as previously discussed



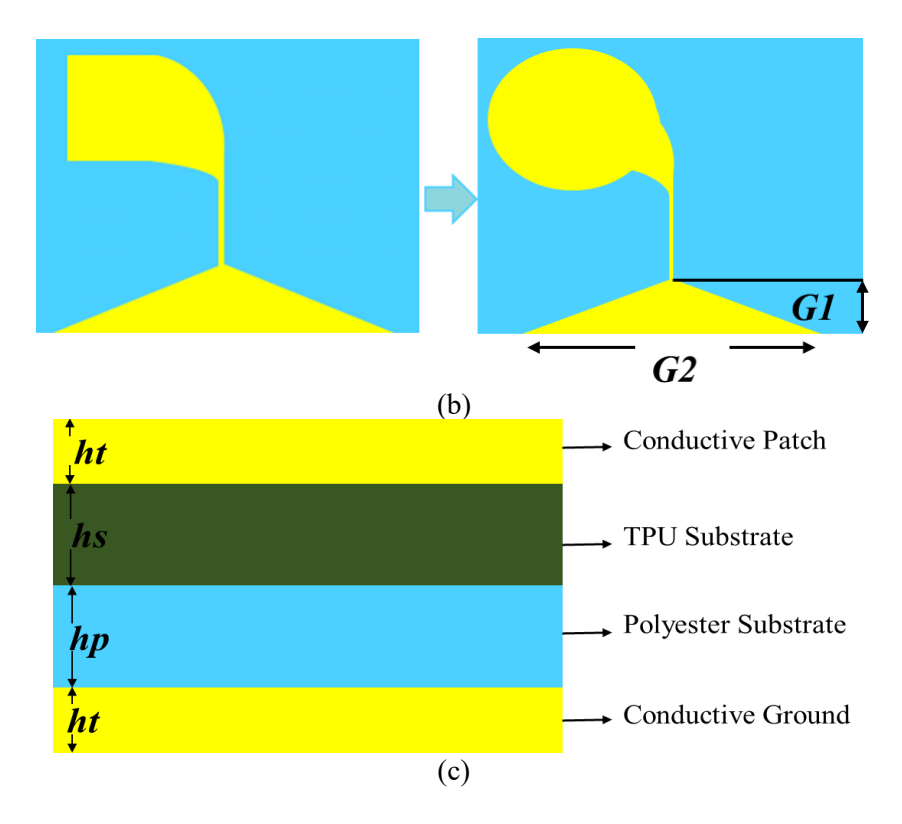


Figure 6.1. Geometry of antipodal Vivaldi antenna (a) Front (b) Back (c) Side view.

Table 6.1 Dimensions of the Antipodal Vivaldi Antenna

<i>W</i> (mm)	L (mm)	R1 (mm)	<i>R2</i> (mm)	f (mm)	G1 (mm)	G2 (mm)	h _t (mm)	<i>h</i> _s (mm)	<i>h_p</i> (mm)
134	98	36	28	1	19	105	0.07	0.35	0.4

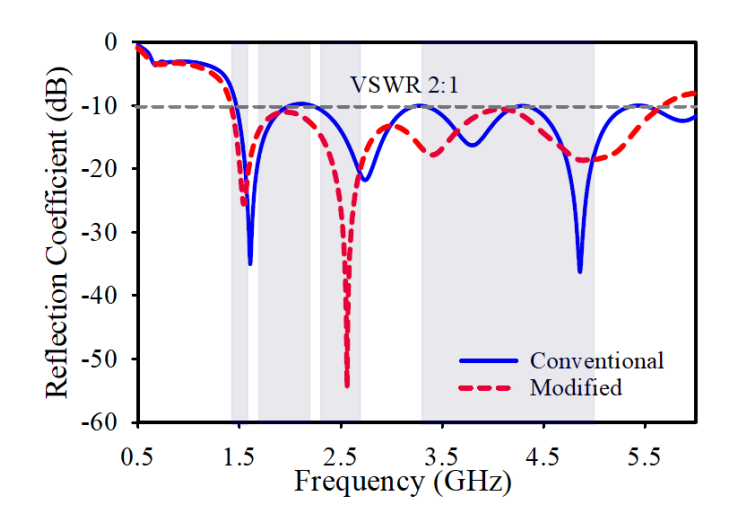


Figure 6.2. Simulated S-parameter result of modified and conventional antipodal.

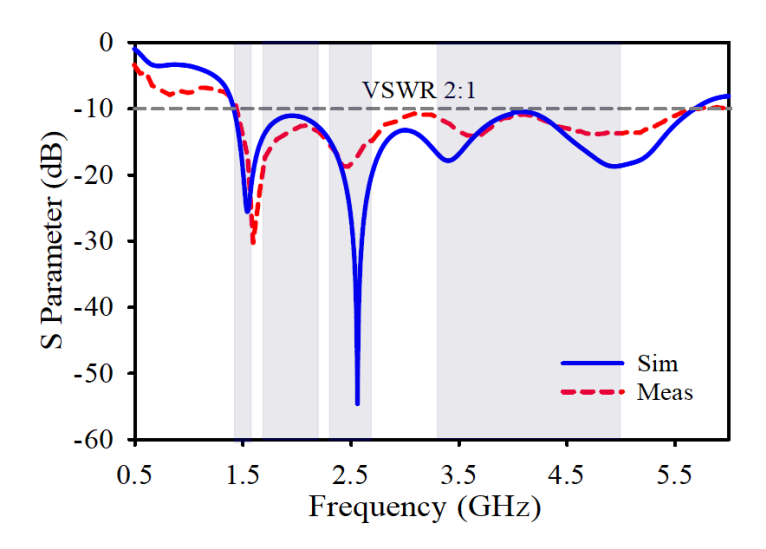


Figure 6.3. Simulated and measured reflection coefficient.

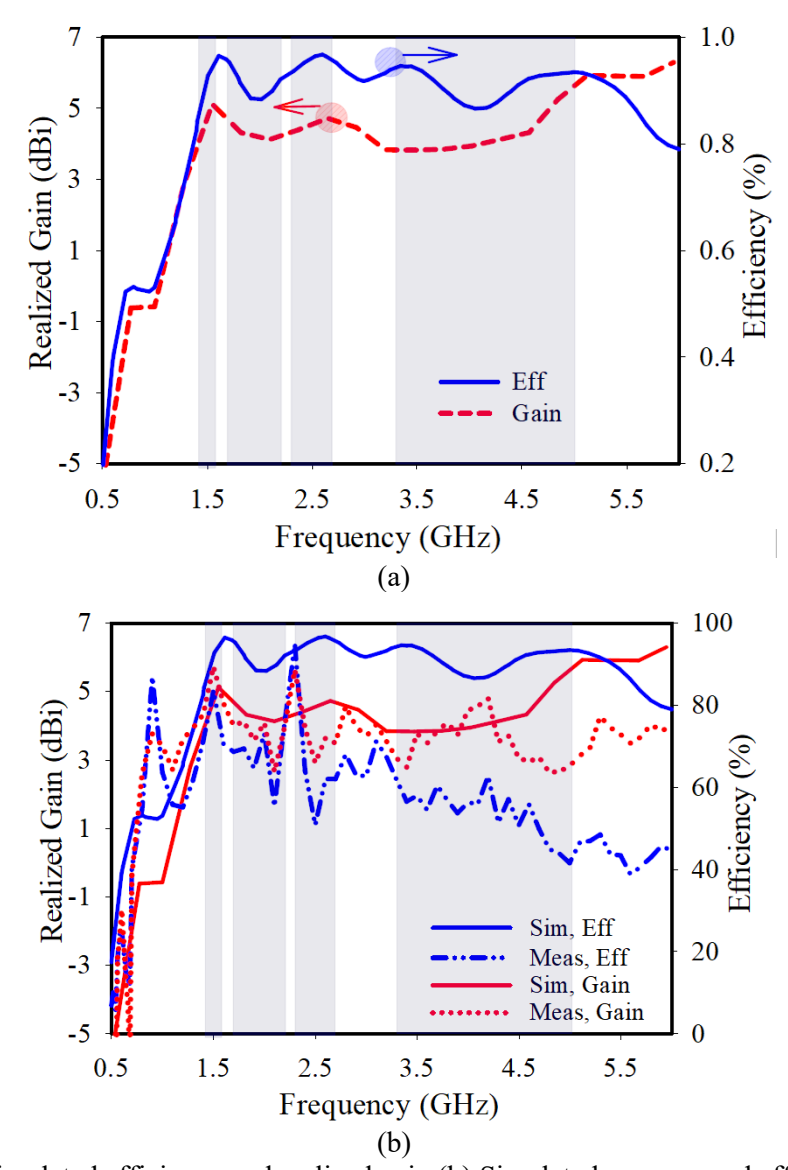


Figure 6.4. (a) Simulated efficiency and realized gain (b) Simulated vs measured efficiency and gain.

DESIGN AND DEVELOPMENT OF SMALL AND LARGE FORM FACTOR ON BODY ANTENNAS FOR SUB-6 GHZ ${\bf 5G}$ APPLICATIONS

Since the antenna is a wearable antenna, when the user wears it (on arms, thighs, chest, or back) it might flex. To determine the antenna's ability to bend at different bending radii compared to the straight position is performed to identify acceptable bending. Fig. 6.5 represents the antenna bending situations with different bending radius in simulation whereas Figure 6.6 shows bending setups for measurement using cylinders that has been mentioned in previous chapter. The simulated performance is illustrated in Figure 6.7 (a) and S₁₁ performance showed shifting compared to the antenna performance in flat conditions. Nevertheless, the antenna demonstrates efficient performance and maintains a similar bandwidth to its performance under flat conditions, except at a 30 mm bending radius. Therefore, a bending radius of 50 mm is identified as the threshold for maintaining efficient antenna performance. The observed decrease and shifting in resonance under bending conditions is attributed to impedance mismatch between the port and feedline caused by the deformation of the antenna structure. The bending performance has also been validated through measurements, as presented in Figure 6.7 (b). The measurement results are in good agreement with the simulations.

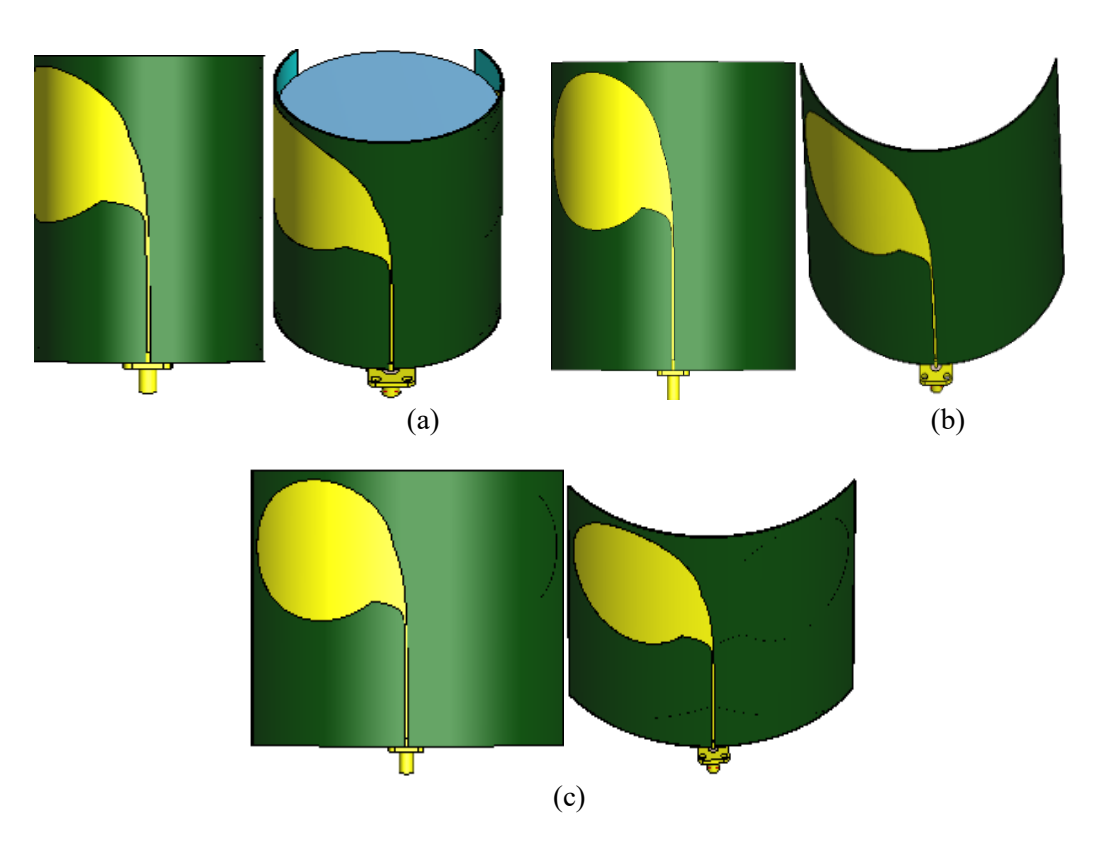


Figure 6.5. Antenna bending situation with different radius of cylinder (a) 30 mm (b) 50 mm (c) 70 mm.

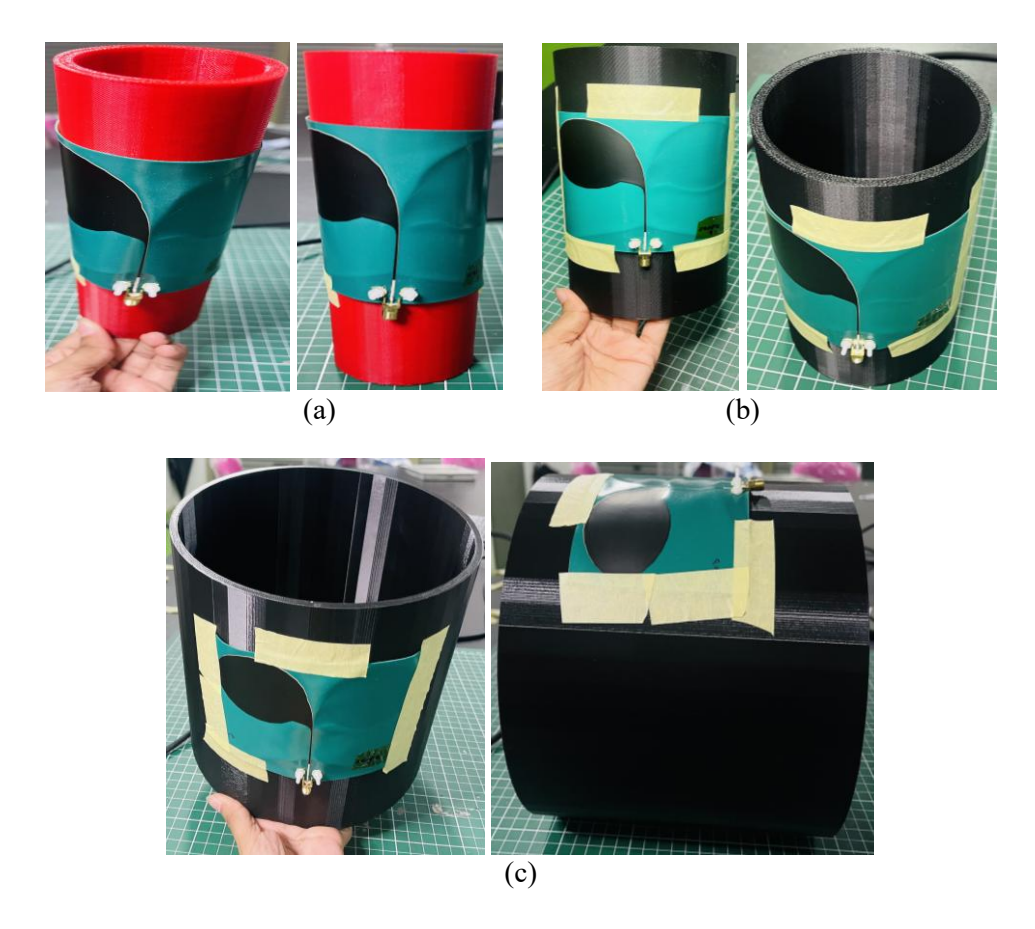
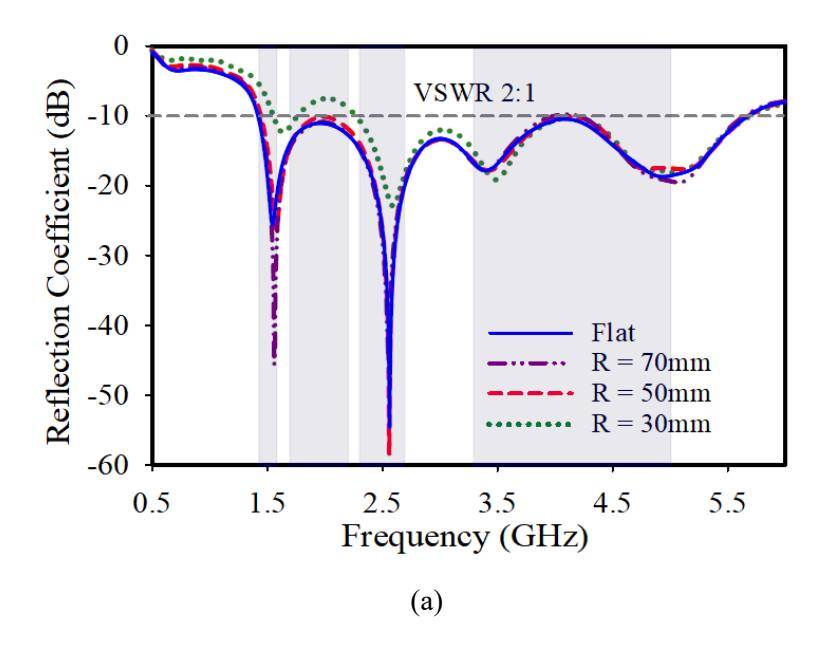


Figure 6.6. Antenna measurement arrangement at bending radius (a) 30 mm (b) 50 mm (c) 100 mm.



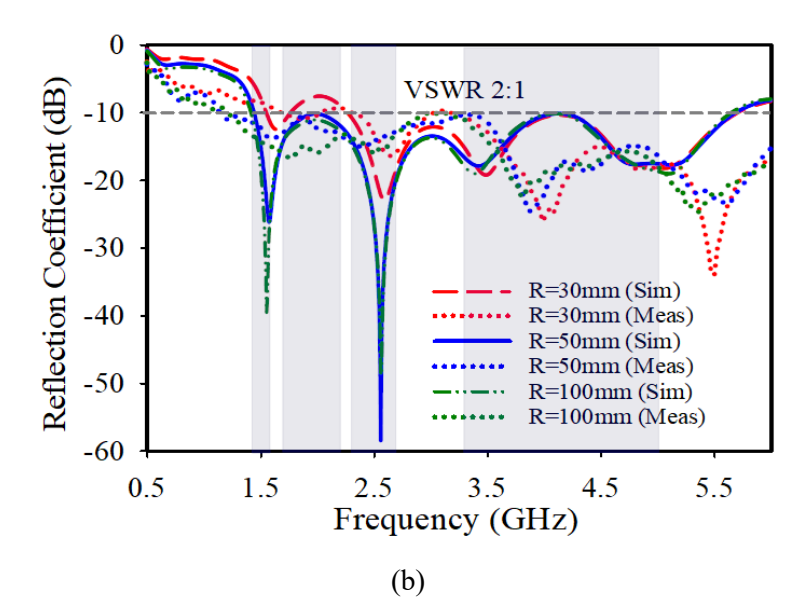


Figure 6.7. (a) Simulated reflection coefficient with different bending conditions vs reflection coefficient in flat condition (b) Simulated vs measured reflection coefficient in bending conditions.

A realistic homogeneous human body model from the CST Microwave Studio has been employed to assess the effect of the human body on antenna performance. The antenna was located at the front (chest) of the human model, according to Figure 6.8, and simulated S₁₁ parameters was observed in Figure 6.9. Because of the high permittivity of the human body, the resonance frequency of the antenna was affected and shifted toward right direction, and the bandwidth of the body-loaded antenna was comparatively less than that of the free space antenna. Hence, the resonance performance of the antenna closely resembles its performance in free space, indicating satisfactory operation when placed near the human body. A distance of 5 mm was established during the simulation between the human model and the antenna due to the SMA connector positioning and the safety of the user.

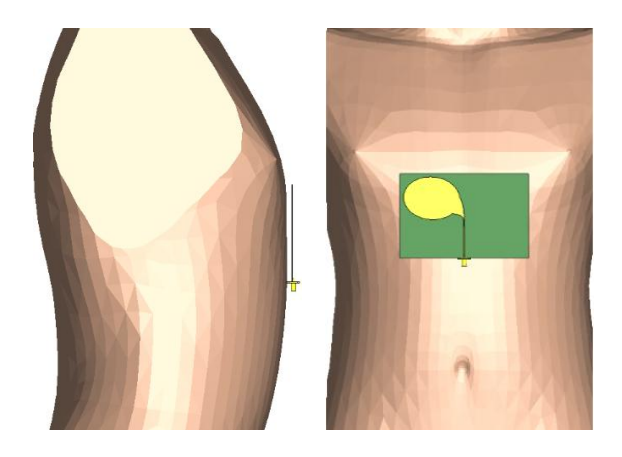


Figure 6.8. Antenna simulated near human body model in computation software.

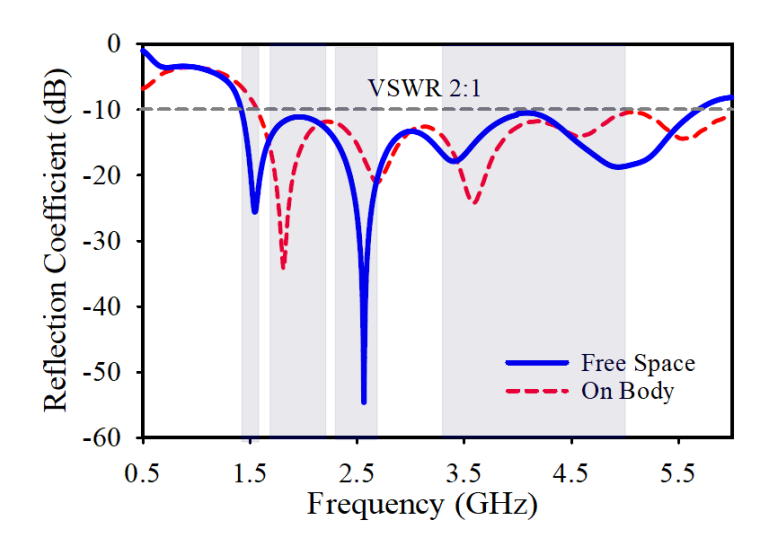


Figure 6.9. Simulated reflection coefficient for on-body condition.

The regulatory organizations (FCC, IEEE, and ICNIRP) defined the SAR restrictions with the goal of ensuring user protection. For the proposed antenna, SAR values are determined considering the ICNIPR standard threshold of 2W/kg per 10g of tissue while antenna placed near human body model. Proposed input power for the antenna has been specified, and the value is 80 mV. Throughout the entire bandwidth, SAR has been calculated in multiple frequencies showing in Figure 6.9, and the value has been presented in Table 6.2. SAR values satisfied the ICNIPR regulation of threshold 2W/kg per 10g of tissue.

Table 6.2 SAR for Single Port Antipodal Antenna

Frequency (GHz)	SAR Values (W/Kg)
0.5	0.284
1.0	0.323
1.5	0.582
2.0	0.654
2.5	0.683
3.0	0.712
3.5	0.810
4.0	0.777
4.5	0.679
5.0	0.674

Afterward, the antenna developed to a two-port structure from single port illustrated in Figure 6.10 (a). In dual-port structure (265×98×0.89 mm³), two port feeding with two-elements were designed, whereby the two-element are located in opposite direction to reduce the mutual coupling, presented in Figure 6.10 (b).

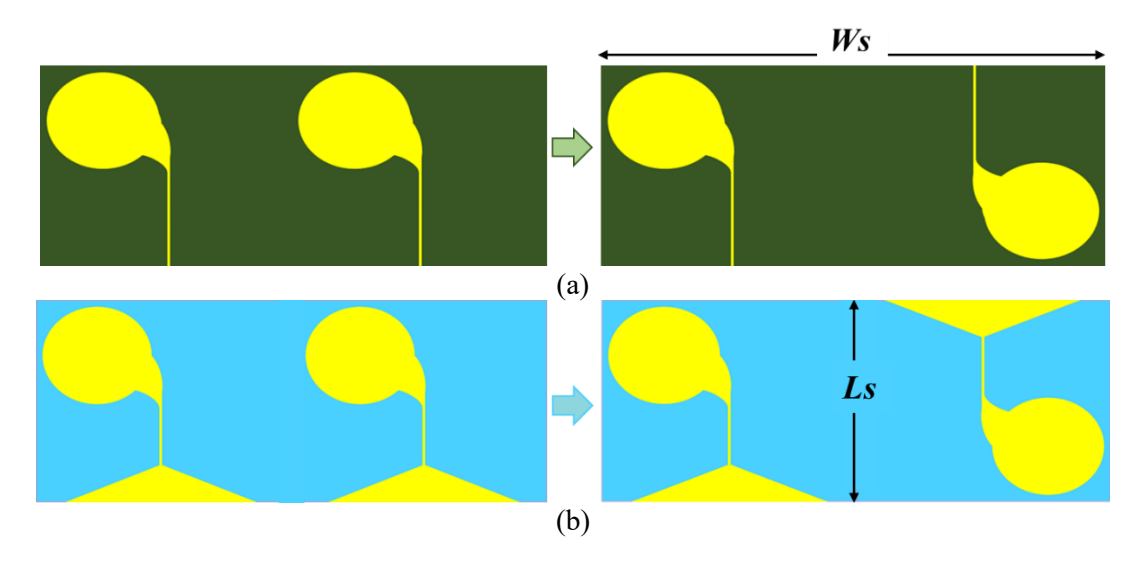


Figure 6.10. Two-port antenna structures (a) Front (b) Rear view.

As illustrated in Figure 6.11, the two-port antenna exhibits similar satisfactory results as the single-element antenna with a bandwidth of 4229 MHz. However, it was observed that mutual coupling was slightly higher in the lower frequency bands, as a result the ports were fed in opposite direction. Subsequently, the mutual coupling was assessed and found to be satisfactory across the entire bandwidth. This adjustment ensures that the two-port antenna maintains optimal performances while effectively minimizing mutual interference between the antenna elements. Additionally, the antenna's performance from Figure 6.12 indicates healthy matching between simulation and measurement, with minor difference (shifting and resonance performance) observed due to the same fabrication procedure errors discussed earlier for the single-element antennas.

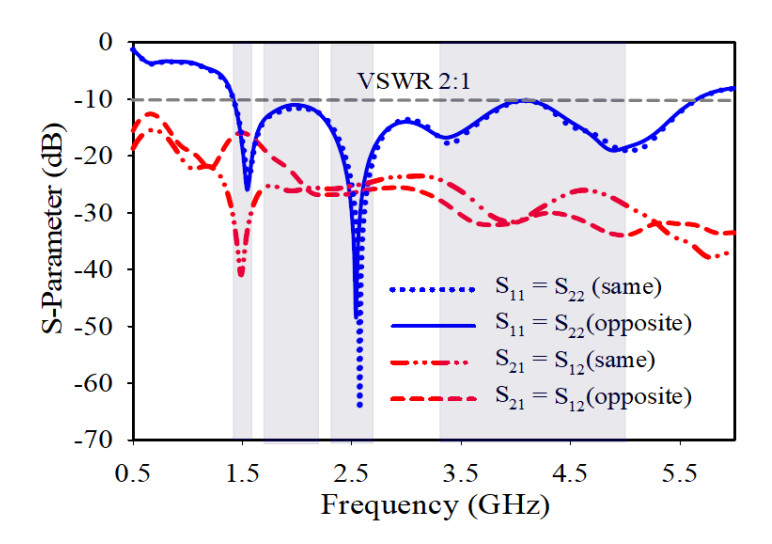


Figure 6.11. Two port simulated S-parameters (feeding in same vs opposite direction).

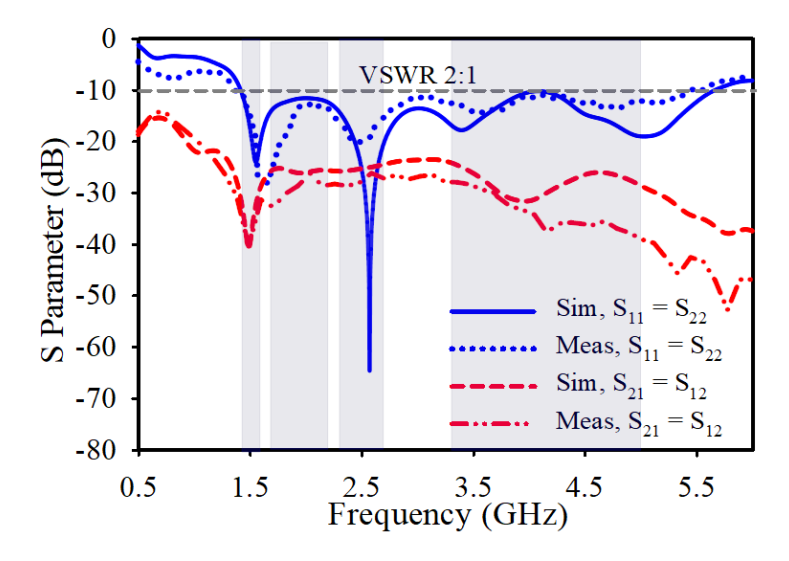
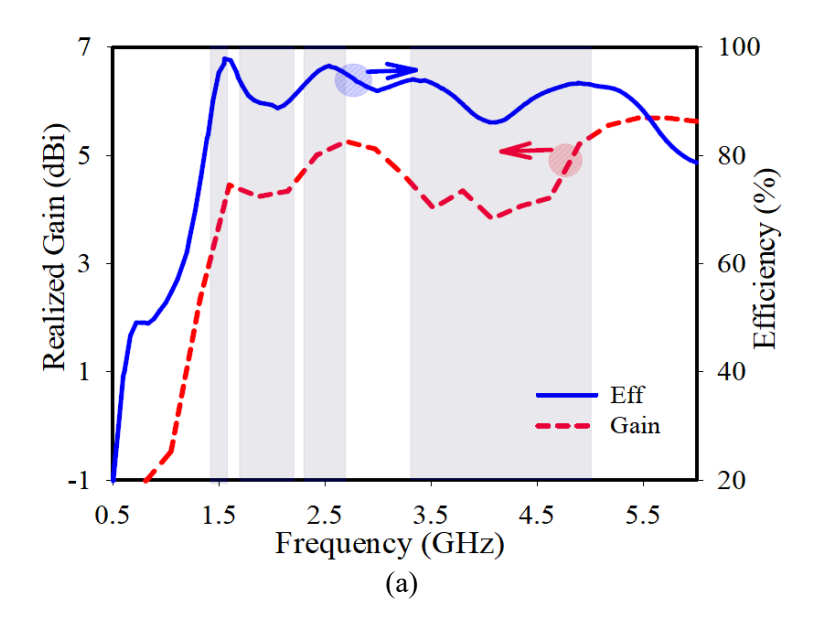


Figure 6.12. Two-port simulated and measured S-parameters.

Furthermore, the antenna demonstrates satisfactory performance, achieving a maximum gain of 5.4 dBi and a peak efficiency of 98%, as illustrated in Figure 6.13 (a). A slight discrepancy between efficiency and gain is observed at higher frequencies, attributed to factors similar to those affecting the single-element antenna. As seen in Figures 6.13 (b) and 6.13 (c), the measured efficiency and gain follow a similar trend to the simulation results and are consistent with the performance of the single-element antenna.



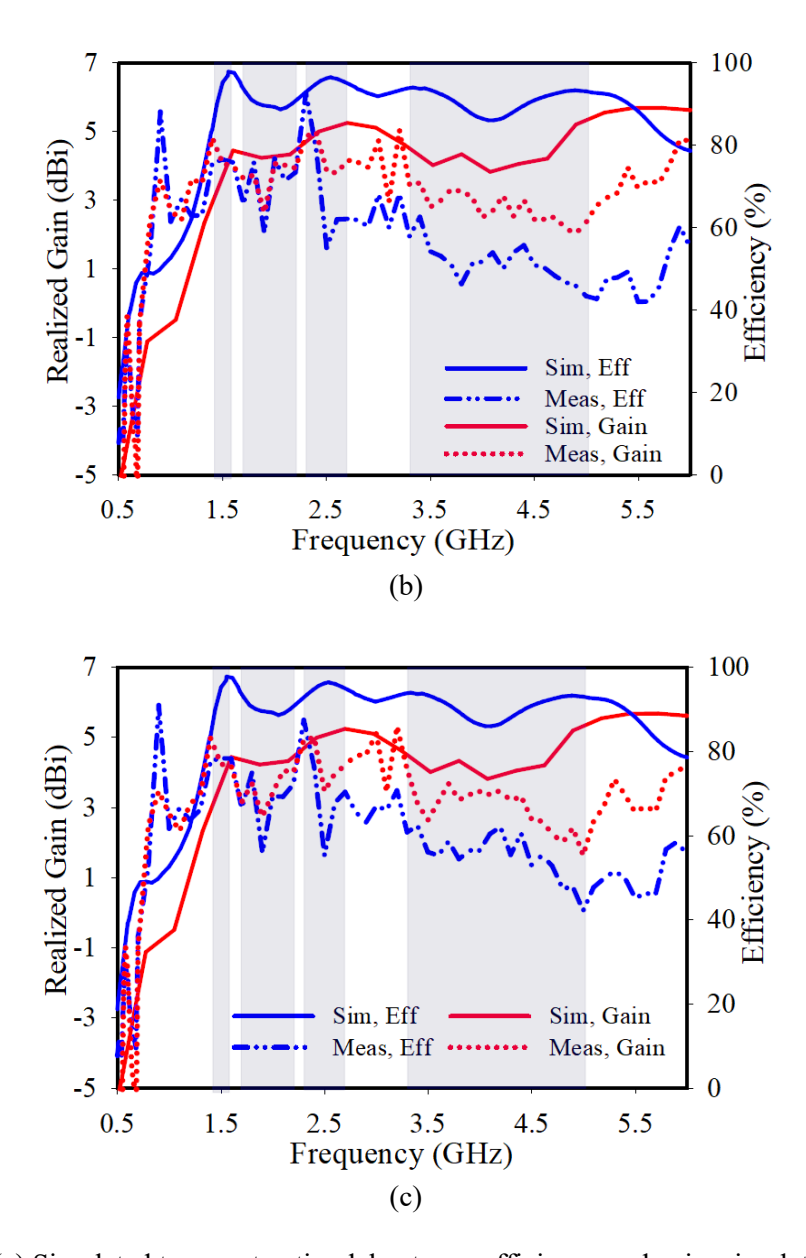


Figure 6.13. (a) Simulated two-port antipodal antenna efficiency and gain; simulated vs measure efficiency vs gain (b) Port 1 (c) Port 2.

Figure 6.14 illustrates the simulated bending scenarios for the antenna under different bending conditions, while Figure 6.15 depicts the corresponding measurement setups. The performance results are presented in Figure 6.16. From Figure 6.16 (a), the simulated S₁₁ performance shows a slight upward shift compared to the flat condition. Despite this, the antenna demonstrates satisfactory performance by achieving the targeted frequency bands and maintaining a bandwidth comparable to the flat condition under bending scenarios. The measurement results, shown in Figure 6.16 (b), align well with the simulations, though minor shifts are observed. Specifically, a leftward shift is noted at a bending radius of 50 mm, and a downward shift is observed at a bending radius of 100 mm, likely due to fabrication variations and the material properties of the cylinder used during measurement. Nevertheless, the antenna successfully covers the required frequency bands in measurement, similar to the simulation, confirming satisfactory performance under bending conditions. The efficiency and gain of the dual-port antenna were also measured under bending conditions. The measured results align well with

the simulations, with minor discrepancies attributed to fabrication inaccuracies and the slight influence of the cylindrical material and results are shown in Figure 6.16 (c) and 6.16 (d).

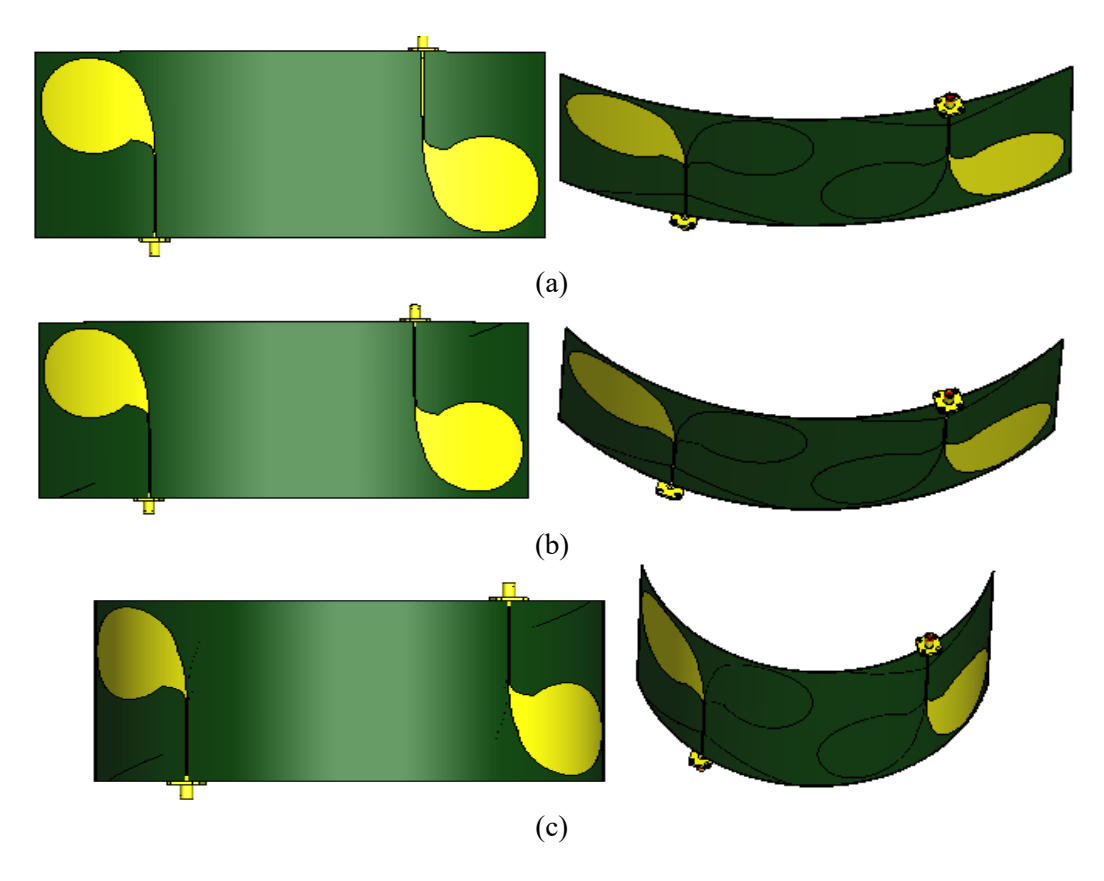


Figure 6.14. Antenna in different bending situation with different radius of cylinder (a) 250 mm (b) 160 mm (c) 100 mm.

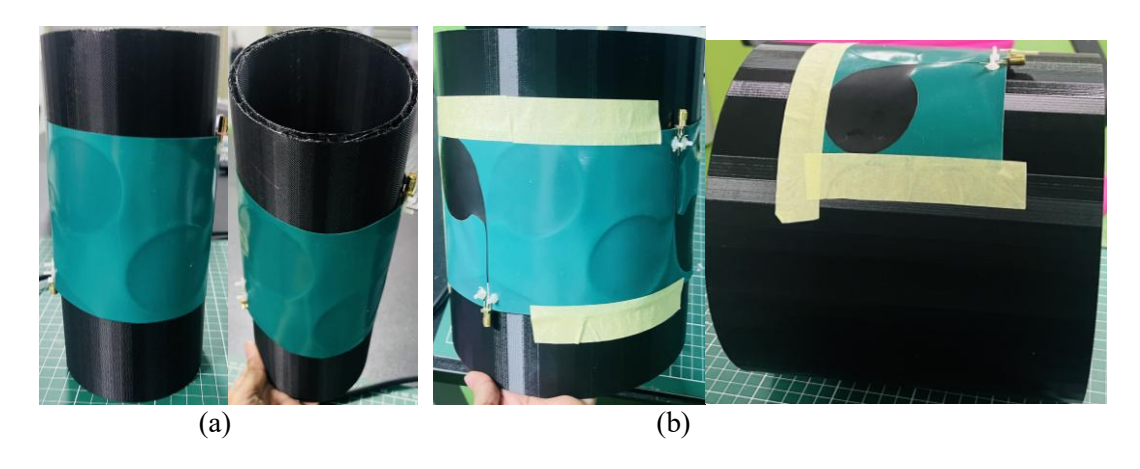
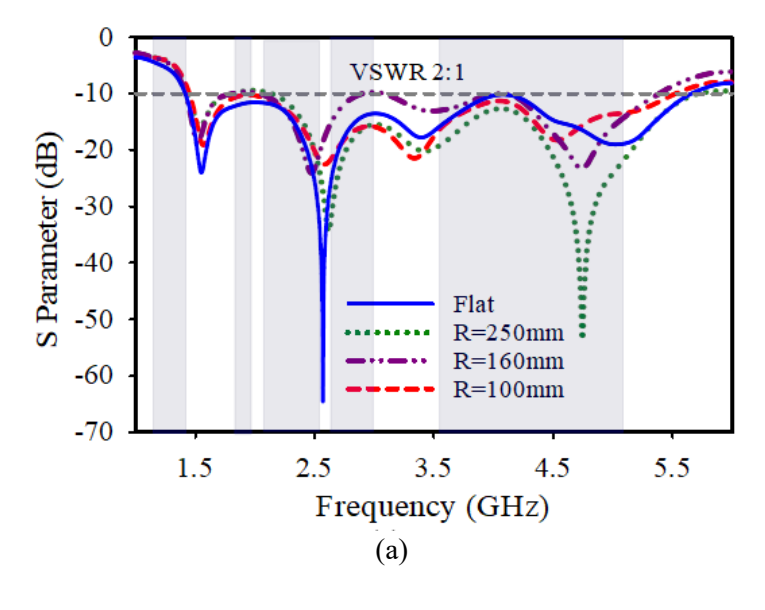
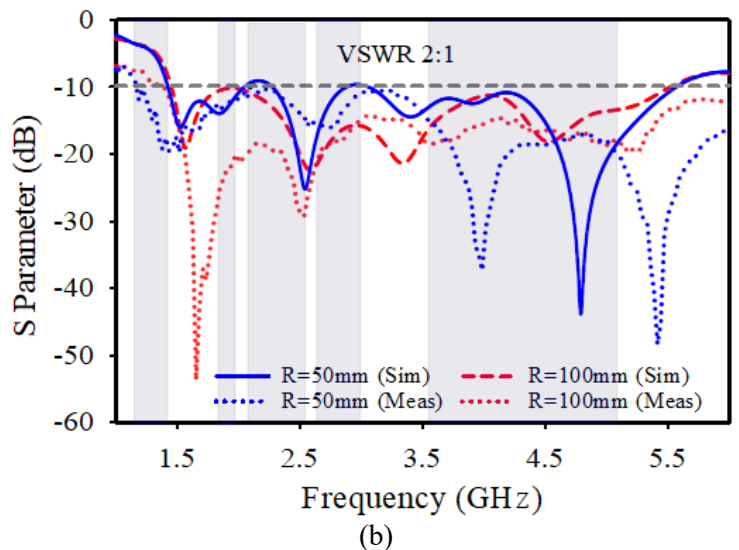
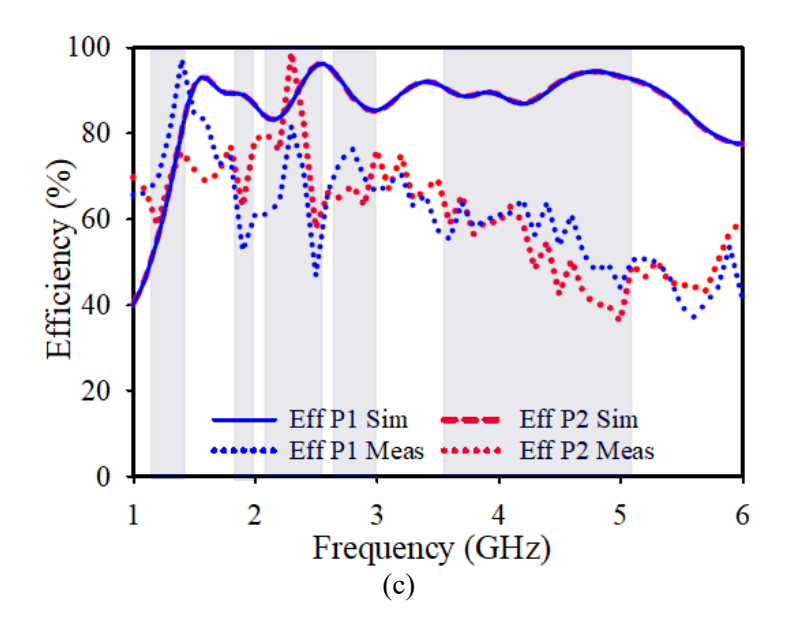


Figure 6.15. Antipodal Vivaldi dual port antenna measurement arrangement at bending radius (a) 50 mm (b) 100 mm.







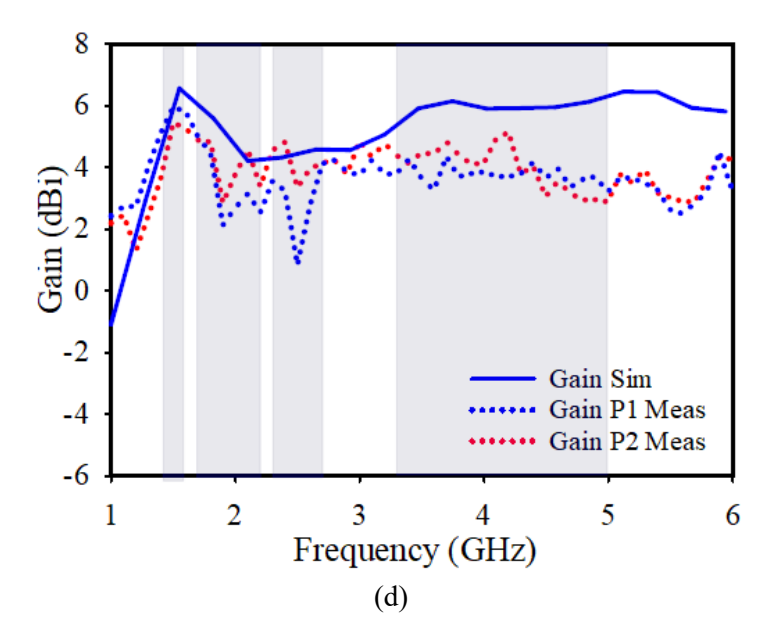


Figure 6.16. (a) Simulated reflection coefficient with different bending conditions vs reflection coefficient in flat condition (b) Simulated vs measured reflection coefficient in bending conditions; simulated vs measured (c) Efficiency (d) Gain.

For antipodal dual port antenna, on-body performance has been analysed as well and it has been portrayed in Figure 6.17. The antenna resonance bandwidth, as shown in Figure 6.18 (a), is comparable to its performance in free space, with a slight rightward frequency shift observed. Besides, higher isolation in comparison to free space is found due to the impact of the human body model. A similar distance of 5 mm was established during the simulation between the human model and the antenna due to the SMA connector positioning and the safety of the user. Figure 6.18 (b) portrays the measurement result with simulation and found to be compatible with each other.

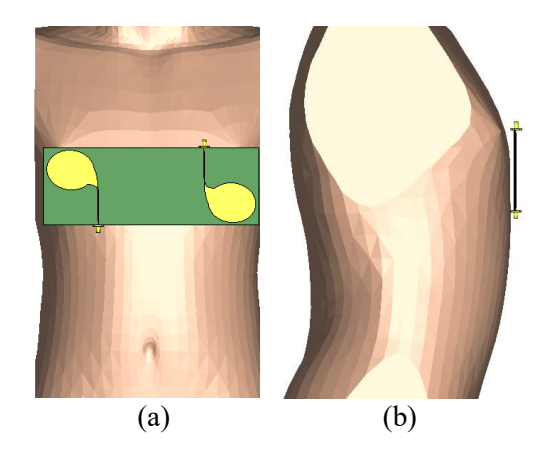


Figure 6.17. Simulated antenna near human body model in computation software.

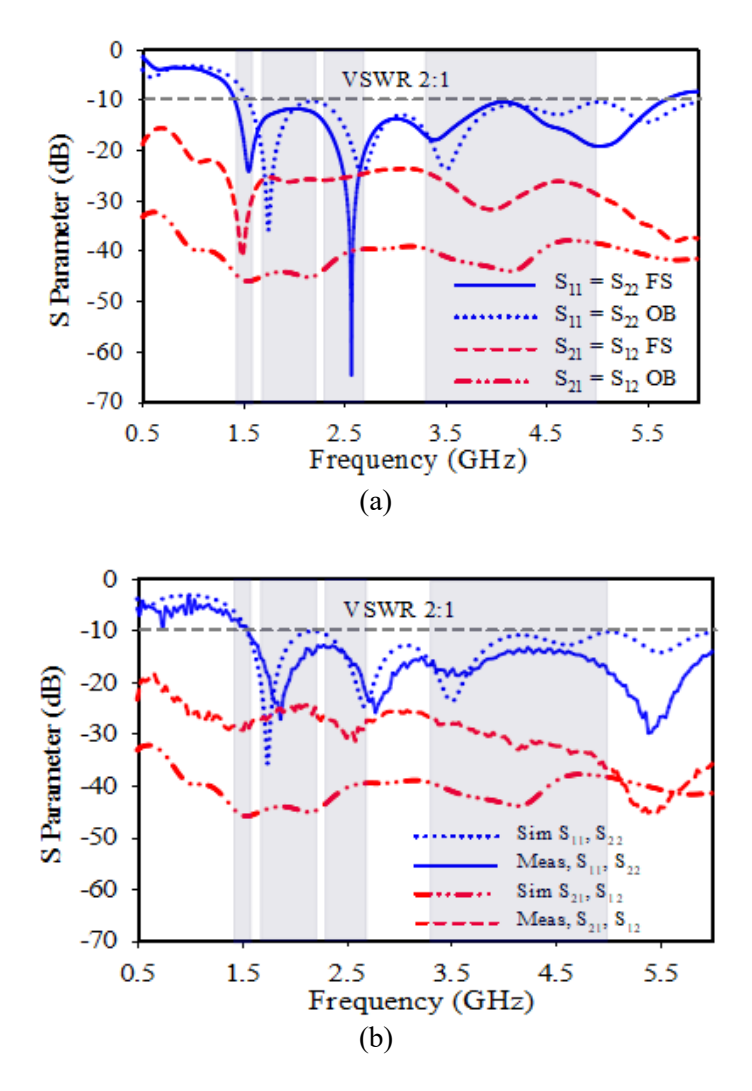


Figure 6.18. (a) Simulated S-parameters for on-body vs free space (b) Simulated vs measured s parameters.

SAR has been determined for the antenna to ensure the safety issue. Throughout the entire bandwidth, SAR has been investigated and the value has been presented in Table 4.3 where SAR values satisfied the ICNIPR regulation of threshold 2 W/kg per 10g of tissue. Additionally, Specific Absorption Rate (SAR) was evaluated for both ports, considering the curved nature of the human body. When positioning the antenna near a human body model, slight variations in distance and body structure were observed near each port area, as they are located on different location (in opposite sides) of the antenna.

TECHNICAL REPORT

 Table 6.3 SAR Values for Two-Port Antipodal Vivaldi Antenna

Frequency (GHz)	SAR Values (W/Kg) Port 1	SAR Values (W/Kg) Port 2
0.5	0.188	0.126
1.0	0.285	0.189
1.5	0.529	0.321
2.0	0.471	0.273
2.5	0.436	0.387
3.0	0.588	0.462
3.5	0.654	0.374
4.0	0.526	0.269
4.5	0.498	0.294
5.0	0.548	0.278

7. CIRCULAR PATCH ANTENNA WITH ANALIS NEAR HUMAN BODY AND UNDER BENDING CONDITIONS

Despite demonstrating excellent performance in both simulation and measurement, the primary objective of the smart garment antenna was to cover all sub-6 GHz frequencies, including those below 1 GHz. However, the previous structure failed to achieve the desired bandwidth below 1 GHz. To address this issue, a new design with the same antenna configuration has been introduced. This new design aims to achieve antenna resonance bandwidth under 1 GHz. Thus, both antennas together will fulfil the original goal of covering the entire sub-6 GHz frequency spectrum while placing on the t-shirt. The single-element prototype was tested in an organized, step-by-step design aspect prior to reaching the ultimate design. Initially, a circular (single-element) patch is placed on top of the substrate layers to create a basic antenna and partial ground to achieve wideband performance. Later, the CST Microwave Studio software was utilized to simulate, and an optimized single-element antenna was achieved through iteration. In addition to simulated analysis, experimental studies were conducted on the $124 \times 153 \times 0.89$ mm³ single-element antenna to validate its performance. The antenna structures both in simulation and fabrication has been presented in Figure 7.1.

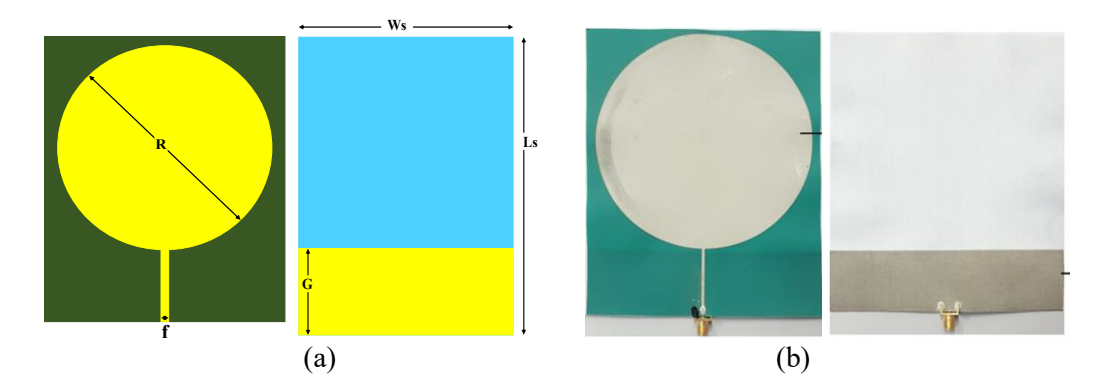


Figure 7.1. Single-port circular patch antenna (a) Simulation (b) Measurement.

Parameter	Description	Dimension (mm)
W_s	Width of the antenna	124
Ls	Length of the antenna	153
R	Radius of circle	57.5
f	Width of feedline	1.9
G	Width of ground	34
ht	Height of conductive silver	0.07
hs	Height of TPU substrate	0.44
hp	Height of Polyester	0.35

Table 7.1 Dimensions of the Single Circular Patch Antenna

The S₁₁ performance of the single-port antenna, observed in both simulation and measurement, is illustrated in Figure 7.2, while Figure 7.3 presents efficiency and gain. As shown in Figure 7.2, the antenna achieves a resonance bandwidth of 885 MHz (-10 dB) ranging from 0.655 to 1.54 GHz in both simulation and measurement, effectively covering the sub-6 GHz frequencies below 1 GHz required for 5G applications. A slight frequency shift was observed in the

measurement, attributed to the screen-printing fabrication technique used, which caused layer diffusion similar to the previously discussed antenna. Nonetheless, the measured S_{11} performance remains consistent with the simulated results, following a similar pattern and successfully covering the desired frequency band. Moreover, the antenna demonstrates satisfactory simulated efficiency and gain across the desired resonance bandwidth, maintaining a consistent pattern between the two parameters. Additionally, in the measurement (showed in Figure 7.3 (b)) the efficiency and gain exhibit compatible performance with simulation and slightly low value compare to simulation is observed due to fabrication error.

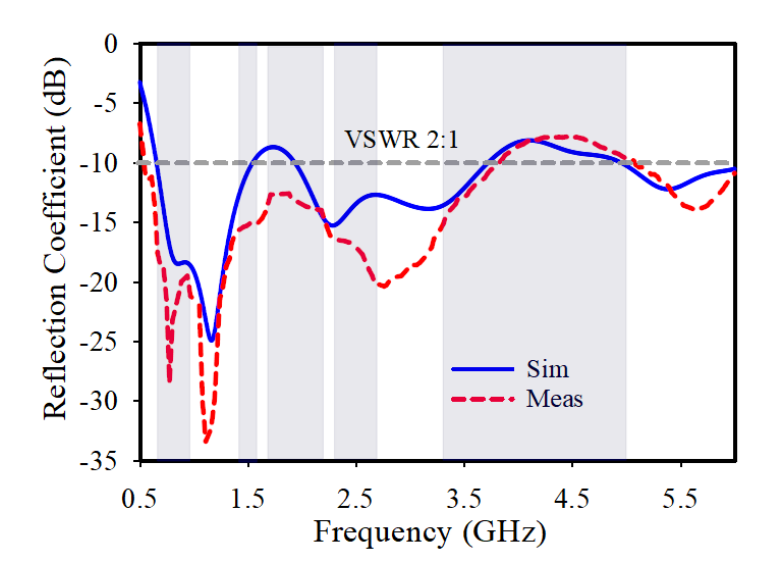
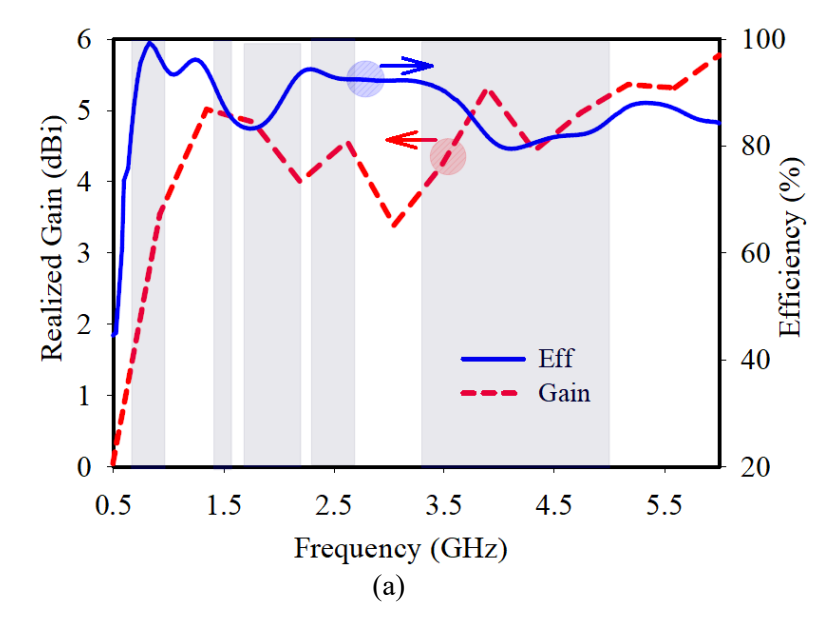


Figure 7.2. Simulated and measured reflection coefficient performance of circular patch antenna.



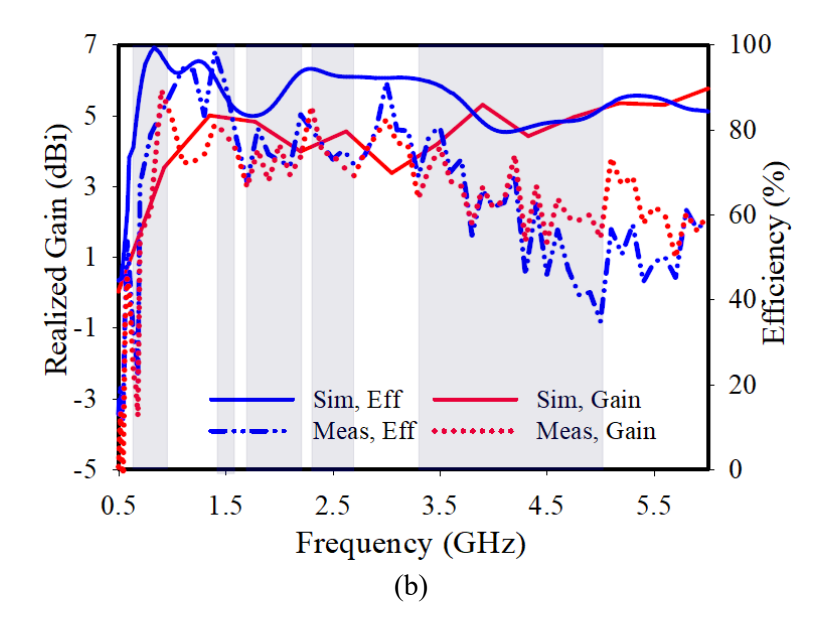


Figure 7.3. (a) Simulated efficiency and gain (b) Simulated vs measurement efficiency and gain.

Bending condition tests were also conducted on the circular patch antenna. The simulation setups for bending conditions are illustrated in Figure 7.4, where the antenna is subjected to various bending scenarios, ranging from mildly bent to significantly bent structures. Similarly, the measurement setup is depicted in Figure 7.5, utilizing a hollow cylinder with different radii. From Figure 7.6, it can be observed that under bending conditions, even with a significantly bent structure the antenna maintains resonance performance comparable to its flat condition, with only minimal resonance shifting. The antenna successfully covers the frequency bands of interest, specifically the sub-6 GHz bands below 1 GHz. Subsequently, the bending performance was validated through measurements, as shown in Figure 7.6 (b). In the lower resonance bandwidth, the measurement results align well with the simulation, following a similar pattern. However, at higher frequencies, slight shifts (toward the right and upward) are observed in the measurement results, attributed to fabrication variations and the material properties of the cylinder used in the setup. Still, in measurement the antenna exhibits satisfactory resonance bandwidth covering frequency of interest (< 1 GHz).

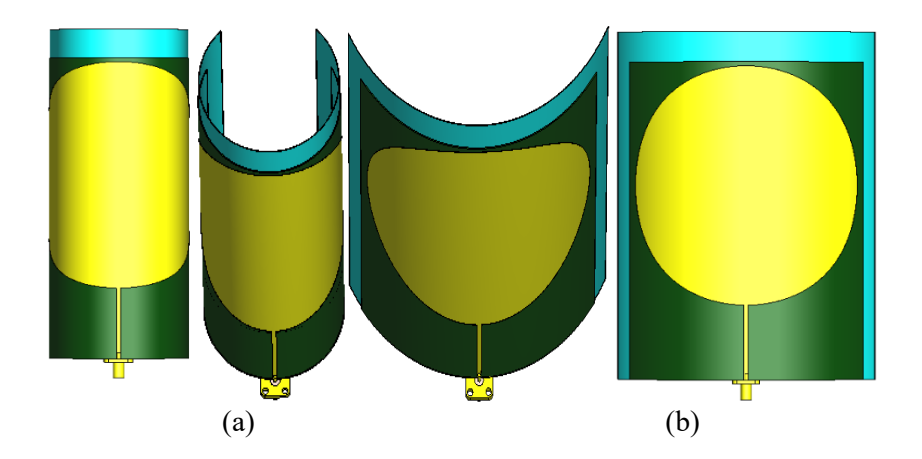


Figure 7.4. Simulated bending setup for single port circular patch antenna.

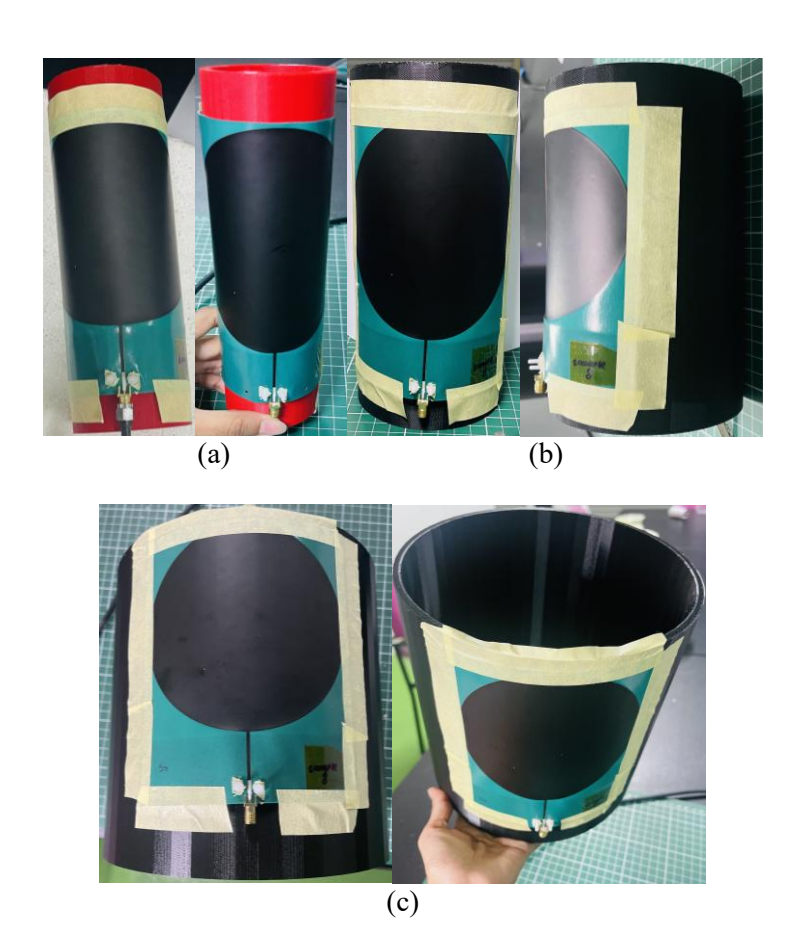
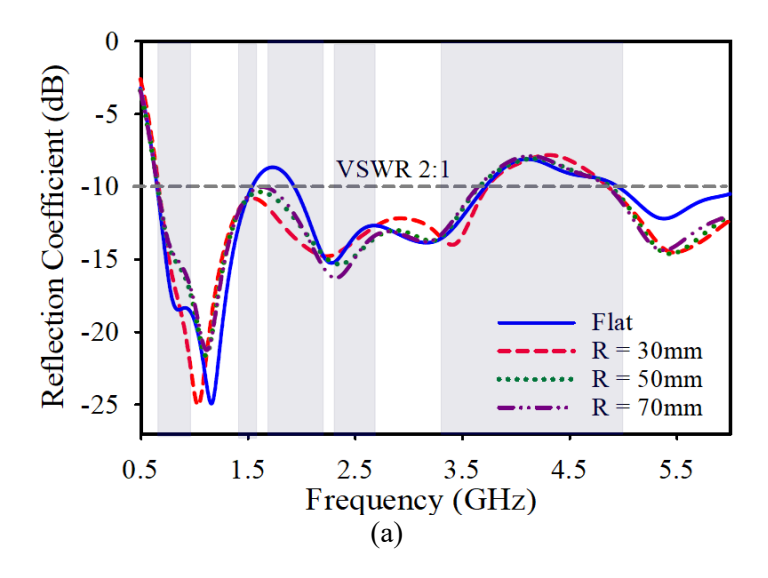


Figure 7.5. Circular patch single port antenna measurement arrangement at bending radius (a) 30 mm (b) 50 mm (c) 100 mm.



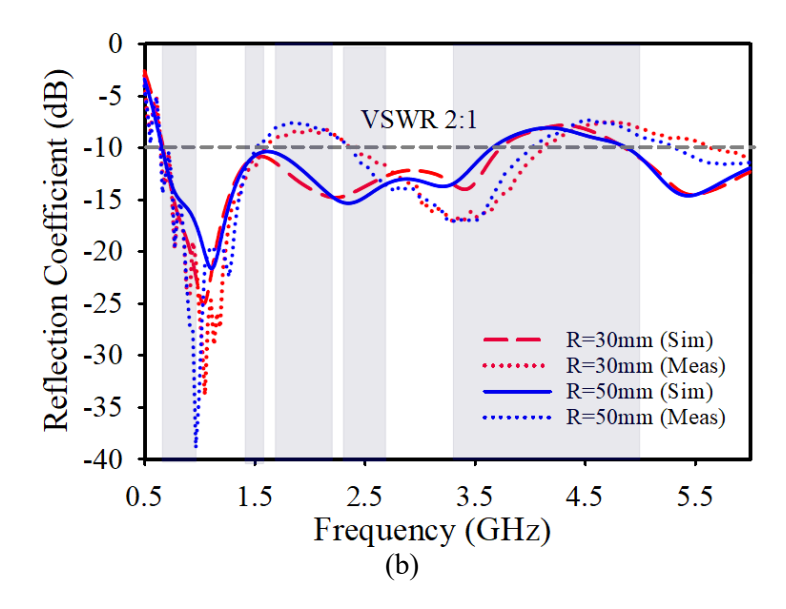


Figure 7.6. (a) Simulated reflection coefficient with different bending conditions vs reflection coefficient in flat condition (b) Simulated vs measured reflection coefficient in bending conditions.

The performance of the circular patch antenna near the human body was analysed, as shown in Figure 7.7. Despite a slight upward frequency shift due to the influence of the human body, the antenna demonstrated satisfactory resonance performance with a bandwidth covering the desired sub-6 GHz frequencies for the single-element circular patch design, as illustrated in Figure 7.8. During the analysis, a consistent distance of 5 mm was maintained between the human model and the antenna to account for the SMA connector positioning and ensure user safety.

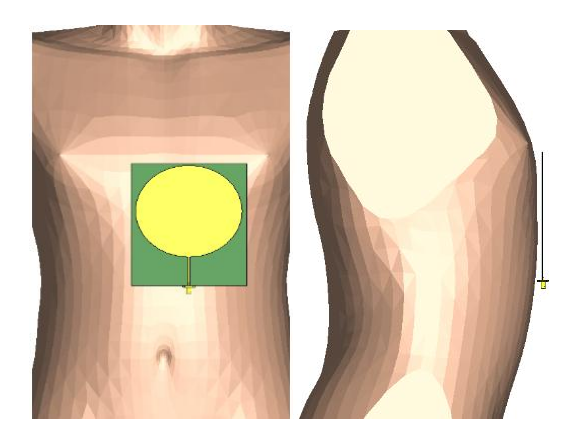


Figure 7.7. Simulated antenna near human body model in computation software.

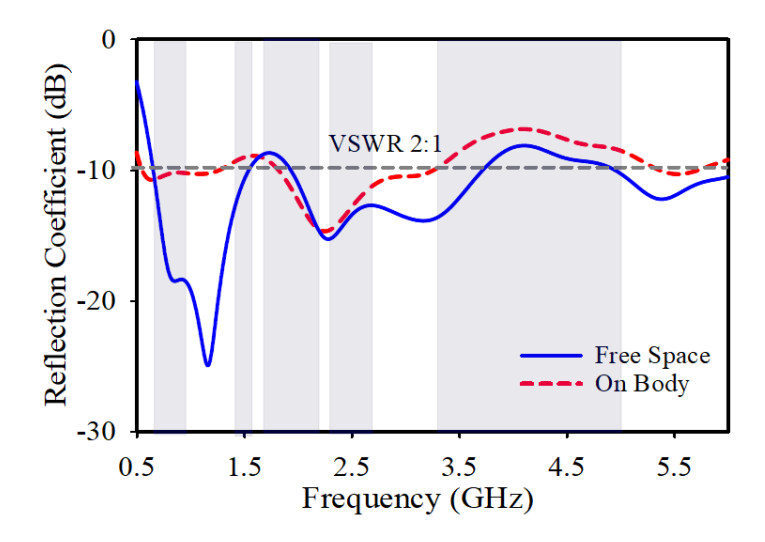


Figure 7.8. Simulated S-parameters for on-body condition.

SAR analysis was performed to ensure user safety using same input power like previous, and values were found to be within safety limits throughout the entire bandwidth and tabulated in Table 7.2. As a result, the antenna can be concluded to be safe to use on the human body.

Table 7.2 SAR Values for Circular Patch Single Port Antenna

Frequency (GHz)	SAR Values (W/Kg)
0.5	1.063
1.0	0.273
1.5	0.345
2.0	0.410
2.5	0.470
3.0	0.596
3.5	0.630
4.0	0.589
4.5	0.614
5.0	0.762

Similar to antipodal, two-port achieving similar ultra-wideband (UWB) coverage as the single-port patch antenna will be major concern for circular patch. For the purpose, a shared radiator multiport antenna with dual ports was simulated, optimized, and evaluated. Adopting a shared radiator approach instead of multiple radiators facilitates a more compact antenna structure. The flow of the design has been presented in Figure 7.9 whereas the final shared radiator antenna presented in Figure 7.10.

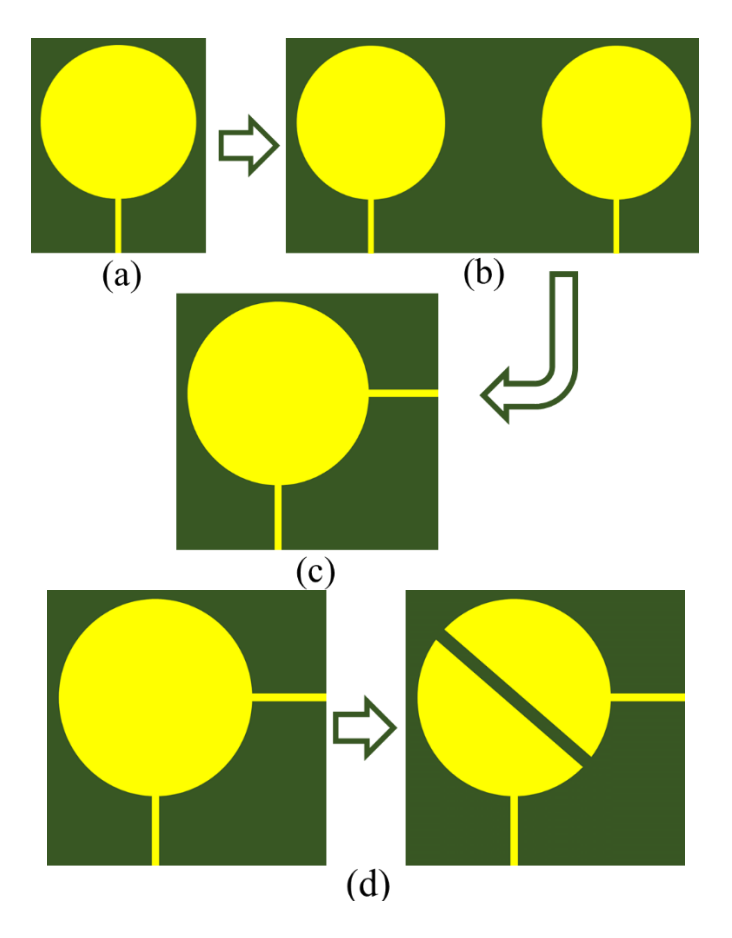


Figure 7.9. Antenna designing steps from (a) Single antenna to (b) Two port two element/ radiator antenna to (c) Shared radiator two port antenna and afterward (d) Inserting slot in the radiator.

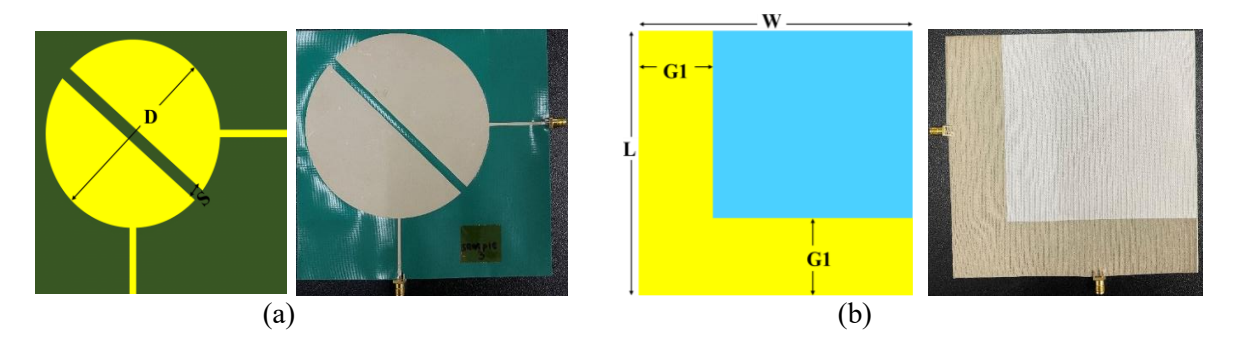


Figure 7.10. Simulated and fabricated finalized two-port circular patch antenna (a) Front view (b) Rear view.

The comparison of scattering parameter results between the single-element antenna, two-element two-port antenna, and shared radiator two-port antennas is showed in Figure 7.11. It is inferred from the figure that with the shared radiator structure, enhanced reflection coefficient performance has been achieved, and the antenna resonance bandwidth not only covering sub-6 GHz 5G band frequencies less 1 GHz but also covers the entire sub-6 GHz 5G frequencies. Thus, the shared radiator antenna not only reduces the overall size but also significantly enhances resonance performance by covering all the desired frequency bands that the previous two-element antenna failed to achieve. This makes the shared radiator design the most promising antenna structure among all configurations explored.

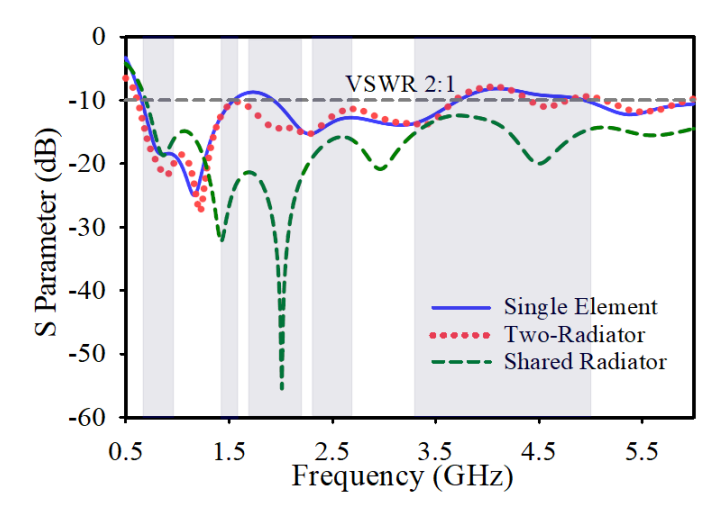
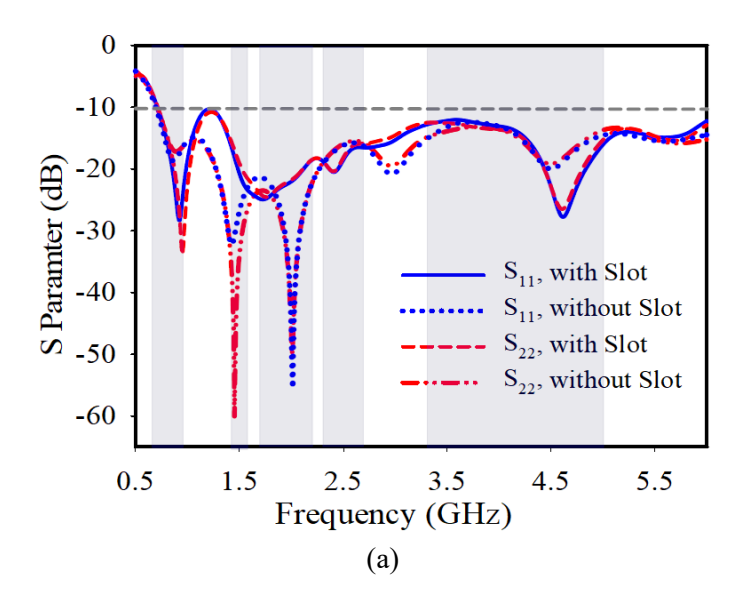


Figure 7.11. Simulated antenna performance S_{11} , single antenna vs shared two-port antenna.

After evaluating the shared radiator multiport antenna structure, a new concern arose regarding the high mutual coupling (particularly toward lower frequencies of the resonance bandwidth) due to the two ports sharing the same radiator. To mitigate this issue, a slot was introduced in the radiating patch. A comparison of mutual coupling before and after including the slot is presented in Figure 7.12 (b), showing a significant reduction in mutual coupling after the slot insertion. Before the slot inclusion, mutual coupling was notably higher, especially in lower bands, hence after the slot insertion, mutual coupling remained under -10 dB across the entire bandwidth. Hence, the insertion of the slot altered the reflection coefficient performance; however, the slot-included antenna maintained satisfactory reflection coefficient characteristics and resonance bandwidth coverage across the desired sub-6 GHz frequencies, as illustrated in Figure 7.12 (a). This makes the antenna structure the optimized design choice.



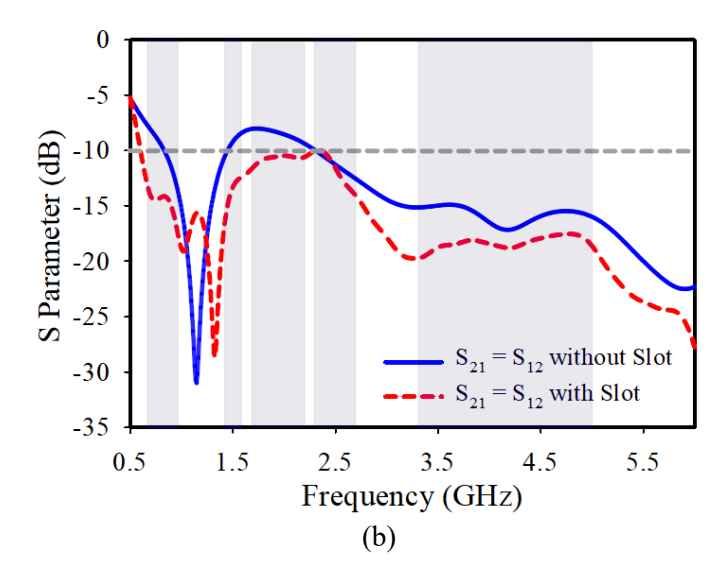


Figure 7.12. (a) S_{11} and S_{22} in two-port (before and after adding slot) (b) S_{21} and S_{12} in two-port antenna (before and after adding slot).

All the S parameters are presented together in Figure 7.13 and Figure 7.14 shows simulation vs measured s-parameters. From Figure 7.14, the simulation and measurement are compatible with each other and due to fabrication error little shifting is observed but the antenna is covering resonance frequency bands of interest in both simulation and measurement.

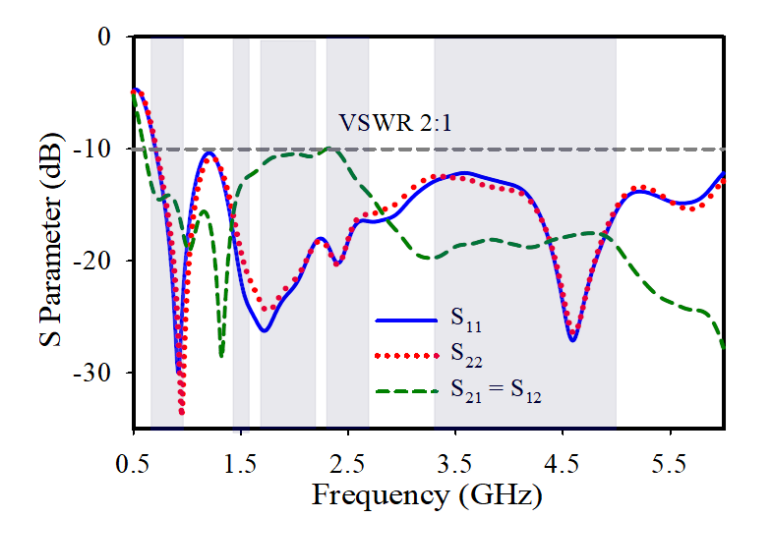


Figure 7.13. Simulated S-parameters in two port circular patch S_{11} , S_{22} , S_{21} , and S_{12} .

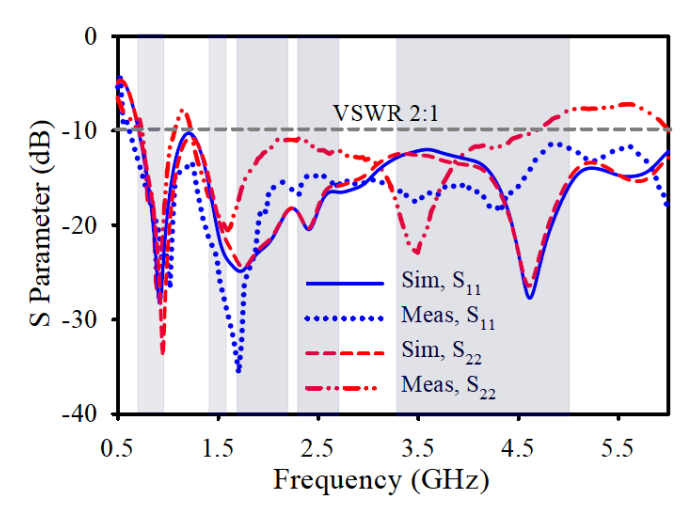
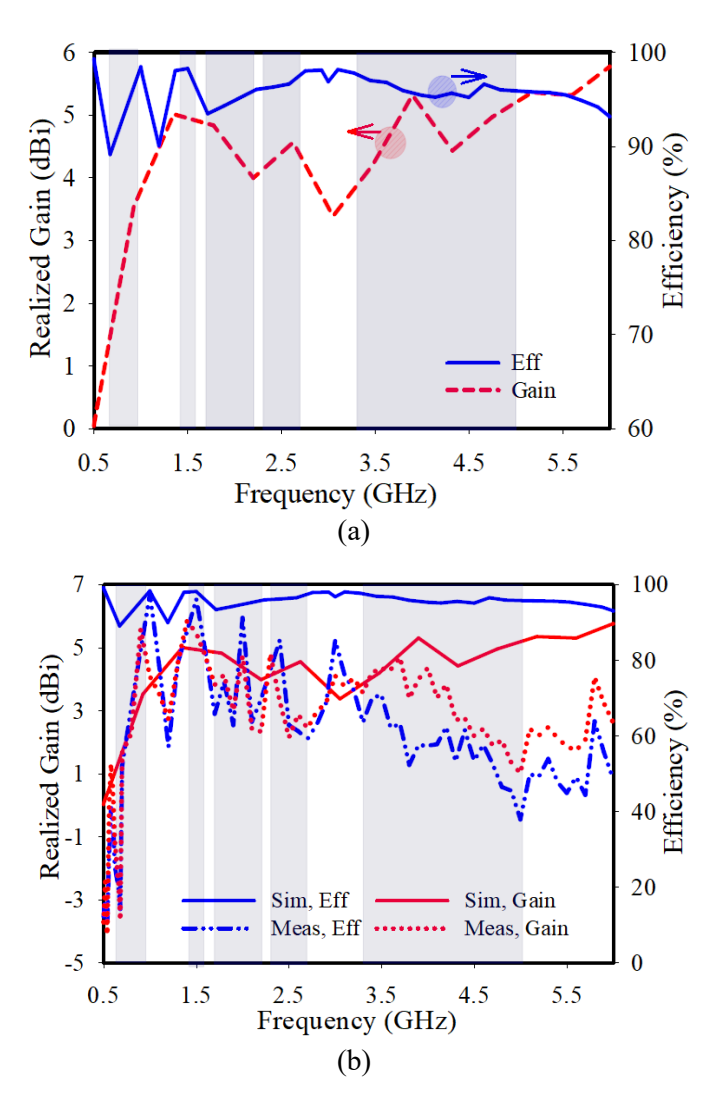


Figure 7.14. Simulated and measured S-parameters in two-port circular patch, S₁₁ and S₂₂.

Figure 7.15 presents the simulated gain and efficiency of the antenna. The results indicate satisfactory performance across the entire resonance bandwidth, with a maximum efficiency of 95.4% and a maximum gain of 5.42 dBi. Measured efficiency and gain has been presented in Figure 7.15 (b) and 7.15 (c) for port 1 and port 2, respectively. The performance was found compatible with simulation.



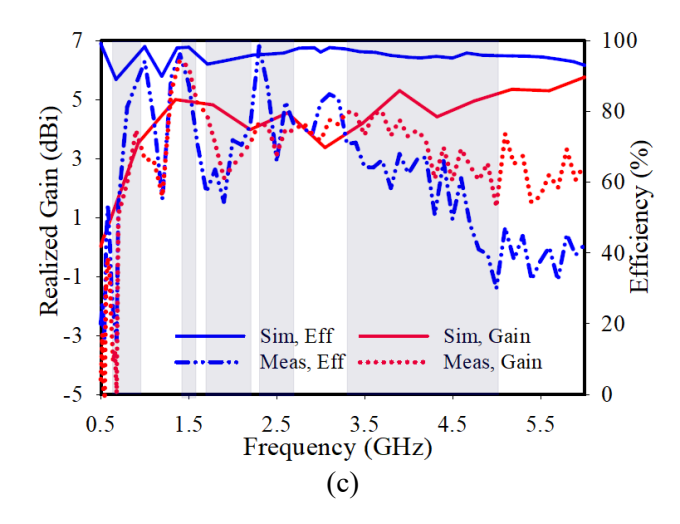


Figure 7.15. (a) Simulated efficiency and gain; simulated vs measured efficiency and gain (b) Port 1 (c) Port 2.

Bending condition tests were conducted in both simulation and measurement, with the simulation setup illustrated in Figure 7.16 and the measurement setup shown in Figure 7.17. Figure 7.18 (a) presents the antenna's resonance performance under different bending conditions compared to the flat condition. The results indicate satisfactory performance, as the antenna maintains a similar pattern to the flat condition, with only a mild upward shift attributed to bending. These results demonstrate that the antenna structure can maintain resonance across all required frequency bands, even under bending conditions. The measurement results, compared with the simulation, are depicted in Figure 7.18 (b). The measurement performance aligns well with the simulation, though a moderate leftward shift is observed in the high-frequency range. This shift is attributed to fabrication processes and the influence of the cylinder material used in the measurement setup. In the gain and efficiency measurement slightly lower than simulation was attained for similar issues, still the simulation and measurement results are compatible.

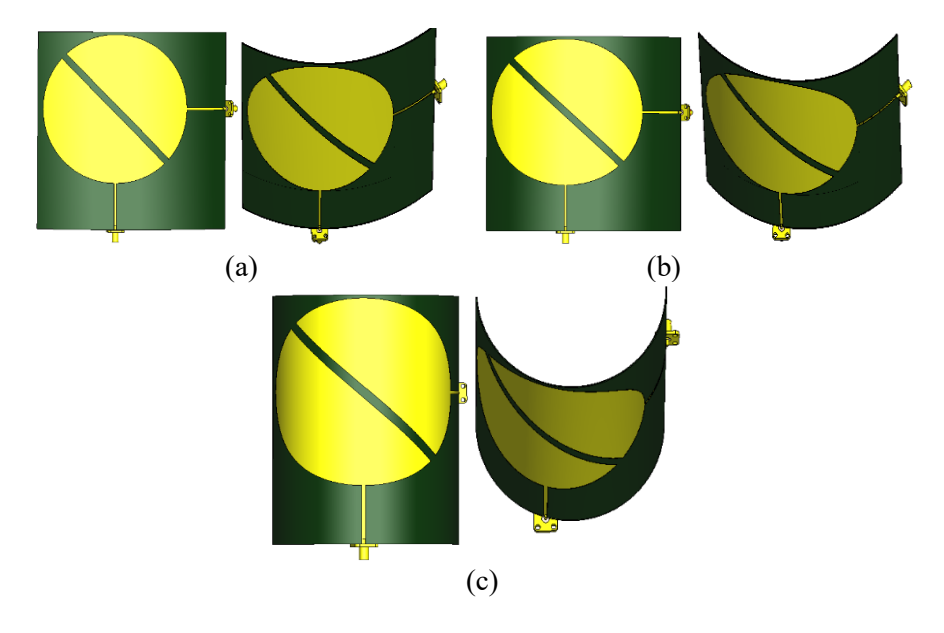


Figure 7.16. Antenna in different bending position with different cylinder radius for bending (a) 150mm (b) 100mm (c) 50mm.

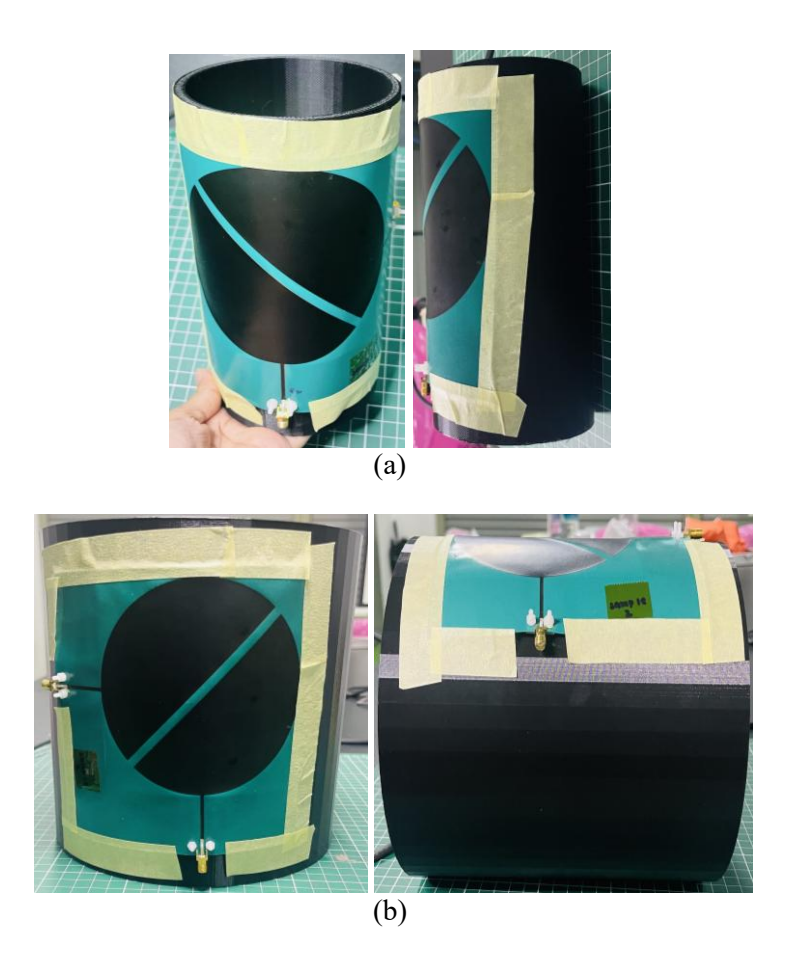
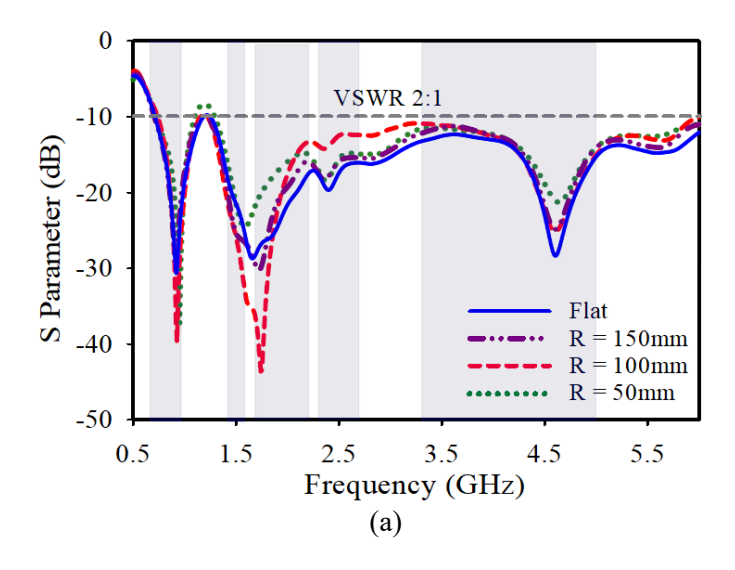


Figure 7.17. Circular patch single port antenna measurement arrangement at bending radius (a) 50 mm (b) 100 mm.



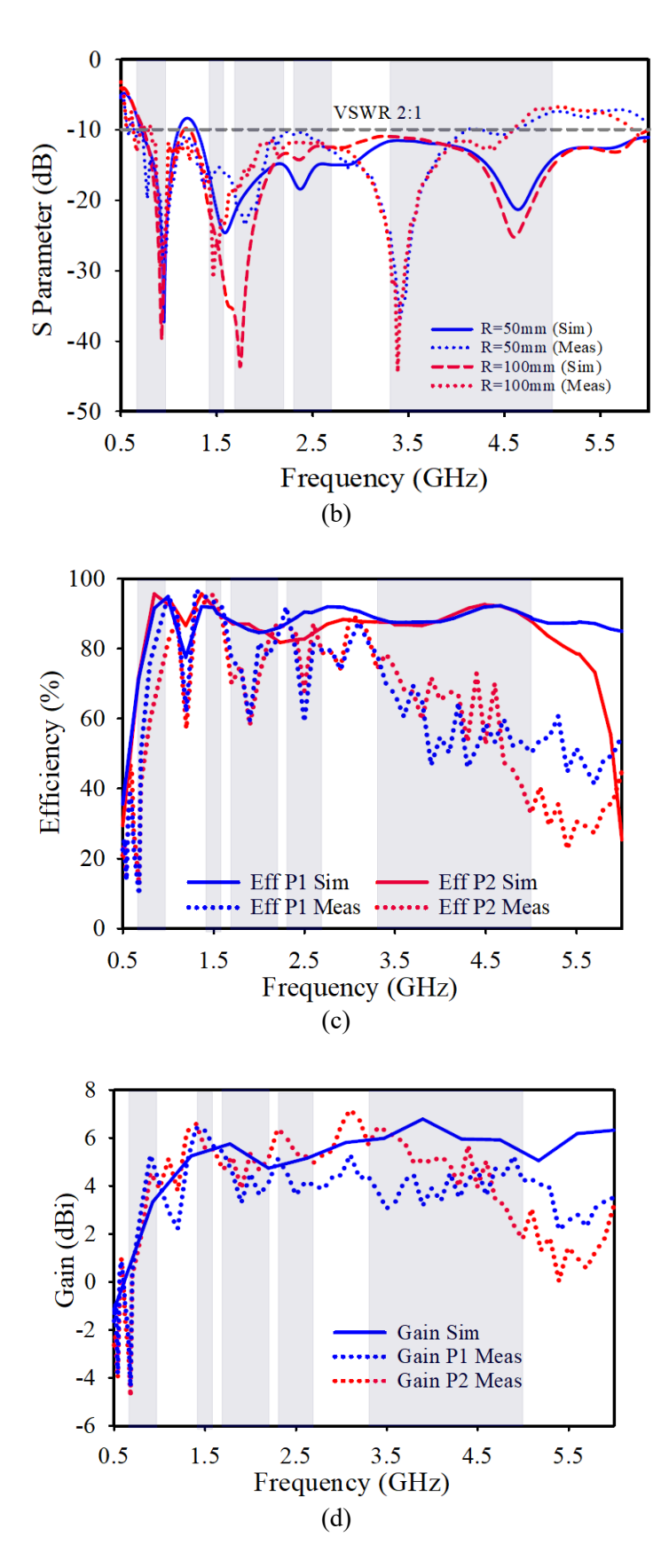


Figure 7.18. (a) Simulated reflection coefficient with different bending conditions vs reflection coefficient in flat condition (b) Simulated vs measured reflection coefficient in bending conditions; simulated vs measured (c) Efficiency (d) Gain.

The performance of the circular patch antenna near the human body was analysed, as shown in Figure 7.19. The antenna demonstrated satisfactory resonance performance, with minor upward shifting and slight pattern changes due to the influence of the human body, as illustrated in Figure 7.20 (a). Additionally, lower mutual coupling was achieved in the presence of the human model. During the analysis, a consistent distance of 5 mm was maintained between the human model and the antenna to account for SMA connector positioning and ensure user safety. Figure 7.20 (b) portrays the measurement result with simulation and found to be compatible with each other.

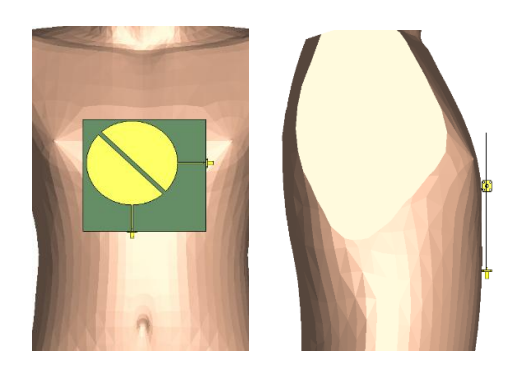


Figure 7.19. On-body analysis simulation set-up.

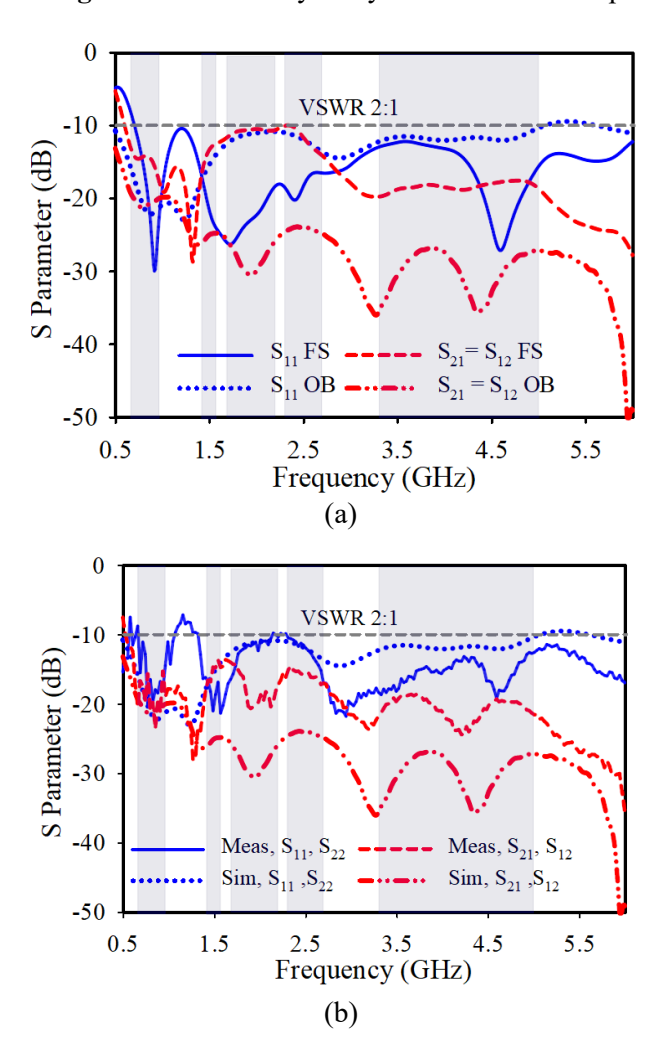


Figure 7.20. (a) Simulated on-body vs free space s-parameters (b) Simulated vs measured s parameters.

8. ANALYSIS OF BENDING AND HUMAN BODY EFFECTS OF COMPACT FULL FLEXIBLE ANTIPODAL VIVALDI ANTENNA FOR 3.5 GHZ IN 5G SUB-6 GHZ WEARABLE APPLICATIONS

In the search for ubiquitous connectivity, the increasing demand for fifth generation (5G) wireless technology has sparked innovation across various sectors, such as biomedical, healthcare, sports, military, smart display, radar, 5G communication, WBAN, WLAN, IoT, Satellite, UHF RFID, tracking, navigation, remote computing, wearable applications, etc [31]. Among the numerous challenges in this domain, the design of compact, flexible antennas capable of operating effectively across the sub-6 GHz spectrum stands as a paramount concern. In this context, the antipodal Vivaldi antenna emerges as a promising contender, offering versatility, compactness, and broadband capabilities crucial for 5G-enabled wearable devices [32].

This research explained an in-depth analysis of the bending conditions and effect of the antenna when placed near the human body, specifically for sub-6 GHz 5G wearable applications. Bending and crumpling introduce mechanical stress, potentially altering the antenna's electrical properties, gain, efficiency, and radiation pattern, which leads to impedance mismatch and signal loss [33]. This can cause changes in the electromagnetic fields around the antenna, resulting in changes to its radiated power and directionality. Moreover, the human body, with its varying dielectric properties and proximity effects, can significantly influence antenna performance [34].

8.1 Antenna Bending and On-body Analysis

Figure 8.1 (a) and (b) show the front and rear side view of the fabricated antipodal Vivaldi antenna, designed using a 100 % polyester substrate with a dielectric constant of 1.34, a loss tangent of 0.005, and a thickness of 0.4 mm, whereas Figure 8.1 (c) shows the measurement setup using a vector network analyzer (VNA; model: E5071C) in the UniMAP laboratory. All the design procedures, parameters and measurement results have been explained more detail in previous work [32]. The total antenna dimensions (i.e. substrate dimensions, $SL \times SW \times ST$) are $33 \times 33 \times 0.4 \text{ mm}^3$.

As this antenna is going to be used in wearable purpose, it is very important to observe antenna's performance under different bending conditions. The antenna is placed upon a cylinder and by varying the radius or angle of the cylinder with reference to the UV-plane, we can bend the antenna with different angles. Figure 8.2 shows the antenna structures with different bending angles from 20° to 120° in both horizontal (H) and vertical (V) directions, whereas Figure 8.3 represents the effect of bending of antipodal Vivaldi antenna on reflection coefficient with different angles in both directions. As the bending angle increases from 20° to 120° in horizontal and vertical directions, resonance shifts towards positive frequencies along with bit degradation in bandwidth. Although, minimal degradation in performance, still it is within required bands, which shows the antenna's function ability under bending conditions. An on-body analysis of the antenna has been performed on different body parts using a homogeneous human model from CST studio, as shown in Figure 8.4. The wideband characteristic of the antenna is very important for less detuned effect on the antenna operational frequency in the presence of body. At first the antenna was placed on chest and back and started varying the gap (x) between the body and the antenna. Even after placing at 10 mm distance, the antenna's performance did not match with the requirement, this is because of the large surface area as compared to small sized antenna. Then the antenna is placed upon arm and started varying the gap (x).

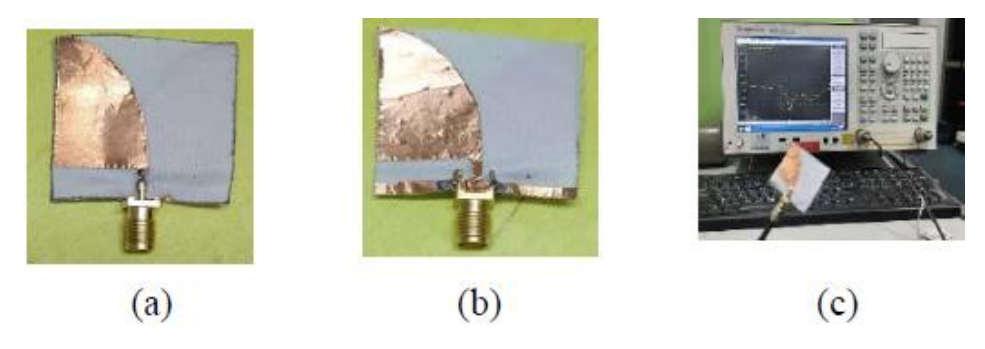


Figure 8.1. Flexible antipodal Vivaldi antenna (a) Front (b) Back side of fabricated antenna (c) Measurement set up.

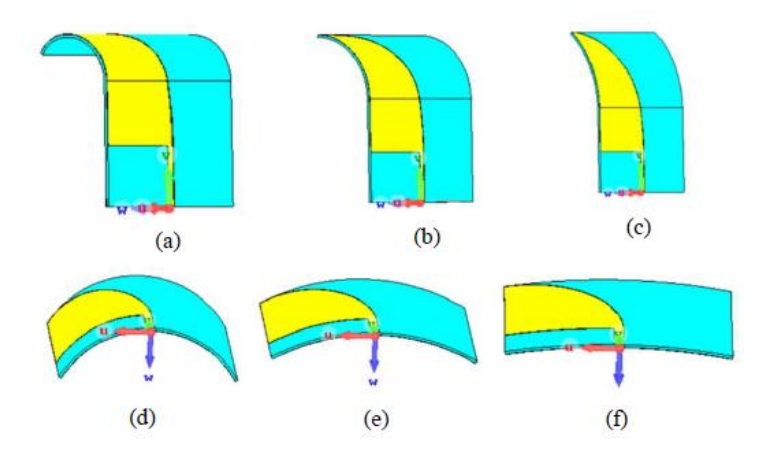


Figure 8.2. Different bending angles of proposed antenna (a) 120° (b) 60° (c) 20° in vertical direction (d) 120° (e) 60° (f) 20° in horizontal direction.

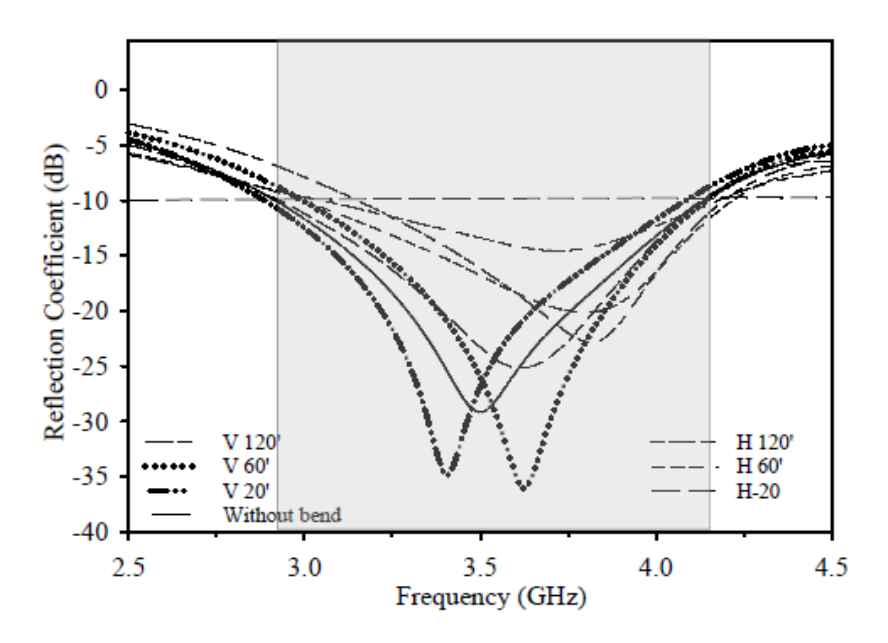


Figure 8.3. Simulated reflection coefficient with its effect in different bending angles in Horizontal (H) and Vertical (V) directions.

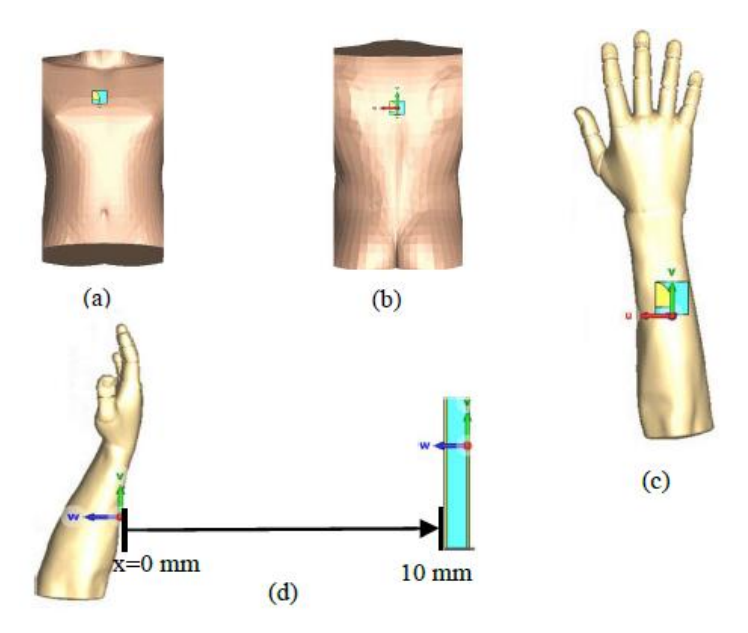


Figure 8.4. Placement of antenna with different body parts (a) Chest (b) Back (c) Arm (d) Gap between arm and antenna, x=0, indicates the antenna is very close to the arm.

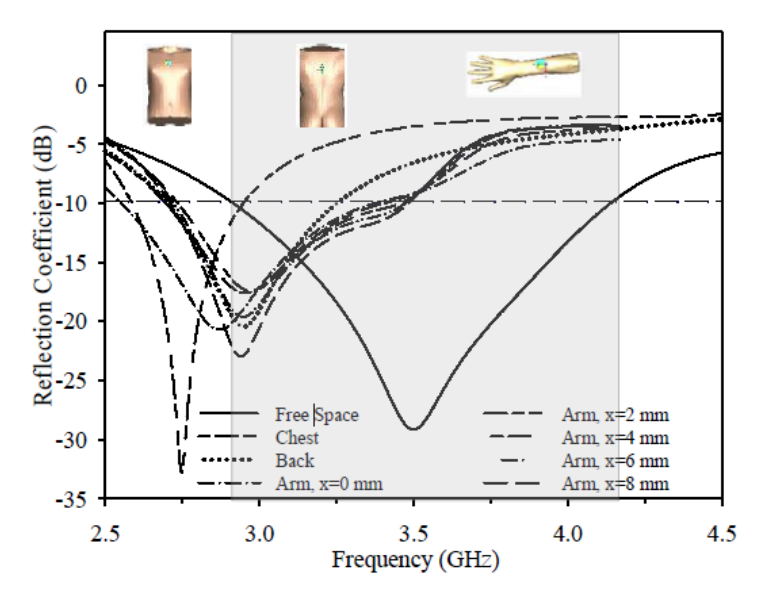


Figure 8.5. Simulated reflection coefficient on different places of body along with in free space.

Figure 8.5 shows the reflection coefficient plot of the antenna with different body parts, along with its effect when placed at specific distances from the arm, it depicts when the antenna is at least 2 mm far away from the arm, its performance maintained. This paper proposes a flexible antipodal Vivaldi antenna for 5G wearable applications. It uses a polyester fabric substrate with a low dielectric value and operates at 3.5 GHz, with a bandwidth of 34.9% (1.224 GHz). Finally, bending, and on body analysis have been proposed. These indicates the antenna's suitability for wearable applications in the 5G n77 and n78 bands. Radiation pattern, gain, efficiency and on body measurements for this design will be investigated in the future.

9. COMPACT FULL FLEXIBLE VIVALDI ANTENNA FOR 3.5 GHZ WEARABLE APPLICATIONS

As technologies are getting more advanced, the demand for high-speed internet is increasing rapidly. The fifth generation of wireless networks (5G) is set to revolutionize the world, offering faster data transfer rates, low latency, and increased connectivity. To make this possible, antennas play a critical role in ensuring efficient and reliable communication [35]. In wireless communication, transfer of data at high rates requires larger bandwidth. Vivaldi Antenna technology, which is considered as one of the most promising solutions for 5G applications and its unique design allows for a wide frequency range and excellent performance in a compact wearable form factor. Low cross polarization, high gain, high efficiency, flexibility, and lightweight nature make it ideal for use in various applications, such as Radar and microwave imaging [36][37], healthcare [38], smart watch for IoT [35], virtual reality, and transportation [39]. Commonly used rigid substrates like FR4, Rogers are not suitable for wearable purposes, so a flexible and elastic antenna made up of wearable substrates like polyester, denim, cotton, Felt, and TPU is the substitute.

9.1 Antenna Performance Analysis, Results, and Discussion

Figure 9.1 (b), and 1 (c) shows the front and rear side view of the fabricated antenna, respectively. Copper tape has been used as the conductive material to design the antenna and ground. A 50Ω SMA connector is attached to the microstrip feedline using a lead solder. Figure 9.1 (d) shows the measurement setup using a vector network analyzer (VNA; model: E5071C) in the UniMAP laboratory. Figure 9.2 (a) on the other hand shows the simulated, and measured reflection co-efficient (dB) results for the Vivaldi antenna, which resonates at 3.5 GHz, with a return loss of -55 dB, and a -10 dB bandwidth above 2 GHz.

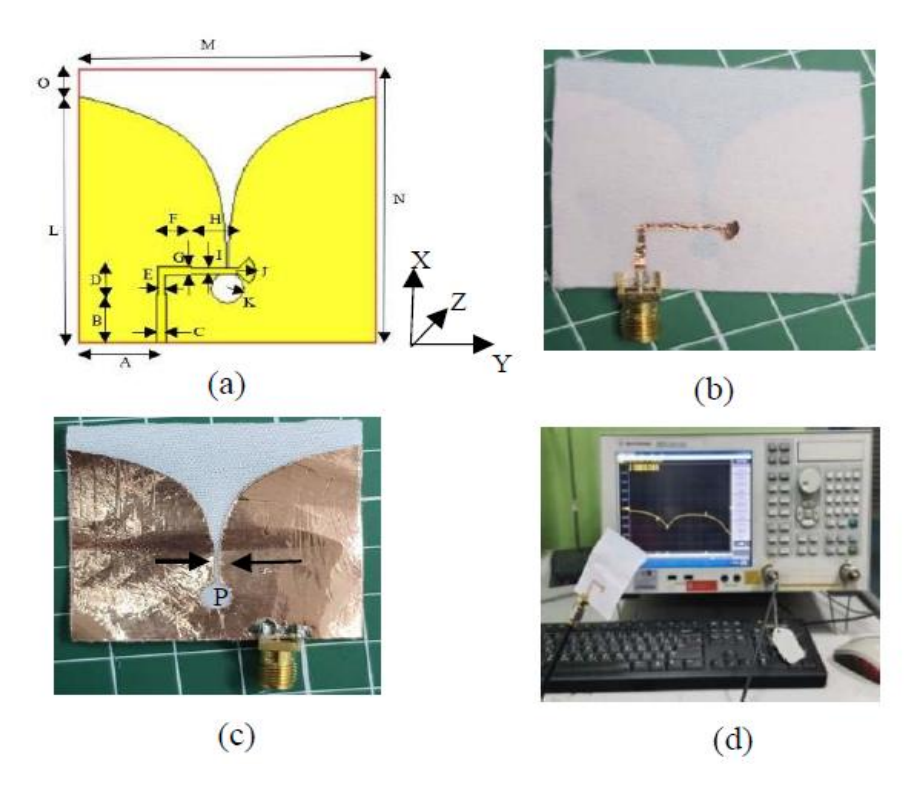
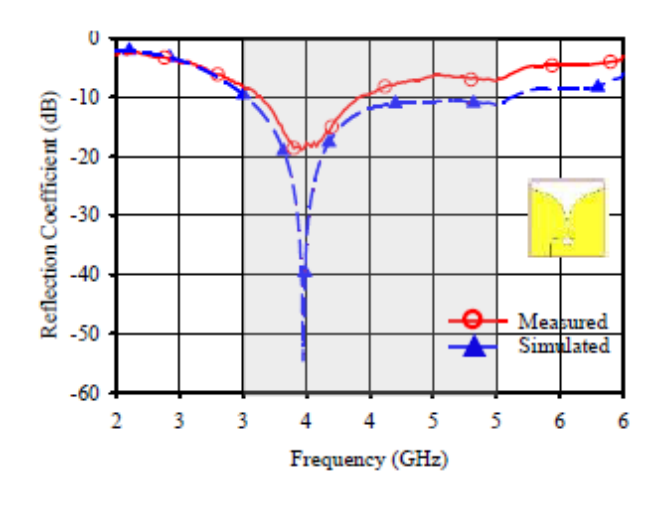
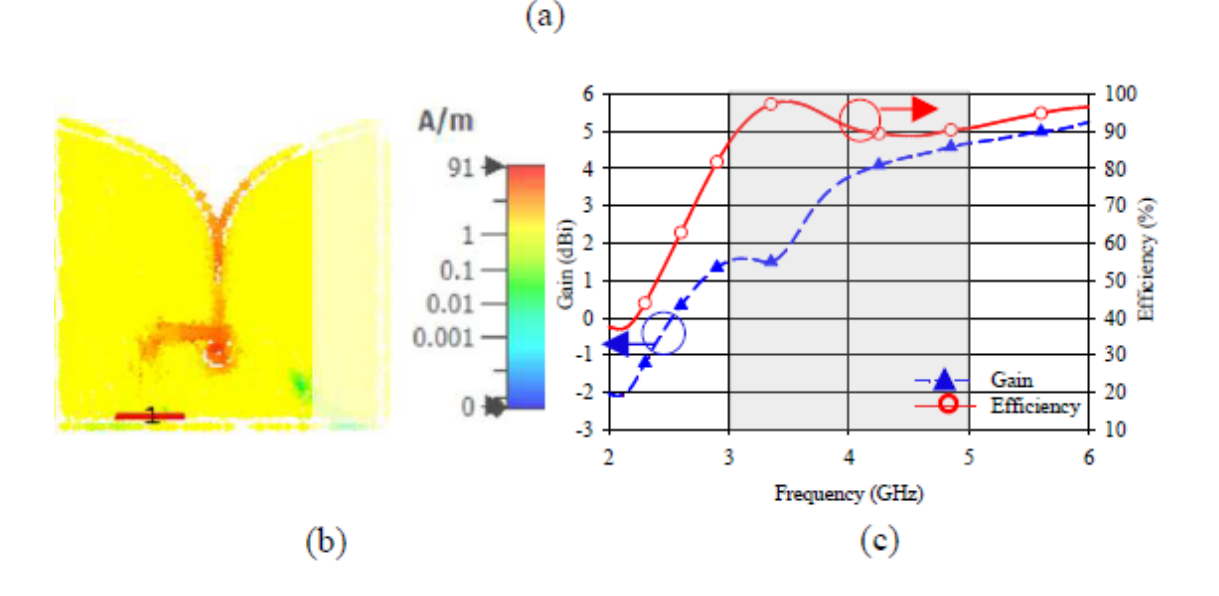


Figure 9.1. (a) Geometry of Vivaldi antenna with all parameters, fabricated antenna (b) Front view (c) Rear view (d) Measurement setup.

Figure 9.2 (b) depicts the current surface density at 3.5 GHz. At the edges of the antenna, these currents are considerably larger compared to the other area on the radiating plane. In addition, the gain, and efficiency of 2 dBi, and 98 %, respectively achieved at desired resonance, are illustrated in Figure 9.2 (c). Moreover, as the frequency increases, the gain increases, and attains a maximum value of 4.7 dBi at 5 GHz, as seen in Figure 9.2 (c). Figures 9.2 (d) and (e) show the radiation patterns for XZ-plane and XY-plane, respectively. The radiation signal in XZ-plane achieves a maximum magnitude of 1.55 dBi at 116°, with a 3 dB angular width of 317.6°.

On the other hand, the radiation signal in XY-plane achieves a main lobe magnitude of 1.54 dBi at 0°, with an angular width (3 dB) of 195.1°, with a side lobe level of -3.1 dB. After measuring the S-parameter the antenna resonates at 3.5 GHz with a reflection coefficient of -18 dB, the shift of reflection coefficient and decrease in bandwidth is due to fabrication tolerance, which can be seen in Figure 9.2 (a).





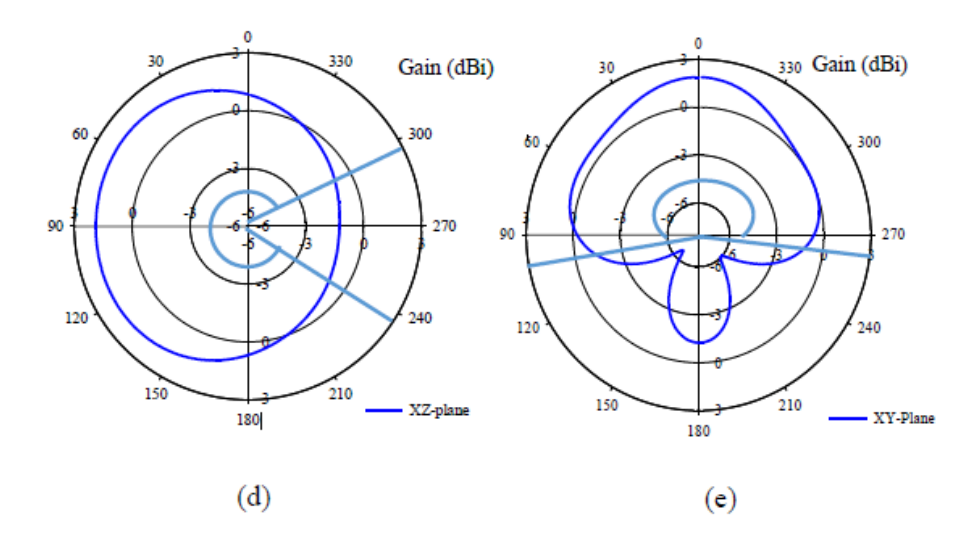


Figure 9.2. (a) Simulated and measured reflection coefficient, simulated (b) Surface current density (c) Gain and efficiency (d) XZ-plane (c) XY-plane radiation pattern.

10. CONCLUSION

The major motivation of this research work is to design and develop antennas for wearable sub-6 GHz 5G applications. The primary challenge is to design antenna that exhibits a wideband performance covering all the sub-6 GHz frequencies on a wearable textile material (polyester). An additional dielectric layer called TPU (Thermoplastic polyurethane) was placed over polyester for long-term durability and suitability for industrial applications. Tunning was performed on antenna parameters to adjust the antenna performance with the new dielectric material (TPU). Later, modifications were done to the antenna structure as well to enhance antenna resonance performance. The 134×96×0.89 mm³ antenna shows resonance bandwidth covering all the sub-6 GHz 5G frequencies over 1 GHz. Besides, the antenna shows excellent performances in terms of efficiency and gain as well (simulation), with a maximum efficiency of 96.90 percent and a maximum gain of 5.65 dBi. Then, from the single-element structure. designing moved toward a two-element structure (265×98×0.89 mm³) where the antennas are fed in opposite directions to reduce the mutual coupling. The two-element antenna shows a satisfactory resonance (covering all the sub-6 GHz 5G frequencies over 1 GHz), efficiency (maximum 98 percent), and gain (maximum 5.4 dBi) similar to the single-element while maintaining a satisfactory mutual coupling as well.

Besides, since the antenna is wearable, the on-body antenna performance has been investigated as well, and the antenna resonance showed some shifting due to the impact of the human body. Even though some shifting has been noticed, the antenna still showed resonance bandwidth covering all the sub-6 GHz 5G frequencies over 1 GHz. The bending performance has been analyzed, too under different bending angles, and the antenna showed satisfactory performance. Additionally, SAR is also determined for the design to ensure the safety of the wearer. Throughout the entire bandwidth, SAR values were found to be within the safety limit (i.e., under 2W/kg per 10g of tissue).

Although the antipodal antenna showed excellent performance bandwidth, sub-6 GHz 5G frequencies under 1 GHz still could not be achieved, and as a result, another antenna is designed to incorporate into the t-shirt, and the shirt will be able to access all the sub-6 GHz frequencies. For this purpose, a circular patch antenna sized 124×153×0.89 mm³ has been proposed to ensure the resonance bandwidth under 1 GHz. The antenna is successfully resonating with a bandwidth from 0.655 GHz to 1.54 GHz covering the sub-6 GHz 5G Bands under 1 GHz with satisfactory gain and efficiency. While shifting toward two-port antenna, the shared radiator technique has been utilized to make the antenna compact and to achieve enhanced performance as well. Afterward, a slot was included in the radiating patch to reduce the mutual coupling since both ports were sharing the same radiator. The shared radiator antenna not only just covered the bands under 1 GHz but also included all the sub-6 bands under its resonance band while maintaining an acceptable mutual coupling. As a result, the design can be chosen as the finalized two-port design. The antenna exhibits excellent performance in terms of bandwidth, efficiency (maximum 95.4 percent), and gain (maximum 5.42 dBi).

The antenna exhibits excellent resonance while placed near the human body as well as still being able to cover all the required frequencies. Antenna performance has also been investigated under bending conditions, and satisfactory performance could be achieved. Besides, SAR has been determined, and throughout the entire bandwidth, values were found under 2W/kg per 10g of tissue, ensuring the safety of the wearer.

REFERENCES

- [1] M. El Atrash, M. A. Abdalla, and H. M. Elhennawy, "A wearable dual-band low profile high gain low SAR antenna AMC-backed for WBAN applications," IEEE Transactions on Antennas and Propagation, vol. 67, no. 10, pp. 6378–6388, 2019.
- [2] P. K. Patnaik, M. Malijeddi, and D. C. Panda, "Wearable microstrip patch antenna for disease detection and WiMAX application," 2021 2nd International Conference on Range Technology (ICORT), 2021.
- [3] T. Le and T.-Y. Yun, "Wearable dual-band high-gain low-SAR antenna for off-body communication," IEEE Antennas and Wireless Propagation Letters, vol. 20, no. 7, pp. 1175–1179, 2021.
- [4] J.-P. Xu, L.-J. Xu, L. Ge, Z. Duan, and Y.-M. Tang, "Flexible wearable antenna based on MIMO technology," 2019 IEEE MTT-S International Wireless Symposium (IWS), 2019.
- [5] G. P. Gao, C. Yang, B. Hu, R. F. Zhang, and S. F. Wang, "A wearable PIFA with an all-textile metasurface for 5 GHz WBAN applications," IEEE antennas and wireless propagation letters, 18(2), 288-292, 2018.
- [6] G. P. Gao, B. Hu, S. F. Wang, & C. Yang, "Wearable circular ring slot antenna with EBG structure for wireless body area network," IEEE Antennas and Wireless Propagation Letters, 17(3), 434-437, 2018.
- [7] H. Li, S. Sun, B. Wang and F. Wu, "Design of compact singlelayer textile MIMO antenna for wearable applications," IEEE Transactions on Antennas and Propagation, 66(6), 3136-3141, 2018.
- [8] T. T. Le and T. Y. Yun, "Wearable dual-band high-gain low- SAR antenna for off-body communication," IEEE Antennas and Wireless Propagation Letters, 20(7), 1175-1179, 2021.
- [9] H. A. Mashagba, H. A. Rahim, I. Adam, M. H. Jamaluddin, M. N. M. Yasin, M. Jusoh,... and P. J. Soh, "A hybrid mutual coupling reduction technique in a dual-band MIMO textile antenna for WBAN and 5G applications," IEEE Access, 9, 150768-150780, 2021.
- [10] C. Hertleer, A. Tronquo, H. Rogier, and L. Van Langenhove, "The use of textile materials to design wearable microstrip patch antennas," Textile Research Journal, vol. 78, no. 8, pp. 651–658, 2008.
- [11] S. B. Roshni, M. P. Jayakrishnan, P. Mohanan, and K. P. Surendran, "Design and fabrication of an E-shaped wearable textile antenna on PVB-coated hydrophobic polyester fabric," Smart Materials and Structures, vol. 26, no. 10, p. 105011, 2017.
- [12] A. Khan and R. Nema, "Analysis of five different dielectric substrates on microstrip patch antenna," International Journal of Computer Applications, vol. 55, no. 14, pp. 40–47, 2012
- [13] Y. Li, R. Torah, S. Beeby, and J. Tudor, "Fully direct-write dispenser printed dipole antenna on woven polyester cotton fabric for wearable electronics applications," Electronics Letters, vol. 51, no. 17, pp. 1306–1308, 2015.
- [14] S.-H. Li, K.-A. Cheng, W.-H. Lu, and T.-C. Lin, "Developing an active emergency medical service system based on WiMAX Technology," Journal of Medical Systems, vol. 36, no. 5, pp. 3177–3193, 2011.
- [15] N. Ferdous, G. Chin Hock, S. Hamidah A.Hamid, M. N. Raman, T. Sieh Kiong, and M. Ismail, "Design of a small patch antenna at 3.5 GHz for 5G application," IOP Conference Series: Earth and Environmental Science, vol. 268, no. 1, p. 012152, 2019.
- [16] A. B. Dey, S. S. Pattanayak, D. Mitra, and W. Arif, "Investigation and design of enhanced decoupled UWB mimo antenna for wearable applications," Microwave and Optical Technology Letters, vol. 63, no. 3, pp. 845–861, 2020.

- [17] K. L. Wong, H. J. Chang, C. Y. Wang and S. Y. Wang, "Verylow- profile grounded coplanar waveguide-fed dual-band WLAN slot antenna for on-body antenna application," IEEE Antennas and Wireless Propagation Letters, 19(1), 213-217, 2019.
- [18] A. Y. Ashyap, Z. Z. Abidin, S. H. Dahlan, H. A. Majid, A. M. A Waddah, M. R. Kamarudin, ... & J. M. Noras, (2018). Inverted E-shaped wearable textile antenna for medical applications. IEEE Access, 6, 35214-35222.
- [19] Z. H. Jiang, & D. H. Werner, (2015). A compact, wideband circularly polarized codesigned filtering antenna and its application for wearable devices with low SAR. IEEE Transactions on Antennas and Propagation, 63(9), 3808-3818.
- [20] S. N. Mahmood, A. J. Ishak, T. Saeidi, H. Alsariera, S. Alani, A. Ismail, & A. C. Soh, (2020). Recent advances in wearable antenna technologies: A review. progress in Electromagnetics Research B, 89, 1-27.
- [21] S. Purohit, & F. Raval, (2014). Wearable-textile patch antenna using jeans as substrate at 2.45 GHz. International Journal of Engineering Research & Technology (IJERT), 3(5).
- [22] G. Casu, C. Moraru, & A. Kovacs, (2014, May). Design and implementation of microstrip patch antenna array. In 2014 10th International Conference on Communications (COMM) (pp. 1-4). IEEE.
- [23] A. Gupta, A. Kansal, & P. Chawla, (2021). Design of a wearable MIMO antenna deployed with an inverted U-shaped ground stub for diversity performance enhancement. International Journal of Microwave and Wireless Technologies, 13(1), 76-86.
- [24] C. Mendes and C. Peixeiro, "A dual-mode single-band wearable microstrip antenna for body area networks," IEEE Antennas Wirel. Propag. Lett., vol. 16, pp. 3055–3058, 2017, doi: 10.1109/LAWP.2017.2760142.
- [25] T. T. Le and T.-Y. Yun, "Wearable Dual-Band High-Gain Low-SAR Antenna for Off-Body Communication," IEEE Antennas Wirel. Propag. Lett., vol. 20, no. 7, pp. 1175–1179, 2021.
- [26] Y. Jandi, F. Gharnati, and O. S. Ahmed, "Design of a compact dual bands patch antenna for 5G applications," in 2017 International Conference on Wireless Technologies, Embedded and Intelligent Systems (WITS), 2017, pp. 18–21. doi: 10.1109/WITS.2017.7934628.
- [27] S. Afroz, A. A. Al-hadi, S. N. Azemi, and W. F. Hoon, "A 3.5 GHz Wearable Antipodal Vivaldi Antenna for 5G Applications," 2023 IEEE Int. Symp. Antennas Propag., vol. 4, no. c, pp. 1–2, 2023, doi: 10.1109/ISAP57493.2023.10388737.
- [28] S. Sankaralingam, S. Dhar, and B. Gupta, "Performance of Fully Fabric Wearable Circular Patch Antennas in the Vicinity of Human Body at 2.45 GHz," in "2013 International Symposium on Electromagnetic Theory," IEEE, 2013, pp. 179–184. doi: 10.1016/j.proeng.2013.09.089.
- [29] M. El Atrash, M. A. Abdalla, and H. M. Elhennawy, "A Wearable Dual-Band Low Profile High Gain Low SAR Antenna AMC-Backed for WBAN Applications," IEEE Trans. Antennas Propag., vol. 67, no. 10, pp. 6378–6388, 2019, doi: 10.1109/TAP.2019.2923058.
- [30] B. M. Mohammed et al., "Fabrication of a Wearable Antenna with Defected Ground Structure on a Flexible TPU-Polyester Substrate," in 2022 IEEE International RF and Microwave Conference, (RFM), 2022, pp. 22–25. doi: 10.1109/RFM56185.2022. 100647.
- [31] B. Hu, G. Gao, L. He, X. Cong, and J. Zhao, "Bending and On-Arm Effects on a Wearable Antenna for 2.45 GHz Body Area Network," IEEE ANTENNAS Wirel. PROPOAGATION Lett., vol. 15, pp. 378–381, 2016.

- [32] B. C. Sahoo et al., "Compact Wideband Wearable Antipodal Vivaldi Antenna for 5G Applications," in 2022 IEEE International RF and Microwave Conference (RFM), 2022, pp. 1–4. doi: 10.1109/RFM56185.2022.10064761.
- [33] A. Y. I. Ashyap et al., "Fully Fabric High Impedance Surface-Enabled Antenna for Wearable Medical Applications," IEEE Access, vol. 9, pp. 6948–6960, 2021, doi: 10.1109/ACCESS.2021.3049491.
- [34] N. I. Zaidi et al., "Analysis on Bending Performance of the Electro-Textile Antennas With Bandwidth Enhancement for Wearable Tracking Application," IEEE Access, vol. 10, pp. 31800–31820, 2022, doi: 10.1109/access.2022.3160825.

APPENDIX

COLLABORATION VISIT ACTIVITY REPORT – 29 APRIL 2024

NO	CRITERIA	DESCRIPTION
1.	COLLABORATOR	UniMAP- JABIL CIRCUIT SDN BHD – EMITS TECHNOLOGY SDN BHD
2.	NAME OF ACADEMIC STAFF	 PROJECT 1: PROFESSOR TS. DR. AZREMI ABDULLAH AL-HADI PROJECT 2: PROF. MADYA. TS. DR WEE FWEN HOON PROF. MADYA IR. TS. DR. SAIDATUL NORLYANA AZEMI PROF. MADYA TS. DR. SOH PING JACK DR. CHE MUHAMMAD NOR CHE ISA DR. SURENTIRAN PADMANATHAN
3.	NAME OF STUDENTS INVOLVED	SADIA AFROZ AINUR FASIHAH BINTI MOHD FAZILAH STUDENT
4.	NAME OF INDUSTRY'S COLLABORATORS	 ZAMBRI SAMSUDIN LIM LAI MING MUHAMMAD IRSYAD MOHD YUSUF FRANCIS TUNG LUN HAO YENSAN LOH SYAHIR
5.	ACTIVITY NAME	VISIT TO JABIL CIRCUIT AND EMITS
	DATE	29 APRIL 2024
	ACTIVITY DESCRIPTION	9.00 am: Arrived at Jabil Circuit 9.15 am: UniPRIMA progress meeting

5.00 pm: Meeting done and group photo taken (See **Figure 6**)





Figure 1. MoA (MTUN Matching Grant) signing.



Figure 2. Group photo.



Figure 3. Lunch at Bangkok Restaurant.



Figure 4. EMITS Technology Introduction presentation.

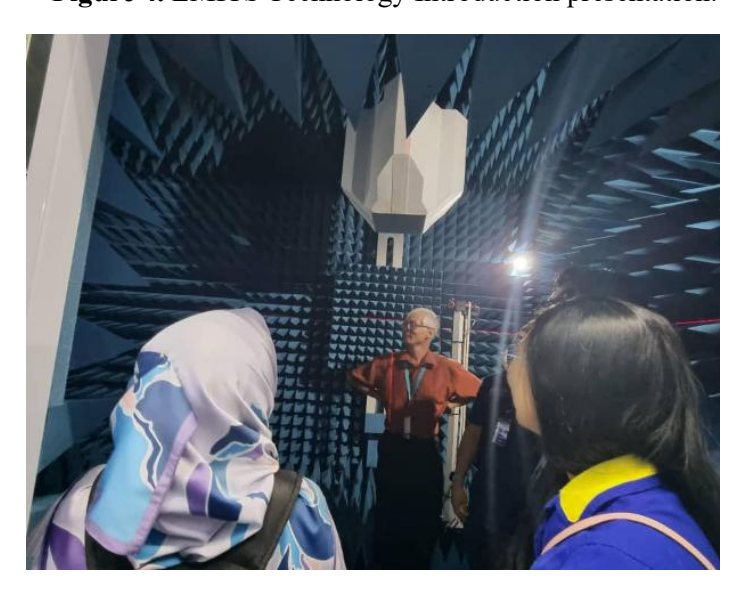


Figure 5. Visited to Antenna Measurement Chamber at EMITS

DESIGN AND DEVELOPMENT OF SMALL AND LARGE FORM FACTOR ON BODY ANTENNAS FOR SUB-6 GHZ 5G APPLICATIONS



Figure 6. Group photo (At EMITS).

COLLABORATION VISIT ACTIVITY REPORT – 23 JUNE 2024

NO	CRITERIA	DESCRIPTION
1.	LOCATION	EMITS TECHNOLOGY SDN BHD
2.	NAME OF ACADEMIC STAFF INVOLVE	 PROF. MADYA IR. TS. DR. SAIDATUL NORLYANA AZEMI DR. CHE MUHAMMAD NOR CHE ISA DR. SURENTIRAN PADMANATHAN
3.	NAME OF STUDENTS INVOLVED	SADIA AFROZ AINUR FASIHAH BINTI MOHD FAZILAH STUDENT
4.	NAME OF INDUSTRY'S STAFF INVOLVE	CS POR
5.	ACTIVITY NAME	ANTENNA MEASUREMENT AT EMITS
	DATE	23 JUNE 2024
	ACTIVITY DESCRIPTION	 9.00 am: Arrived at EMITS TECHNOLOGY 9.15 am: Antenna measurement and Discussion (See Figure 1) 5.00 pm: Meeting done and group photo taken (See Figure 2)





Figure 1. Antenna Measurement and Discussion.



Figure 2. Group photo.

COLLABORATION VISIT ACTIVITY REPORT – 8 AUGUST 2024

NO	CRITERIA	DESCRIPTION
1.	LOCATION	EMITS TECHNOLOGY SDN BHD
2.	NAME OF ACADEMIC STAFF INVOLVE	PROF. MADYA IR. TS. DR. SAIDATUL NORLYANA AZEMI DR. CHE MUHAMMAD NOR CHE ISA DR. SURENTIRAN PADMANATHAN
3.	NAME OF STUDENTS INVOLVED	1. SADIA AFROZ
4.	NAME OF INDUSTRY'S STAFF INVOLVE	CS POR
5.	ACTIVITY NAME	ANTENNA MEASUREMENT AT EMITS (6)
	DATE	8 AUGUST 2024
	ACTIVITY DESCRIPTION	10.00 am: Arrived at EMITS TECHNOLOGY 10.15 am: The team was welcomed and briefed by the staff on the setup and safety protocols for the Antenna measurement 10.30 am: Measurement activities O Conducted on-body measurements from 500 MHz to 6 GHz. The measurements were performed 3 different type antenna which are: [antipodal single-port, circular patch single-port, circular patch dual-port], and on body measurements. All necessary equipment and tools were provided by Emits Technology Sdn Bhd, and the process was overseen by the technical staff, Mr Por Chee Siong. 5.00 pm: Measurement activities II The measurements were successfully conducted without any major issues. Initial data analysis indicates sma
		connection with feedline required to be more secured. The equipment used was calibrated and functioning as expected. The visit was successful, with all planned measurements completed within the expected time frame.

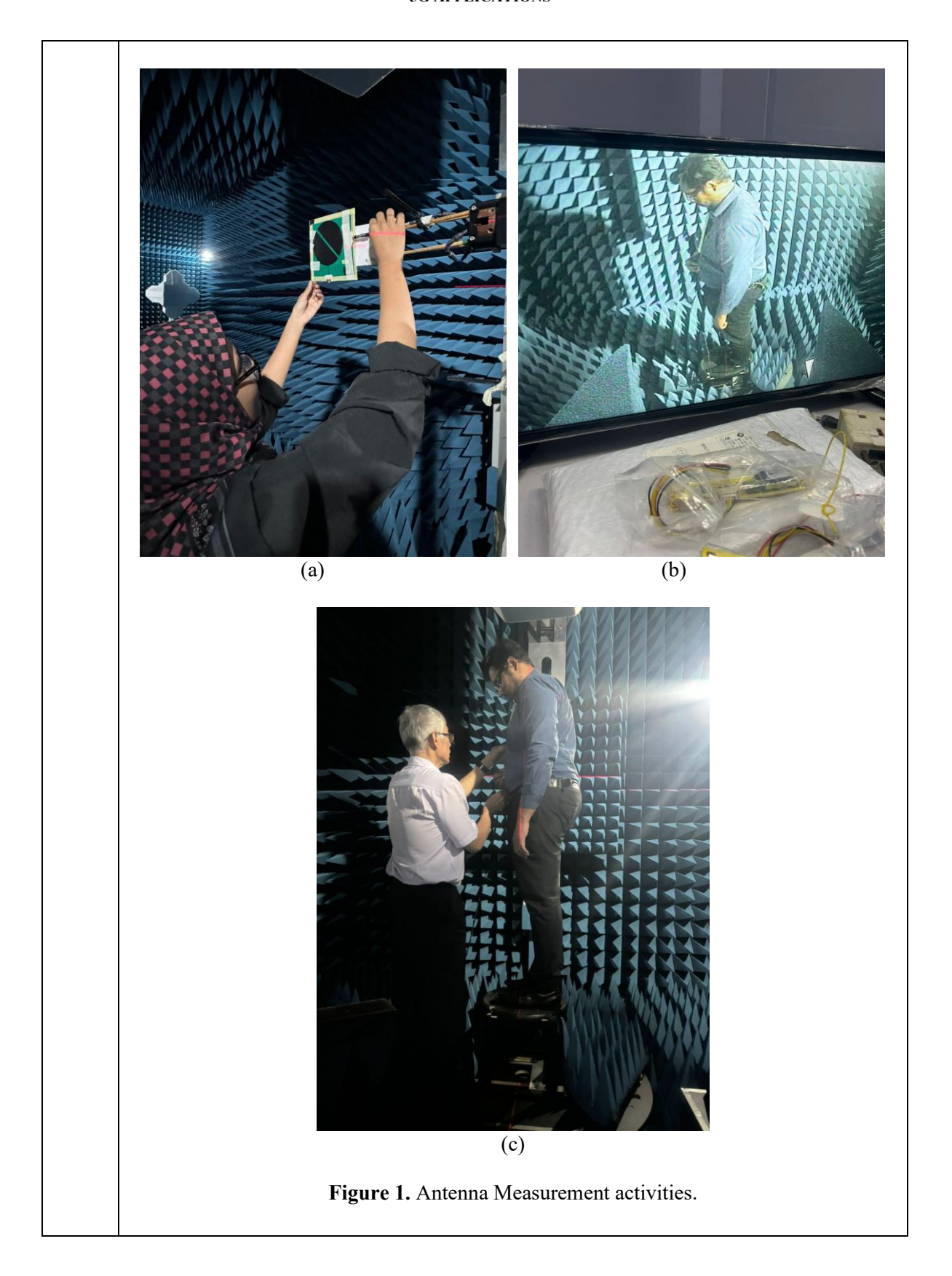




Figure 2. Group photo.